Long Term Two-Phase Flow Analysis of the Deep Low Permeability Rock at the Bruce DGR Site

by

Huiquan Guo

A thesis
presented to the University of Waterloo
in fulfillment of the
thesis requirement for the degree of

Master of Applied Science
in
Civil Engineering

Waterloo, Ontario, Canada, 2011

I hereby declare that I am the sole author of this thesis. This is a true copy of the thesis, including any required final revisions, as accepted by my examiners.

I understand that my thesis may be made electronically available to the public.

Abstract

Abnormal pressures have been measured in the deep boreholes at the Bruce site, southern Ontario, where a deep geologic repository for low and intermediate level radioactive waste disposal has been proposed. The pressure regime in the stratigraphic units exhibits either higher than hydrostatic pressure (over-pressured) or lower than hydrostatic pressure (under-pressured) are considered to be abnormal. At the Bruce site, the Ordovician sediments are under-pressured while the underlying Cambrian sandstone and the overlying Guelph carbonate are over-pressured. Hypotheses have been documented in literature to explain the phenomenon of abnormal pressures. These hypotheses include osmosis, glacial loading and deglaciation unloading, exhumation of overlying sediments, crustal flexure and the presence of an immiscible gas phase. Previous work on the Bruce site has shown that the under-pressures in the Ordovician limestone and shales could not be explained by glaciation and deglaciation or by saturated analyses. The presence of a gas phase in the Ordovician formations has been determined to be a reasonable cause of the under-pressure developed in the Ordovician shales and limestones at the Bruce site. Support for the presence of a gas phase includes solution concentrations of methane, concentrations of environmental isotopes related to methane and estimates of water and gas saturations from laboratory core analyses.

The primary contribution of this thesis is the sensitivity analyses performed on the hydrogeologic parameters with respect to a one dimensional two-phase flow model. First, a one dimensional two-phase air and water flow model was adopted and reconstructed to simulate the long-term evolution of the groundwater regimes at the DGR site. Then the hydrogeologic parameters which impact the presence of under-pressure in the groundwater are investigated. Data required to quantify the properties of geologic media and groundwater are adopted directly from borehole testing and laboratory testing results. The permeable boundaries of the domain are assumed to be water saturated and pres-

sure specified (using hydrostatic conditions in the Guelph Formation and hydrostatic with 120 m over-pressure condition in the Cambrian and Precambrian). Isothermal conditions were assumed, thus constant water density and viscosity values are estimated for the average total dissolved solids (TDS) concentration of the modelled stratigraphic column. A constant diffusion coefficient (a diffusivity of 0.25×10^{-8} m^2/s) of air in water is assumed with a saturation-dependent tortuosity. The air generation rate is assumed to simulate the gas phase generated in the Ordovician formations. The numerical simulation of up to 4 million years provides a means to explore the behaviour of gas phase dissipation due to partitioning into the water phase and diffusive transport in the solute phase. Results confirmed that the presence of a gas phase would result in the under-pressure in water.

The sensitivity analyses are designed to see the impact of variations in the initial conditions, air generation rate and diffusion coefficient on the evolution of abnormal under-pressure. The numerical model replicated the high pressures measured in a discontinuity in the Ordovician shale. Gas phase diffusion in simulation dominates the development of under-pressures of the water phase. In the sensitivity analysis of diffusion coefficient, it indicates that a low diffusion coefficient is required for long-time under-pressure exists in the low permeability media.

Acknowledgements

I would like to thank all the people who made this possible.

I would like to present my sincere gratitude to my supervisor Dr. Jon F. Sykes for the continuous support of my study, for his guidance, patience, motivation and knowledge in helping me finish this thesis. It would be impossible to finish this study without Jon's help.

I would like to present my special thanks to Dr. Stefano Normani and Dr. Yong Yin, for their skills and technical assistance, for their generous help and insightful comments. I appreciate their contributions of time, ideas and knowledge.

Last but not the least, I would like to thank my family and friends, for their encouragement and support behind me.

Table of Contents

List of Tables

List of Figures

Chapter 1

Introduction

Geological abnormal zones with pressures that are higher than the hydrostatic pressure (over-pressured) or lower than the hydrostatic pressure (under-pressured) have been globally observed in deep sedimentary basins. These zones first attracted attention because of difficulties involved in drilling over-pressured formations (*Bethke*, 1986). Now they have drawn the attention of the petroleum industry as they could be a potential reservoir of natural gas/oil resources. Numerous hypotheses and mechanisms have been developed to explain abnormal pressures; popular theories include compaction disequilibrium, tectonics, hydrocarbon generation and migration, aquathermal pressuring, osmosis and faults.

Neuzil (1995) summarized two distinct conceptual theories for abnormal pressures. One is static and the other is dynamic. He postulated that abnormal pressures could exist in either equilibrium or disequilibrium flow regimes. The equilibrium-type abnormal pressures generally result from topographically-driven flow or a result of osmosis or fluid density contrasts, while the disequilibrium type is more common and caused by natural geologic processes, such as compaction, diagenesis and deformation (*Neuzil*, 1995).

Ontario Power Generation (OPG) has proposed the development of a Deep Geologic Repository (DGR) at the Bruce site, Ontario, for long-term management of radioactive waste (Figure 1.1). The proposed repository is to be formed at a depth of 680 m in the Cobourg Formation, which is surrounded by an extensive low permeability limestone and overlain by extremely low permeability shales (Figure 1.2). Observations made from borehole drilling and field tests at the Bruce site reveal a distinct under-pressured regime

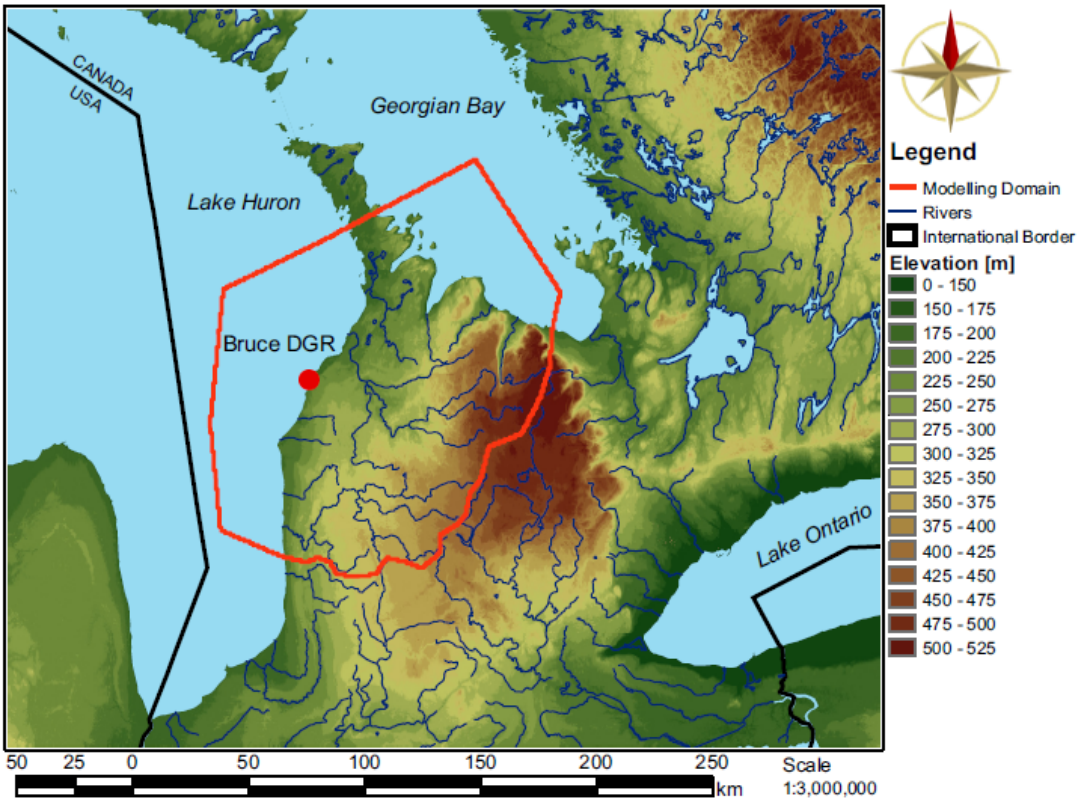

Figure 1.1: Location of proposed DGR site. Adopted from *Sykes et al.* (2011).

in the Ordovician formations and an over-pressured zone in the underlying Cambrian formation. The extensive overlying and underlying low permeability media is a requirement for Cambrian over-pressure to persist over the Paleozoic period.

In order to characterize the site-scale geology, hydrogeology and hydrogeochemistry, 6 DGR boreholes are installed at the Bruce site (Figure 1.3). The DGR borehole laboratory testing results are the main source of data used in this thesis.

1.1 Statement of Purpose

In this thesis, a two-phase gas and water flow conceptual model has been evaluated and the sensitivity analyses are performed to see the presence of abnormal pressures and the impact of the hydrogeologic parameters. The numerical modelling process simulates gas-water transport in the deep geologic settings where conceptual hydrostatic pressures

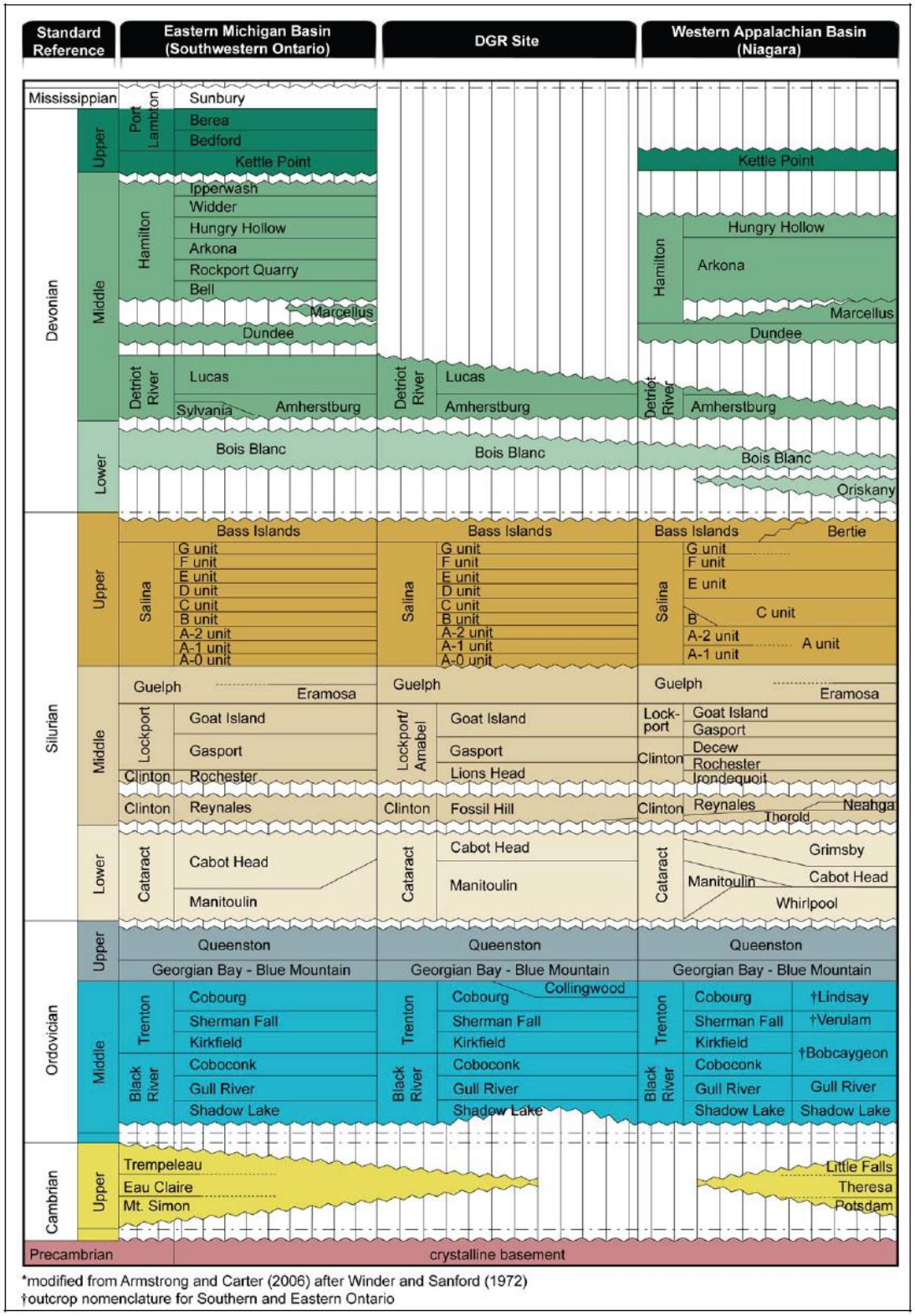

Figure 1.2: Paleozoic stratigraphy of southwestern Ontario. Adopted from *AECOM and ITASCA CANADA* (2011).

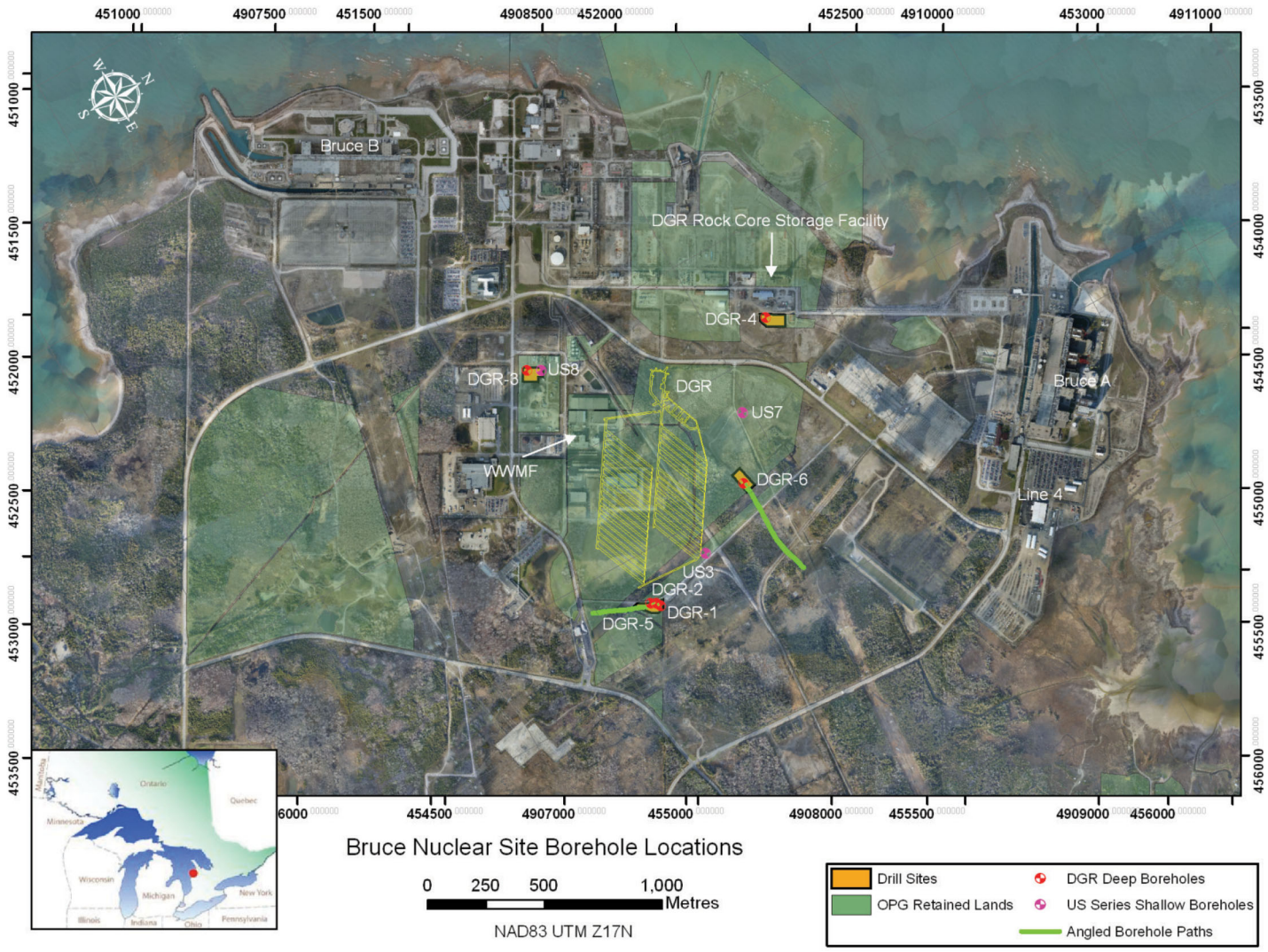

Figure 1.3: DGR borehole, US borehole and the proposed DGR layout at the Bruce site. Adopted from *INTERA* (2011).

evolve to be abnormal. In addition, we see the impact of gas generation in these low permeability units on fluid pressures. A computer program TOUGH2-MP (*Pruess et al.*, 1999) has been utilized to solve the two-phase flow problem, which is too complicated to solve analytically. The computer program used in this study describes two-phase flow and thermodynamic transport in porous and fractured media.

In the two-phase flow analyses, hydrogeologic parameters are perturbed for different scenarios in a sensitivity analysis to understand the impact of rock properties and environmental conditions on the change of groundwater pressure and fluid content.

1.2 Scope of Study

This thesis briefly introduces the geology and hydrogeology of the Michigan Basin, and summarizes previous work on abnormal pressures and two-phase flow. A detailed one-dimensional modelling domain has been developed in this study to cover the vertical flow regime at the Bruce site, including 17 vertically layered formations ($\sim$ 350 m – 970 m in depth) and discretized into 983 grid blocks for numerical simulation. Transient simulations of the 1-D domain were run using the computational program TOUGH2-MP.

The numerical modelling requires predefined rock properties, fluid properties, initial conditions, time-steps and source/sink terms. It produces results of fluid pressures, saturations, and temperature for every grid block with respect to the defined break time points for output. From the simulations we can investigate the trend and critical features of the flow regime and make quantified assessments for site development.

1.3 Overview

Chapter 2 briefly describes the environment and geology of the Michigan Basin and characterizes the geological properties of the brief sedimentary units. Regional-scale studies and the relevant modelling framework are reviewed to provide a conceptual strategy for this research.

Chapter 3 describes the regional-scale geochemical framework and the DGR site data. The data are summarized from the Hydrogeologic Modelling Report by *Sykes et al.* (2011).

Chapter 4 introduces theories for two-phase flow in low permeability media. It provides a description of the two-phase flow model used in this research. Existing models developed for two-phase flow analysis are reviewed and the advantages of these models are discussed. The equation-of-state module adopted in this research and the research methodology are described.

Chapter 5 develops the conceptual model for site-scale analysis. It describes the in-situ fluid phase properties, specifically hydraulic and thermal, and discusses the most basic functions for two-phase flow. The selection of proper parameters for simulation is discussed.

Chapter 6 defines the input data and initializations for the computational model. Various cases have been analyzed to investigate the impact of parameters. The base case scenario is compared with other scenarios to illustrate the effect of gas generation rate and capillary pressure functions. This is followed by the sensitivity analysis for further evaluation of determinant parameters.

Chapter 7 presents the final conclusions and suggestions for this study and further studies of this research.

Chapter 2

The Michigan Basin

The Michigan Basin, shown in Figure 2.1, is one of several cratonic basins in North America. Others include the Illinois, Williston and Hudson Bay basins. This nearly circular basin is centered on the lower peninsula of Michigan state and it gently dips from the edge toward its center with a nearly uniform structure. The radius of this nearly circular basin is about 250 km and its central part deepens to 4.9 km. Continuous subsidence in the Michigan Basin during the Paleozoic era resulted in the deposition of a nearly complete stratigraphic sequence of sedimentary rocks from the oldest Precambrian units to Jurassic "red beds", the youngest bedrock unit in the basin.

2.1 Geologic Framework of the Michigan Basin

In the DGR Phase I Geology Report, *AECOM and ITASCA CANADA* (2011) developed a 3D Regional Geological Framework (3DGF). The original purpose of the 3D Geological Framework was to capture and present the current geological understanding of the Paleozoic sedimentary formations within southern Ontario including a portion of the Michigan Basin. A rectangular region covers 160 km $\times$ 200 km, which centered on the DGR site, is designed to be the Regional Study Area (RSA) for hydrostratigraphic modelling (Figures 2.2 and 2.3).

The data source for the regional framework was the Oil, Gas, and Salt Resources Library (OGSR) Petroleum Wells Subsurface Database (*NWMO*, 2011). Figure 2.4 shows the

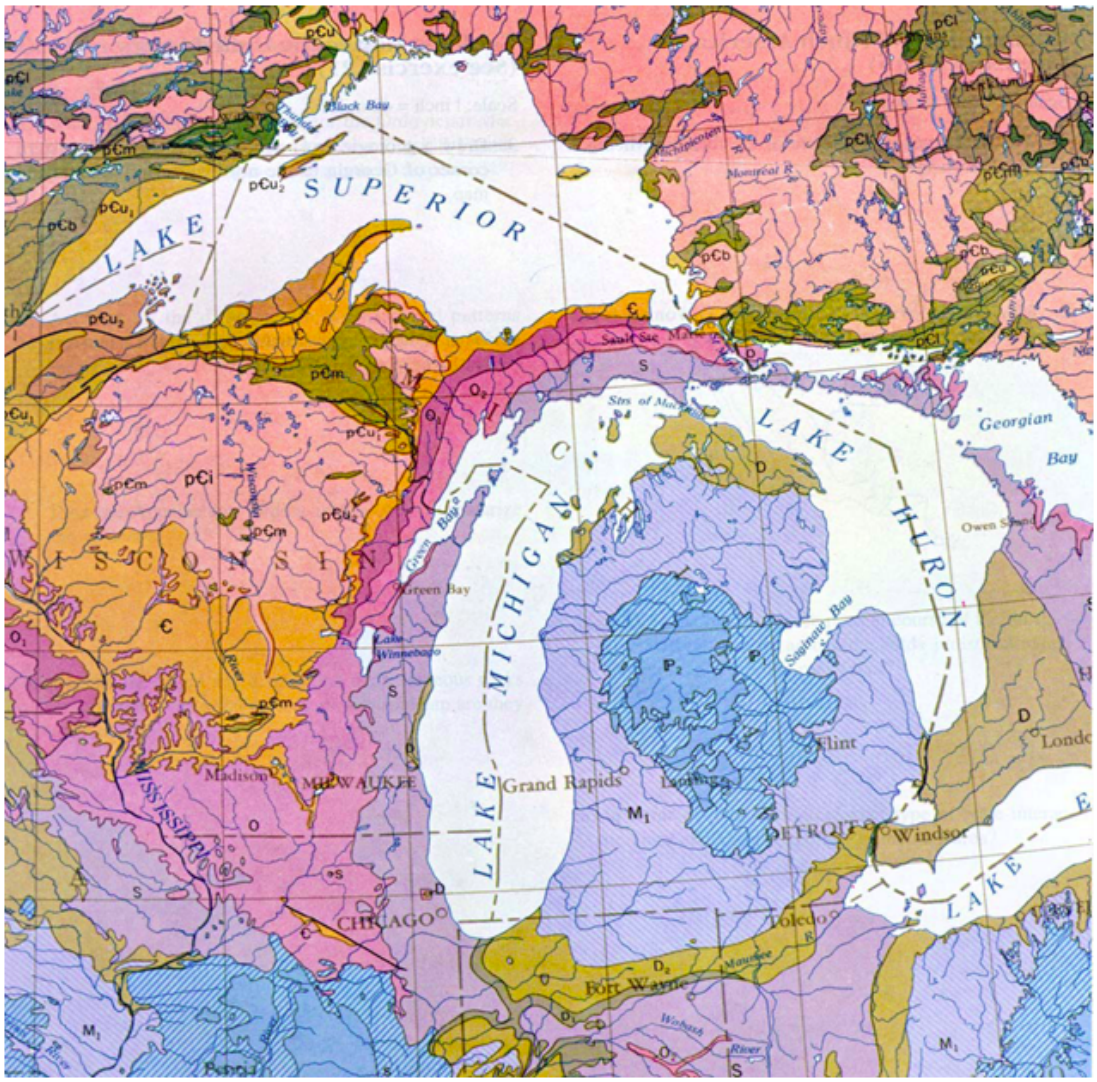

Figure 2.1: Geologic map of the Michigan Basin. Adopted from *Sykes et al.* (2011).

location of these wells in southwestern Ontario. Records from tens of thousands of petroleum wells provide detailed information on geological formation interfaces, water pressure, brine concentration and gas/oil content. The OGSR well logs indicate the extent of southern Ontario gas/oil production fields. Fewer wells were located in the RSA, indicating the lack of oil and gas resources in this area (*Sykes et al.*, 2011). Other data sources are from the Michigan State Geological Survey Digital Well Database, and from *Armstrong and Carter* (2006). *Armstrong and Carter* (2006) generated a series of geologic cross-sections across southern Ontario, which is a good reference for the 3DGF development.

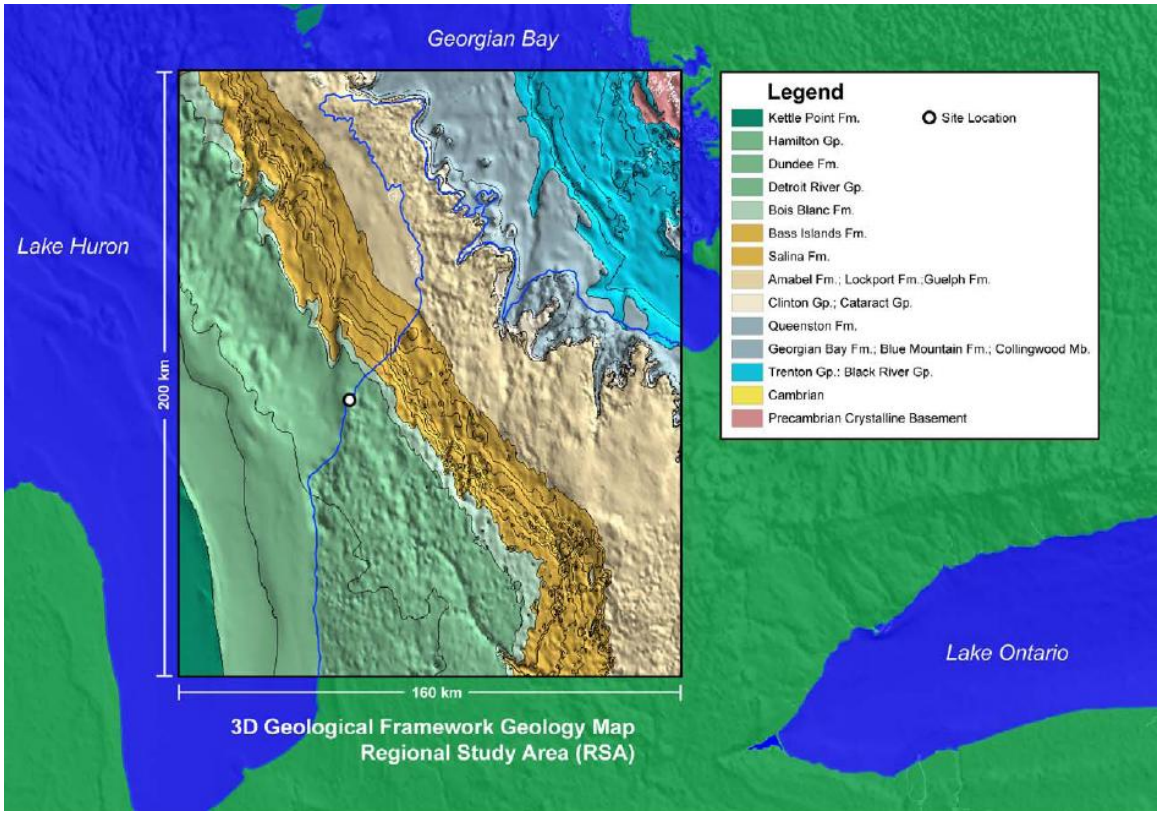

Figure 2.2: 3D Geological Framework study boundary with Paleozoic geology derived from 3D model. Adopted from *AECOM and ITASCA CANADA* (2011).

2.2 Regional Geology and Evolution of the Michigan Basin

The Michigan Basin is one of the sedimentary basins formed on the Earth's crust during the ancient Paleozoic period, between about 544 and 286 million years ago.

Having experienced more than 200 million years of continuous subsidence and compaction, the Michigan Basin is gently dipped from the edge toward its center with a nearly uniform structure. The deposited sediments have a maximum thickness of about 5 km below ground surface. Deposits are accumulated in the subsiding areas during the long and slow earth movement and ocean retreating and transgression era, resulting in deposition of a nearly complete stratigraphic sequence of sedimentary rocks (Figure 2.5). These sediments are dominated by sandstone, limestone and shale. Beneath these Paleozoic sediments, there lie the Precambrian rocks.

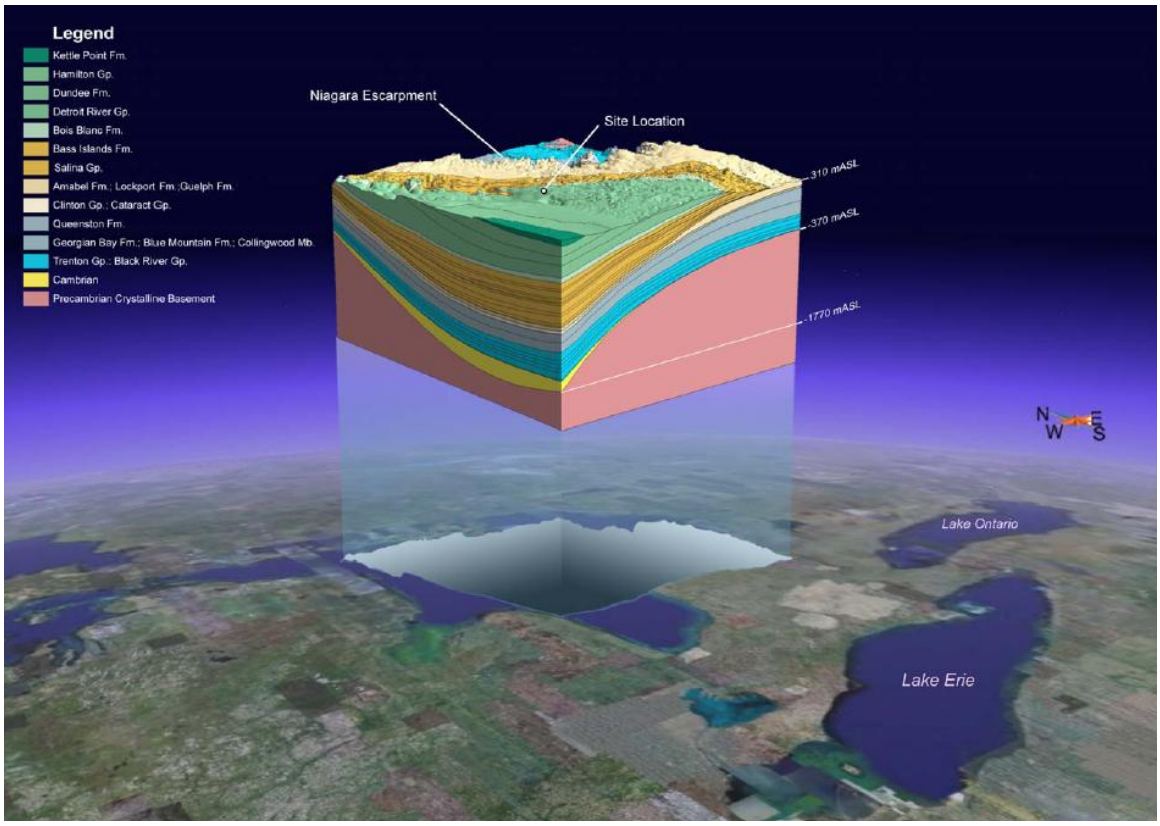

Figure 2.3: 3D Geological Framework box diagram of the Regional Study Area. Adopted from *AECOM and ITASCA CANADA* (2011).

2.3 Abnormal Deep Groundwater Regime

There is evidence showing that the groundwater within the Paleozoic sediments is undisturbed and stagnant. According to the Hydrogeologic Modelling report (*Sykes et al.*, 2011), three distinct groundwater regimes at the Bruce DGR site are distinguished:

- A shallow zone characterized by Upper Silurian and Devonian units that have higher permeability and a relatively Low Total Dissolved Solids (TDS). It is expected that topography strongly affects the flow pattern of groundwater in the shallow zone;
- An intermediate zone characterized by low permeability Upper Silurian carbonates, shale, salt and evaporite units, the more permeable Niagaran Group (comprised by the Guelph, Goat Island, Gasport and Lions Head Formations) and the Lower Silurian carbonates and shales (Figure 2.6);

- A deep zone characterized by low permeability shales and carbonates of the Ordovician and the more permeable sandstones and dolomites of the Cambrian Formation. The TDS of pore water can exceed 300 g/L, which corresponds to a specific gravity of 1.2 for the fluids. The deep horizon is isolated by the low permeability units in the shallow zone and from the influence of local topography.

According to the DGSM (Descriptive Geosphere Site Model) report (*INTERA*, 2011), significant abnormal pressures in the deep saline system were discovered. An under-pressure phenomenon exists in the Ordovician shales and limestones, and additionally an over-pressure condition in the Cambrian sandstones. The significant over-pressure responds to the extreme low permeability formations overlying the Cambrian formations, and only thick low permeability media could preserve the excess pressures for a million years or longer without dissipation through fluid migration.

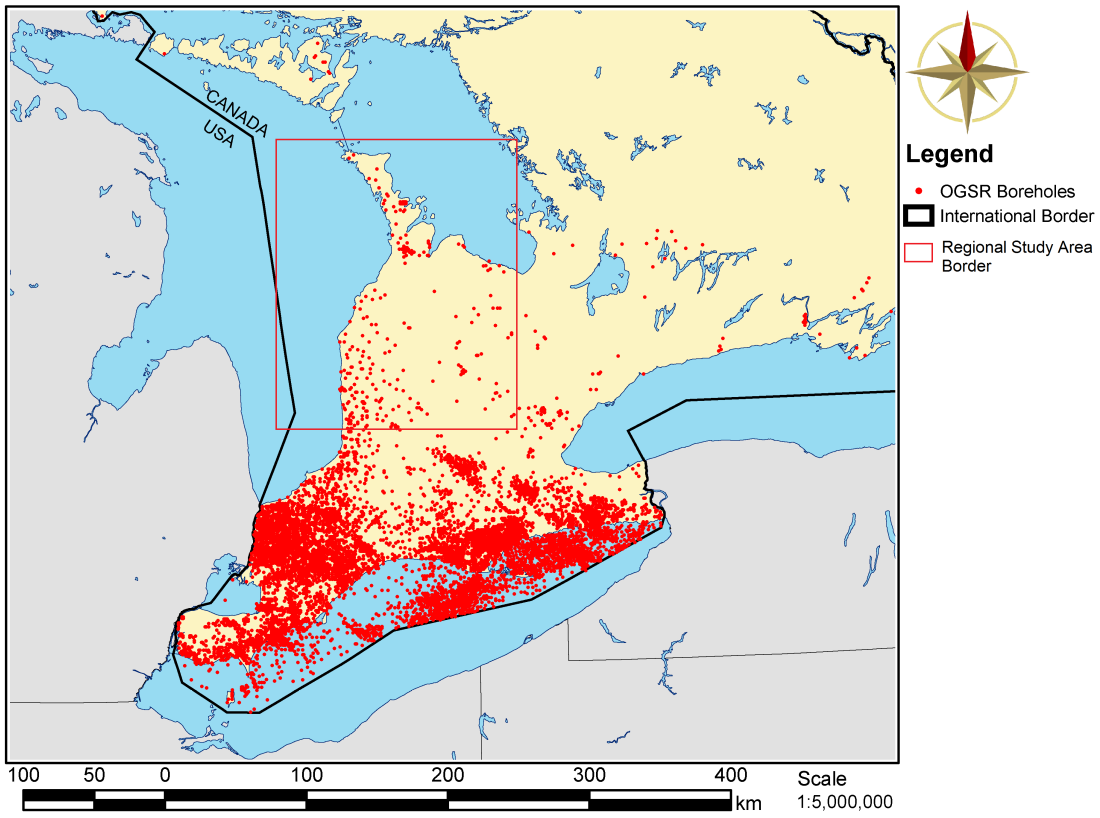

Figure 2.4: Locations of Oil, Gas, and Salt Resources Library (OGSR) petroleum wells in southwestern Ontario. Adapted from *Sykes et al.* (2011).

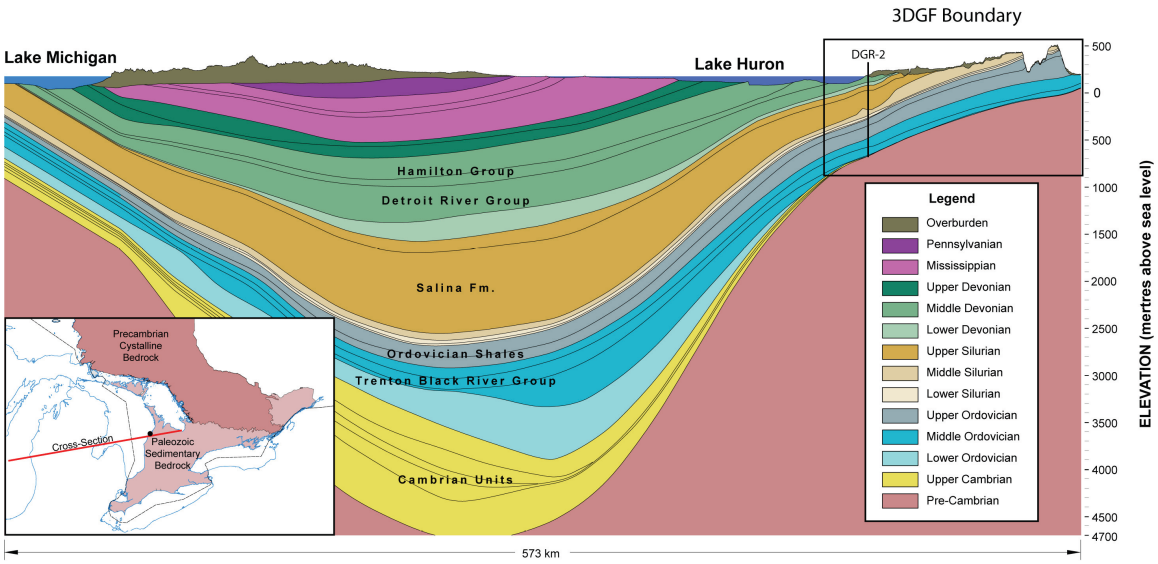

Figure 2.5: The Michigan Basin cross-section. Adopted from *AECOM and ITASCA CANADA* (2011).

2.4 Regional Sedimentary Units

The Michigan Basin has experienced ocean transgression and regression alternately during the Paleozoic. The conditions were changed under the movements of the seas, and sediments from the ocean have been deposited and transformed into different rock types.

This indicates that the Michigan Basin was developed continuously during six subdivisions of the Paleozoic, including the Cambrian, Ordovician, Silurian, Devonian, Mississippian and Pennsylvanian (Figure 2.1). However, the Mississippian and Pennsylvanian rocks are absent in southern Ontario (see Figure 2.7). Figure 1.2 illustrate the Paleozoic stratigraphy of southern Ontario, in the Appalachian Basin, the DGR site, and the Michigan Basin. The Geological stratigraphy map of southern Ontario also shows the outcrops of Proterozoic and Paleozoic sediments, proceeding from the Precambrian basement to Upper Devonian formations (Figure 2.7). Expressed with respect to geologic time, the dominant sedimentary units in the Michigan Basin are described in the following paragraphs.

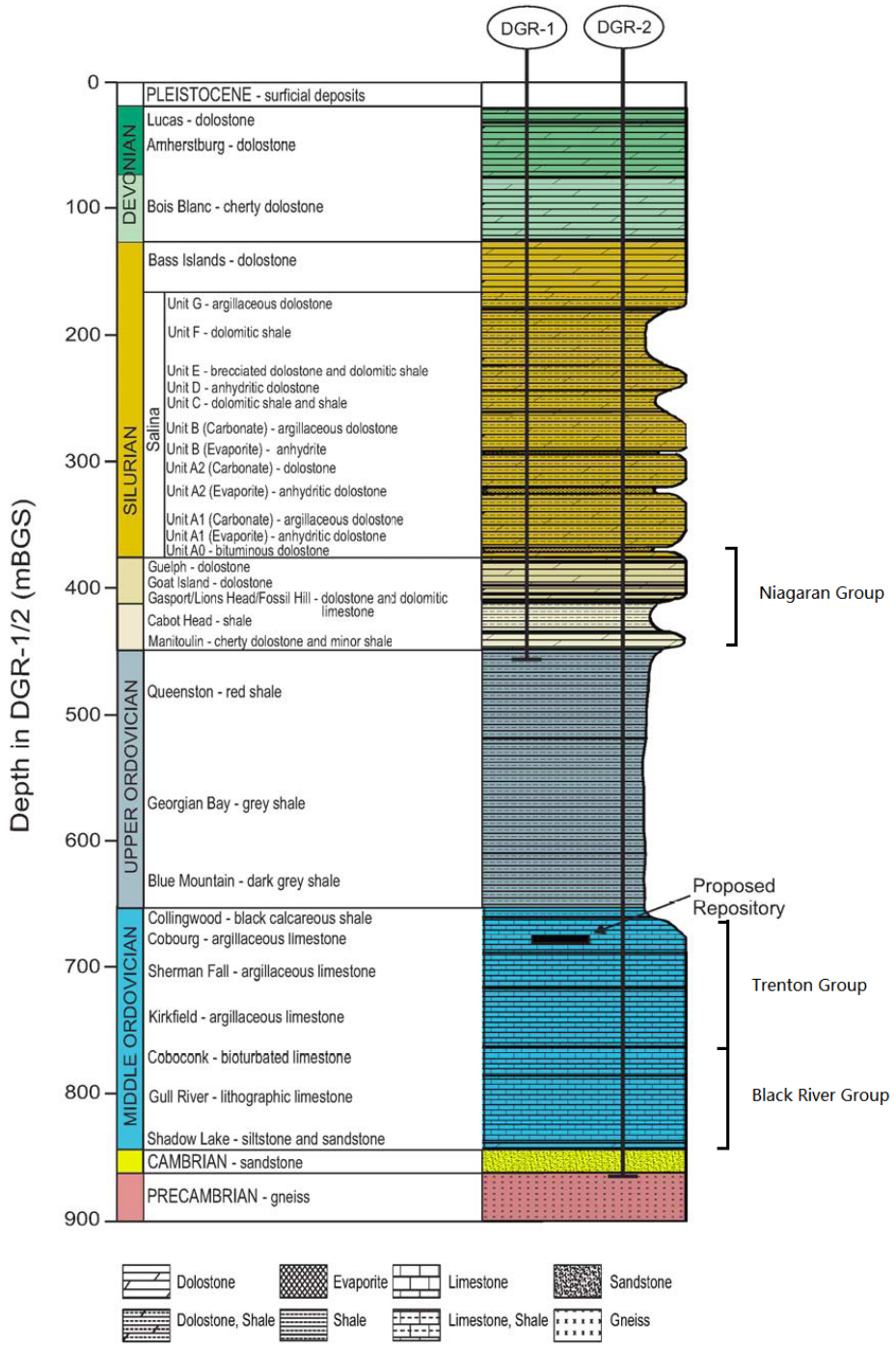

Figure 2.6: Stratigraphic column at the Bruce site based on DGR-1 and DGR-2 borehole data. Adapted from *Sykes et al.* (2011).

2.4.1 Precambrian Basement (4000 Ma - 544 Ma)

Precambrian rocks are the oldest rocks in southern Ontario region, serving as the basement of Paleozoic sediments and younger deposits. The main exposure area of the Precambrian rocks is in eastern and central Canada, encircling Hudson Bay. The outcrop area is called the Canadian Shield. The western upper peninsula of Michigan has Precambrian rock outcrops. The nearest outcrop of Precambrian basement rock occur approximately 150 km to the northeast of the DGR site, along the north shore of Georgian Bay (*NWMO*, 2011).

Precambrian rocks are considered to have been relatively tectonically stable (*AECOM and ITASCA CANADA*, 2011). Precambrian rocks in many cases formed the continental cratons. The North American craton which includes the Precambrian shields of Canada has remained coherent and relatively rigid since the Precambrian (*Hoffman*, 1988). Beneath the Michigan Basin, it is a nearly uniform dip caused by tectonic warping. The depth of Precambrian rocks at the Michigan Basin is about 5000 m in the center. The Precambrian rocks under the Michigan Basin also include a rift zone (*Hinze et al.*, 1975). As an extension of the Mid-Continent rift system, the rift zone formed around 1.1 billion years ago (*NWMO*, 2011).

2.4.2 Paleozoic Era (544 Ma - 286 Ma)

2.4.2.1 Cambrian

As the oldest Paleozoic rocks deposited in the basin, these rocks were interestingly deposited under relatively shallow water conditions (*Catacosinos and Daniels*, 1991). Maximum water depths were probably tens of meters. The lithology of the Cambrian units ranges from fine to medium crystalline dolostone, sandy dolostone, argillaceous dolostone to fine to coarse quartzose sandstone (Hamblin, 1999). These Cambrian sandstone deposits resulted from sandy sediment compaction. These coarse sandy sediments are brought from bare lands by the streams during the early Paleozoic time. Its deposits extend from the Appalachian Basin to the Michigan Basin but have largely been eroded over the Algonquin Arch [Bailey Geological Services Ltd. and R. O. Cochrane, 1984a], see Figure 2.8.

Generally, the Cambrian consists of sediments which are comparatively permeable. It acts as a groundwater aquifer. The high pressure in Cambrian is isolated by overlying low permeability sediments. Although the Cambrian is permeable, the fluid in it is thought to be stagnant. Referring to the Hydrogeologic Modelling Report (*Sykes et al.*, 2011), the Cambrian sandstone outcrops in Wisconsin, and it is absent at the Algonquin Arch (Figure 2.1), it also outcrops north of Sault Ste. Marie, Ontario. The distance is more than 300 km to the northwest of the DGR site. A potential fluid pathway may exist to the west where the unit deepens and thickens towards the center of the Michigan Basin (*Sykes et al.*, 2011).

Measured TDS concentration in the Cambrian at the DGR-1 and DGR-2 boreholes is 235 g/L and pore water chemistries are Na-Ca-Cl brine (*NWMO*, 2011). The only Cambrian production of oil and gas in Ontario, Canada, is on or near the axis of the Algonquin Arch at the eastern edge of the basin; production is from stratigraphic traps in dolomite and porosity pinchouts or from fault blocks in dolomite.

2.4.2.2 Ordovician

The Michigan Basin was submerged by ocean during much of the Ordovician Period. In southern Ontario part of the Michigan Basin region, the Ordovician has two distinct lithologies: Middle Ordovician Carbonates and Upper Ordovician Shales. The Lower Ordovician rocks have been removed from southern Ontario due to erosion, but it is present in the center of the basin (Figures 1.2 and 2.5).

The Middle Ordovician Carbonates are subdivided into seven units:

- Shadow Lake Formation, Gull River Formation and Coboconk Formation, which belong to the Black River Group;
- Kirkfield Formation, Sherman Fall Formation and Cobourg Formation which belong to the Trenton Group.

A major marine transgression (the sea invades the continent) was responsible for the development of carbonate sequences. *Coniglio et al.* (1990), in their study of Ordovician carbonate diagenesis, commented that these stratigraphic sequences comprise supratidal

and tidal flat siliciclastics and carbonates, through lagoonal carbonates, into offshore carbonates.

2.4.2.2.1 Middle Ordovician The Shadow Lake Formation lies at the base of the Black River Group and is characterized by poorly sorted, red and green sandy shales, argillaceous and arkosic sandstones, minor sandy argillaceous dolostones and rare basal arkosic conglomerate (*Armstrong and Carter*, 2006). The Gull River Formation and Coboconk Formation consist mainly of limestones, fine to medium grained (*NWMO*, 2011). Thin shale beds and partings may be present (*Armstrong and Carter*, 2006).

The Kirkfield Formation and Sherman Fall Formation are characterized by fossiliferous, argillaceous limestones with thin shale interbeds and partings. The DGR horizon is located in the Cobourg Formation, which is characterized similarly to the Kirkfield Formation and Sherman Fall Formation by fossiliferous limestones and argillaceous limestones.

2.4.2.2.2 Upper Ordovician Shales The extensive Upper Ordovician shale sequences are comprised of the Blue Mountain, Georgian Bay and Queenston formations (*NWMO*, 2011).

The Blue Mountain is primarily dominated by uniform soft and laminated shale with minor siltstone and carbonate. The facies in the Blue Mountain Formation are primarily open marine (*NWMO*, 2011). The Georgian Bay Formation is composed of shale with minor siltstone and limestone. The Queenston Formation is characterized by shale with varying amounts of carbonate.

The only currently active natural gas reservoir is in the Ordovician aged Arthur pool, southeast of the RSA (*NWMO*, 2011). Nearly 25 percent of cumulative oil produced is from the hydrothermal dolomite reservoirs of the Ordovician (*NWMO*, 2011). The Middle Ordovician has currently become a target of petroleum exploration.

2.4.2.3 Silurian

During the middle and late Silurian, the Michigan Basin was filled by a warm, shallow sea and reefs started to grow in this ideal condition (*Coniglio et al.*, 2003). The reefs

tend to grow close to the sea level to obtain optimum light, food and oxygen. Therefore, they may build a column of reef rock hundreds of meters high.

The barrier reefs located around the shallow boundary of the Michigan Basin. Outward from the reefs, in the deeper water, mud rich in calcium carbonate accumulated on the floor of the vast shallow seas, generally producing thinly bedded dolomite that contains few fossils (*Davis*, 1964). Also, carbonate deposits formed in shallower water due to the reefs.

2.4.2.3.1 Lower and Middle Silurian Carbonates and Shales The Lower Silurian is divided into two formations: the Manitoulin Formation and overlying Cabot Head Formation. The Manitoulin is carbonate dominated while the Cabot Head Formation is described as noncalcareous shales that may contain some sandstone and carbonate interbeds (*Armstrong and Carter*, 2006).

2.4.2.3.2 Middle Silurian The Middle Silurian rocks are comprised of the Fossil Hill, Lions Head, Gasport, Goat Island and Guelph formations.

The Fossil Hill Formation and Lions Head are composed of thin to medium bedded fossiliferous dolostone. The top of Fossil Hill Formation is a regional discontinuity and records a regional marine regression (the sea retreats from the continent) during the Middle Silurian (*NWMO*, 2011). Erosion and tectonic movements further deformed the geological settings within the Michigan Basin. The marine transgression that followed was responsible for the deposition of the Lions Head, Gasport, Goat Island and Guelph formations.

The Gasport Formation is a thick bedded dolostone which may contain some limestone. The Goat Island is similar to the Lions Head but more argillaceous.

The Guelph Formation is the first permeable layer on top of the 280 m low permeability formations that overlay the DGR horizon. The small thickness of the Guelph Formation is 4.1 m at the DGR-1 borehole. The permeability is about four orders of magnitude higher than the underlying formations. Therefore, the Guelph Formation is an aquifer in the intermediate zone. Above the Guelph Formation are further low permeability shale and anhydrite units within the Silurian deposits (*NWMO*, 2011). The Guelph Formation aquifer contains Na-Cl brine with a high TDS of 330 g/L.

2.4.2.3.3 Upper Silurian The Upper Silurian includes the Salina Group and the Bass Islands formations. In the Michigan Basin, the Salina Group is produced by repeated deposition of carbonate, evaporate and argillaceous sediments, and on top covered by a shaley strata.

Pinnacle reefs and the associated sedimentary rocks are tremendous sources of oil and gas. The annual production from the Niagaran reef reservoirs in Michigan has reached 30 million barrels of oil and 150 billion cubic feet of natural gas which accounts for 70 percent of oil and 90 percent of gas produced in the state (*Aminian et al.*, 1982).

A thin porous and permeable aquifer exists in the Upper Silurian, the thickness depicted in DGR-1 is 3.7 m. The aquifer is the uppermost part of the Salina A1 Upper Carbonate (*INTERA*, 2011). This shallow aquifer is isolated by 50 m thick low permeability Salina dolostone and evaporite from the Guelph Formation.

2.4.2.4 Devonian Carbonates

The midland uplifting deformed the shape of the Michigan Basin in the Devonian Era. At early Devonian, this movement locked the in-land sea to a narrow and shallow basin. This is followed by a deposition of carbonates, limestone, shale and evaporite during the mid-Devonian retreat event.

The Devonian sediments are fully developed in the Michigan Basin; however, they are weathered severely on the upper edge of the basin (Figure 1.2). *Golder Associates Limited* (2003) investigated the unconformity of the Silurian-Devonian in the southeastern Michigan, and found the upper 2 to 8 m of the Bass Islands Formation in the Devonian is soft, weathered and relatively permeable. At the DGR site, from the middle Devonian period, most of the sediments are fully decomposed probably by deglaciation or weathering (Figure 1.2). At the western Appalachian basin, the top of the upper Devonian and the Mississippian deposits are also removed from the geologic sequence (Figure 1.2).

In early Middle Devonian, continued transgression and regression of seas across the Michigan Basin, in an arid climate, deposited limestone offshore (*Dorr and Eschman*, 1970). A lot of muddy sediments were brought into the Michigan Basin due to a uplift in the northern Appalachian region (*Dorr and Eschman*, 1970). These organic-rich mud formed

the Antrim Shale in Michigan, which has become a successful nature gas production field in Michigan (*Dorr and Eschman*, 1970; *Martini et al.*, 1996; *Catacosinos et al.*, 1991).

2.4.2.5 Mississippian

The Mississippian formation only appears in Michigan and is absent in southern Ontario (Figure 2.5). The central Michigan Basin was covered by a small sea from the Late Devonian to the Early Mississippian. *Dorr and Eschman* (1970) indicate that the inland sea possibly disappeared during the Middle Mississippian, because the Middle Mississippian rocks are missing. Seas invaded again in the Late Mississippian and withdrew during basin uplifting, depositing a new set of formations in the central area.

The most common rocks include shale, siltstone, and sandstone. The Michigan Basin subsidence was most rapid during early Mississippian. The sediment depositional patterns were similar. However, the sediments were coarser and the area of deposition is smaller in very late Mississippian time. Due to the uplift of the Michigan Basin during late Mississippian period, this is possible (*Dorr and Eschman*, 1970). This causes erosion of the older formation and is represented by a gap to the overlying Pennsylvanian.

2.4.2.6 Pennsylvanian

This is the last period before the great lost interval in the Michigan Basin. The Pennsylvanian is known for its extensive coal-bearing strata (*Holman*, 1995). It is absent in southern Ontario.

2.4.2.7 Post Pennsylvanian

This era can be divided into two parts (*Dorr and Eschman*, 1970): *The Lost Interval* and *The Great Ice Age*.

2.4.2.7.1 The Lost Interval At the end of the Pennsylvanian, a great general uplift occurred in the eastern part of North America, as the gently downward-curving layers of sedimentary rocks in the Michigan Basin were slowly pushed upward (*Holman*, 1995).

Rocks of the Latest Pennsylvanian, Permian, nearly all of the Mesozoic (except for the Late Jurassic), all of the Cenozoic are missing. It is likely that most of them would have been swept away by erosion in such an area of general uplift (*Dorr and Eschman*, 1970). The exhumation of these layers has allowed the underlying rocks to dilate, reducing the pore pressure in the rock.

2.4.2.7.2 The Great Ice Age The Ice Age began about 2 million years ago in the Early Quaternary Period (*Dorr and Eschman*, 1970). The complex climate changes were worldwide, and most land on earth was covered by glaciers. About 4 periods of glaciation occurred over the Michigan Basin, with warm interglacial periods in between. During the Ice Age, several great ice sheets advanced and retreated in North America. The Michigan Basin was buried under approximately 2000 m or more of ice. The movement of glacial ice sheets acts as another form of deposition/erosion, which changed the topography of the Michigan Basin at that time. The Great Lakes are products of the bedrock topography produced during the Paleozoic era, the subsequent vast erosion of these rocks, and finally the recent glacial processes of the Pleistocene (*Holman*, 1995). The Great Lakes also grew deeper and wider with advances and retreats of the ice sheet. The Ice Age contributes to the features and landforms we see in Michigan.

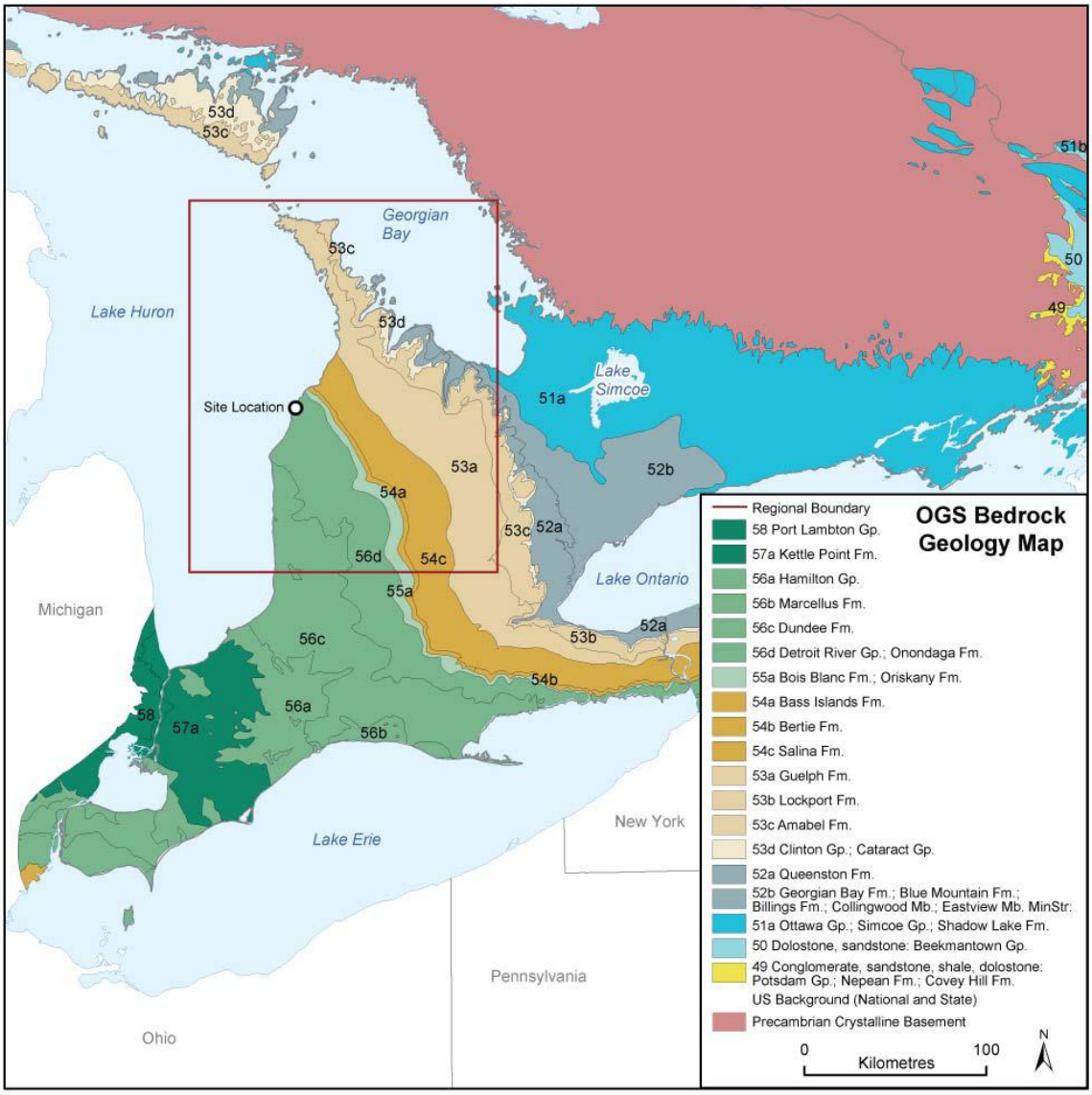

Figure 2.7: Bedrock geology of southern Ontario. Adopted from *AECOM and ITASCA CANADA* (2011).

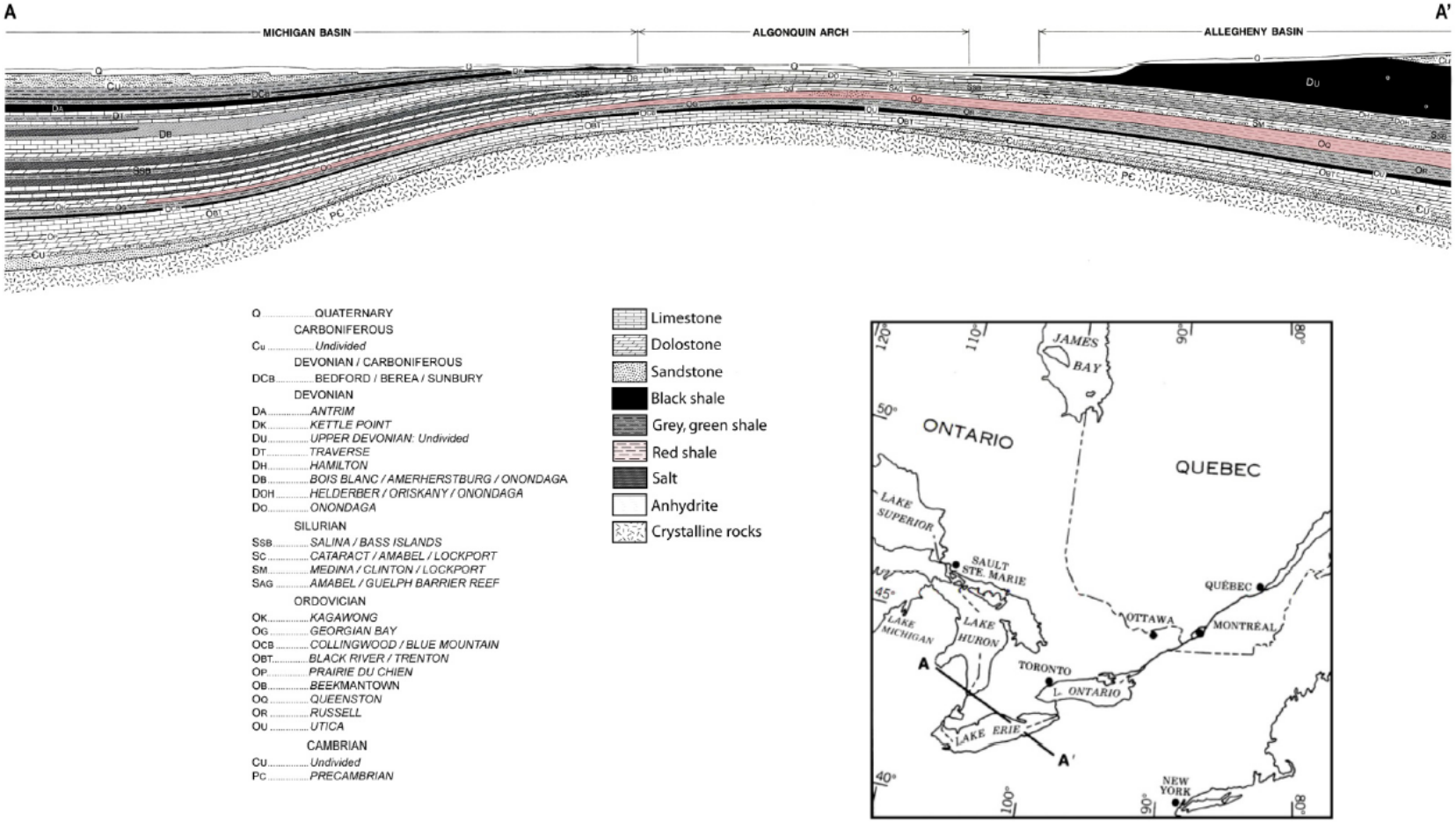

Figure 2.8: Geological cross-section from the Allegheny (Appalachian) to the Michigan Basin. Adopted from *Sanford* (1993).

Chapter 3

Regional-Scale and DGR site data

Most of the descriptions in this chapter refer to the Conceptual Model section of the Hydrogeologic Modelling Report of *Sykes et al.* (2011). The Hydrogeologic Modelling report includes the key components of the regional-scale conceptual model and summarizes data from the Geosynthesis study for the regional-scale and site-scale modelling (*NWMO*, 2011). Some of the important features of these reports that are adopted for this thesis, include the regional-scale geochemical framework and the DGR site data.

3.1 Regional-Scale Geochemical Framework

The regional-scale geochemical data have been summarized and analyzed by Hobbs et al. through two periods of study (*Hobbs et al.*, 2011). The geochemical framework for the DGR site is defined by both the data obtained from the DGR boreholes and a geochemical database (*Sykes et al.*, 2011). Referring to *Hobbs et al.* (2011), the geochemical database is based on the chemical and isotopic compositions of waters collected from multilevel research wells and producing wells across southwestern Ontario, central Michigan Basin and the western margin of the Appalachian Basin.

Two geochemical systems are characterized at the regional scale by *Hobbs et al.* (2011):

i) A shallow system (depth $<$ 200 m). The pore water is less saline fresh water and brackish water, which is characterized as Na-Cl, Na-Mg-Ca-Cl, Ca-SO_4 or Ca-Na-Cl

type based on major ion concentrations. The stable isotopic compositions of $\delta^{18}O$ and $\delta^{2}H$ in pore water indicate the more saline waters mixed with glacial waters or dilute meteoric waters;

ii) An intermediate to deep system (depth > 200 m). The pore water has high TDS concentration (200,000 mg/L – 400,000 mg/L), with the presence of hydrocarbons. Brines are characterized as Na-Ca-Cl or Ca-Na-Cl type. The stable isotopes are consistent with typical sedimentary basin brines (TDS > 100,000 mg/L).

3.1.1 Regional-Scale TDS Distribution

According to *Hobbs et al.* (2011), in order to characterize the groundwater in Michigan and southern Ontario regions and develop a regional-scale geochemical framework, 202 groundwater samples were collected across central Michigan and southwestern Ontario (Figure 3.1). In southwestern Ontario, samples were collected from Cambrian to Devonian formations. The observed TDS has a large variation at a given depth and the values range from less than 1,000 mg/L to more than 400,000 mg/L (Figure 3.2). In Figure 3.2, most TDS values are high in concentration between 140,000 and 400,000 mg/L. The classification scheme developed by *Carpenter* (1978) was used to classify the waters by TDS: 67% of the waters are brine, 20% are saline, 10% are brackish and only 3% are fresh waters (*Hobbs et al.*, 2011). The highest salinity in the database is in central Michigan with TDS of approximately 400,000 mg/L in Ca-Na-Cl type, at a depth of 1,200 – 1,400 m and 3,200 m.

Figure 3.1 and Figure 3.2 indicate that the distribution of TDS concentration has a large variation at a given depth and little water samples are collected at the DGR site. In addition, the water type varies over the study area, and there is a lack of data to define the chemical evolution of pore fluids (*Sykes et al.*, 2011). Hence, it is difficult to estimate the spatial distribution of TDS concentration over the regional-scale domain. In the Hydrogeologic Modelling Report, *Sykes et al.* (2011) defined an approach to obtain the regional-scale TDS distribution for their density-dependent flow analysis. The concept was to let TDS concentration evolve and redistribute in a representative domain with an assigned initial concentration for each layer.

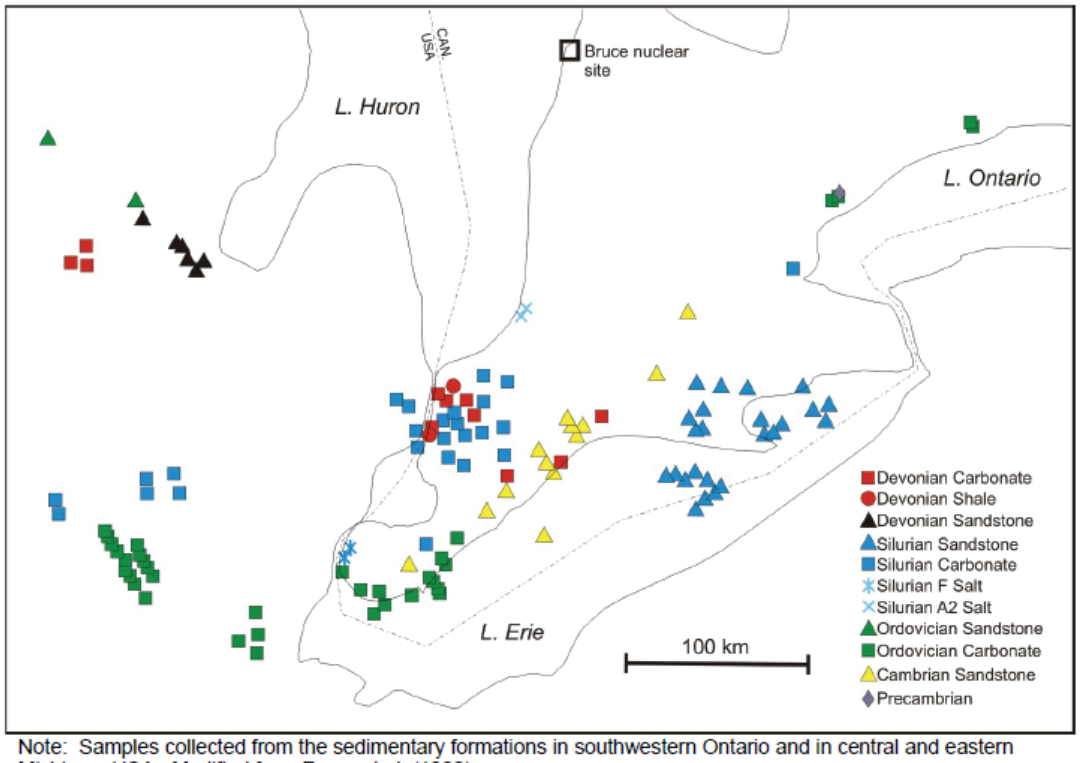

Figure 3.1: Locations of the groundwater samples. Adopted from *Hobbs et al.* (2011).

3.1.2 Stable Isotopes ^{2}H and ^{18}O

The study of isotopes of water and solutes is useful in identifying the origin of groundwater. *Clayton et al.* (1966) first adopted the use of isotopic compositions to prove that the origin of groundwater in a set of sedimentary basins is predominantly of local meteoric origin. Reactions between water and minerals, dissolved species, associated gases, and other liquids with which they come into contact can modify the isotopic composition of water, especially the value of $\delta^{18}O$ (*Kharaka and Hanor*, 2005).

The stable isotopic composition of $\delta^{18}O$ versus $\delta^{2}H$ for all water samples are plotted with the Global Meteoric Water Line (GMWL) (Figure 3.3). The GMWL (defined by *Craig* (1961)) states the average hydrogen and oxygen isotope ratios in natural terrestrial waters. In Figure 3.3, the majority of waters are on the right side of the GMWL line, indicating the waters from the Cambrian to Devonian are enriched in $\delta^{18}O$. In addition, compared to the standard modern day seawater (VSMOW), a majority of $\delta^{18}O$ and $\delta^{2}H$ are in the negative range, means that the waters are depleted in ^{2}H and ^{18}O. Only a few

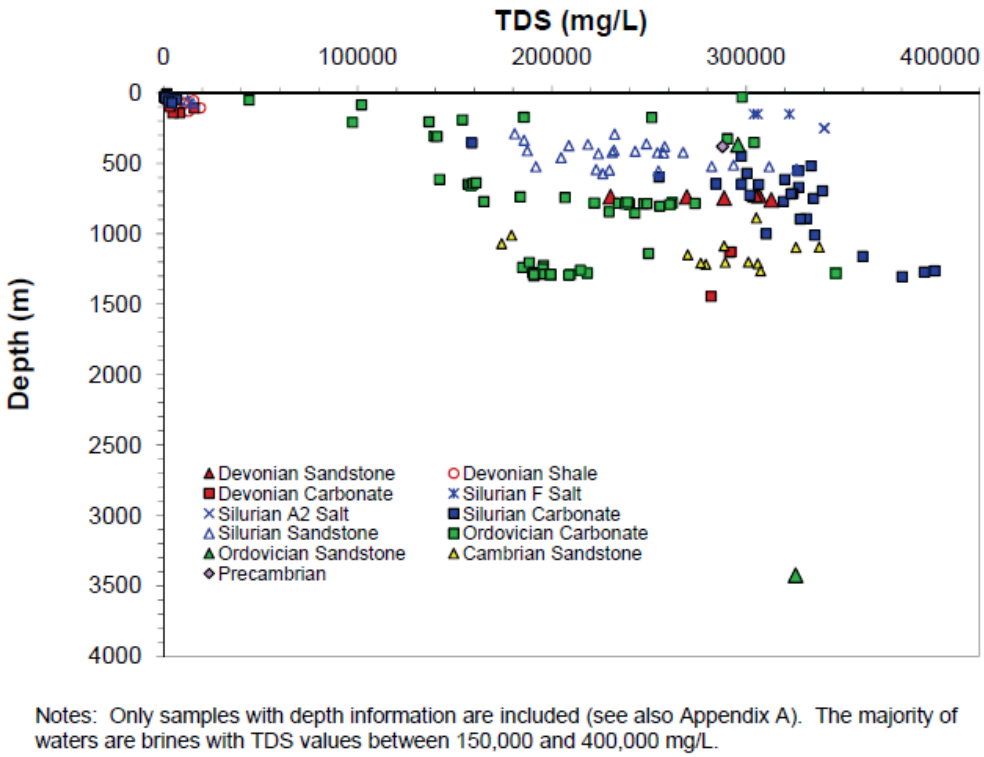

Figure 3.2: Total Dissolved Solids measured in formation waters from southwestern Ontario plotted as a function of sampling Depth. Adopted from *Hobbs et al.* (2011).

waters in Silurian and Devonian are enriched in ^{18}O. Possible processes controlling the oxygen and hydrogen isotopic compositions in these formations are the mixing with between various end members, seawater evaporation, hydrothermal activity, and water-rock interactions (*Hobbs et al.*, 2011).

3.2 DGR Site Data

A majority of the DGR site data is relevant to the 1-D modelling in this thesis. This section introduces and overviews the laboratory and DGR borehole data which has also been summarized in the Descriptive Geosphere Site Model (*INTERA*, 2011).

The DGR site stratigraphy is represented by the DGR-1 and the DGR-2 borehole data (Table 3.1). The actual thickness and depth of the geologic units listed in Table 3.1 are

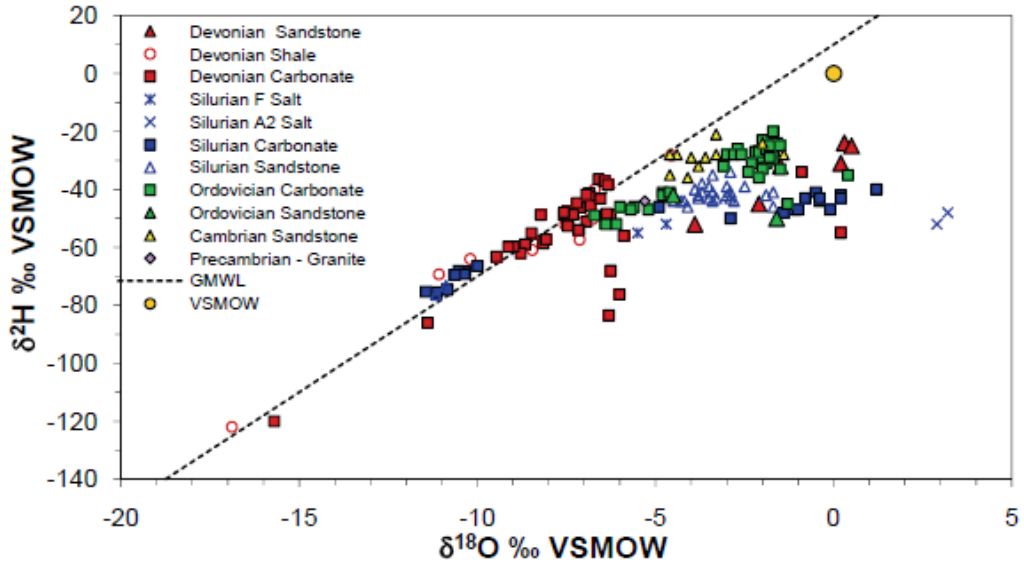

Note: The Global Meteoric Water Line (dashed line) and modern day seawater (VSMOW) are also shown.

Figure 3.3: Hydrogen versus oxygen isotopic signatures for all waters within the geochemical database. Adopted from *Hobbs et al.* (2011).

also adopted to construct the 1-D geologic domain for two-phase simulations presented in this thesis.

Chapter 2 briefly describes the composition of formation rocks and their evolution through the geologic periods. In the following section, details of the site-scale fluid saturation and concentration, pore water isotopic composition, measured pressure and groundwater parameters are summarized for the two-phase gas and water flow simulation.

3.2.1 TDS Concentration and Stable Isotopic Composition

Profiles of major ions and TDS concentration in the DGR boreholes are plotted in Figure 3.4 and Figure 3.5. The majority of the TDS concentrations from the Middle Silurian to Cambrian are more than 200 g/L with some data more than 300 g/L. The variation of TDS in intermediate and deep zones is relatively insignificant for general high salinity brine water.

The concentration of the major ions (Na, Ca, Mg and Cl) has significant variation between different DGR boreholes, and distribute sparsely with a distinct variation between

Table 3.1: Unit Thickness, Depth to Top of Formation and TDS Data for DGR-1 and DGR-2

Unit	Thickness [m]	Depth to Top [m]	TDS [g/L]
Drift	20.0	0	0.5
Lucas/Amherstburg	55.0	20.0	0.5
Bois Blanc	49.0	75.0	3.2
Bass Islands	45.3	124.0	6.0
Salina			
G Unit	9.3	169.3	14.8
F Unit	44.4	178.6	59.6
E Unit	20.0	223.0	124
D Unit	1.6	243.0	200
C Unit	15.7	244.6	249
B Unit	30.9	260.3	321
B Anhydrite	1.9	291.2	321
A-2 Carbonate	26.6	293.1	126
A-2 Evaporite	5.8	319.7	45.6
A-1 Carbonate	41.5	325.5	28.6 to 192
A-1 Evaporite	3.5	367.0	325
A-0 Unit	4.0	370.5	360
Guelph	4.1	374.5	370
Goat Island	18.8	378.6	300
Gasport	6.8	397.4	300
Lions Head	4.4	404.2	300
Fossil Hill	2.3	408.7	300
Cabot Head	23.8	411.0	306
Manitoulin	12.8	434.8	350
Queenston	70.3	447.6	310
Georgian Bay	90.9	518.0	308
Blue Mountain	42.7	608.9	295
Collingwood	7.9	651.6	225
Cobourg	28.6	659.5	272
Sherman Fall	28.0	688.1	270
Kirkfield	45.9	716.1	234
Coboconk	23.0	762.0	255
Gull River	53.6	785.0	203
Shadow Lake	5.2	838.6	200
Cambrian	16.9	843.8	235
Precambrian		860.7	300

adjacent formations and even within the same formation. Especially in the Middle Ordovician, the concentration exhibits a wide variation compared to the lower Cambrian formation. *Sykes et al.* (2011) hypothesized that the impact of diffusion in solute transport is diminished in the Ordovician shale and limestone, and the chemistry has weak spatial dependence.

The stable isotopic composition of $\delta^{18}O$ and δD ($\delta^{2}H$) is plotted versus depth in Figure 3.6 and Figure 3.7. The trend in Lower Silurian - Ordovician shows a gentle decrease

downward in both $\delta^{18}O$ and δD values. The $\delta^{18}O$ in the Ordovician shows depletion with depth from the Guelph Formation ($\delta^{18}O \sim$ -2.5‰) to the minimum value in the top of the Gull River Formation ($\delta^{18}O \sim$ -9‰). It increases to about -5‰ in the Cambrian (*INTERA*, 2011). δD is comparatively more variable but also decreases with depth in the Ordovician and increases in the Cambrian. Both show enrichment in the intermediate and deep zones compared to the shallow zone. The implication made by *INTERA* (2011) according to the lower stable isotopic composition in the Devonian and Upper Silurian sequence is a gradual mixing of fluids in the shallow zone with meteoric water. The more enriched Cambrian is separated from the overlying Ordovician indicating that cross-formational mixing and exchange may have occurred at the Cambrian (*INTERA*, 2011). The majority of the Ordovician has enriched stable isotopic compositions; this possibly implies that the impact of mixing is quite low compared to the shallow zone.

3.2.2 Measured DGR Borehole Pressures

Figure 3.8 plots the estimated environmental head, the hydrostatic freshwater pressure and density compensated hydrostatic pressure, and the measured formation pressure at the DGR-4 borehole. The estimated environmental head is converted from the formation pressure based on the measured or estimated water density at the same depth. The surface elevation is 181.6 mASL at the site. Comparing the environment head values with the hydrostatic head, it is obvious that the Cambrian and the Niagaran are slightly over-pressured and the Ordovician is significantly under-pressured. The hydraulic gradients imply there is a upflow from the Cambrian to the Ordovician, and downflow from the Niagaran to the Ordovician (*Sykes et al.*, 2011).

3.2.3 Fluid Saturations

DGR core petrophysical tests indicate the presence of a gas phase in the Silurian and Ordovician formations (Figure 3.9). The presence of gas phase significantly reduces the effective diffusivity, according to *Saripalli et al.* (2002) by one or two orders of magnitude. During the drilling of the DGR boreholes, hydrocarbons were encountered from the Devonian, Silurian and Ordovician formations (*INTERA*, 2011). Figure 3.10 shows the concentration of methane in the DGR cores. An obvious increase in methane con-

centration is observed from the Queenston to Cobourg Formation where it achieves its maximum (Figure 3.10).

Based on the solubility study for CH_4 of *Duan and Mao* (2006), *INTERA* (2011) indicated that the maximum solubility of methane is approximately 0.02 mol/kgw under the pressure and temperature conditions in the Ordovician rocks. *INTERA* (2011) thus suggested that gas phase methane could be present in the Salina A1 Unit and between the Georgian Bay Formation and Coboconk Formation.

Summarized by *Sykes et al.* (2011), the stable isotope data indicates that the methane in the Upper Ordovician shale is biogenic origin, and the methane in the Middle Ordovician limestone is thermogenic origin.

3.2.4 DGR Site Data for Two-Phase Flow Parameters

3.2.4.1 Hydraulic Conductivity

The horizontal hydraulic conductivities for the units at the the Bruce DGR are obtained from field testing of DGR and US boreholes. The vertical hydraulic conductivity (K_V) values can be calculated from the anisotropy ratios. The permeabilities (k_x, k_y are the horizontal permeabilities and k_z is the vertical permeability) for each formation are converted from the hydraulic conductivity with a liquid viscosity of 0.002 Pa·s and a groundwater density of 1,250 kg/m^3. The estimated representative values for hydrogeologic model are summarized by *INTERA* (2011) and listed in Table 3.2. Table 3.4 shows all the hydrogeologic parameters required for two-phase flow analyses, where the terms used to define the capillary pressure function and the relative permeability are described in equations 4.2 and 4.3. The horizontal hydraulic conductivity (K_H) values are geometric mean of the straddle-packer testing results (*INTERA*, 2011).

The anisotropy ratios for the units are also listed in Table 3.2. It was suggested by *INTERA* (2011) in the Descriptive Geosphere Site Model (DGSM), that most low permeability formations have a typical $K_H : K_V$ of 10:1 based on laboratory core testing. The permeable layers (Salina A1, Guelph, and Cambrian aquifers) are considered to be isotropy ($K_H : K_V$=1:1).

Table 3.2: Recommended estimates of hydraulic conductivities and anisotropy ratios of hydrogeological model layers

Model Layer	K_H (m/s)	$K_H : K_V$	Reference
Clay till overburden	8E-10	2:1	*NWMO* (2011), Table A1
Lucas	1E-06	10:1	*NWMO* (2011), Table A1
Amherstburg (upper 20m)	1E-06	10:1	*NWMO* (2011), Table A1
Amherstburg (lower 20m)	1E-07	10:1	*NWMO* (2011), Table A1
Bois Blanc	1E-07	10:1	*NWMO* (2011), Table A1
Bass Islands (upper 20m)	1E-04	10:1	*NWMO* (2011), Table A1
Bass Islands (lower 25m)	1E-05	10:1	*NWMO* (2011), Table A1
Salina G Unit	1E-11	10:1	*NWMO* (2011), Table A1
Salina F Unit	5E-14	10:1	*NWMO* (2011), Table A1
Salina E Unit	2E-13	10:1	*NWMO* (2011), Table A1
Salina D Unit	2E-13	10:1	*NWMO* (2011), Table A1
Salina C Unit	4E-13	10:1	*NWMO* (2011), Table A1
Salina B Unit - Carbonate	4E-13	10:1	*NWMO* (2011), Table A1
Salina B Unit - Evaporite	3E-13	10:1	*NWMO* (2011), Table A1
Salina A2 Unit - Carbonate	3E-10	10:1	*NWMO* (2011), Table A1
Salina A2 Unit - Evaporite	3E-13	10:1	*NWMO* (2011), Table A1
A1 Unit Upper Carb	2E-07	1:1	*NWMO* (2011), Table A1
A1 Unit Lower Carb	9E-12	10:1	*NWMO* (2011), Table A1
Salina A1 Unit - Evaporite	3E-13	10:1	*NWMO* (2011), Table A1
Salina A0 Unit	3E-13	10:1	*NWMO* (2011), Table A1
Guelph	3E-08	1:1	*NWMO* (2011), Table A1
Goat Island	2E-12	10:1	*NWMO* (2011), Table A1
Gasport	2E-12	10:1	*NWMO* (2011), Table A1
Lions Head	5E-12	10:1	*NWMO* (2011), Table A1
Fossil Hill	5E-12	10:1	*NWMO* (2011), Table A1
Cabot Head	9E-14	10:1	*NWMO* (2011), Table A1
Manitoulin	9E-14	10:1	*NWMO* (2011), Table A1
Queenston	2E-14	10:1	*NWMO* (2011), Table A1
Georgian Bay	3E-14	10:1	*NWMO* (2011), Table A1
Blue Mountain	5E-14	10:1	*NWMO* (2011), Table A1
Cobourg Collingwood Member	2E-14	10:1	*NWMO* (2011), Table A1
Cobourg - Lower	2E-14	10:1	*NWMO* (2011), Table A1
Sherman Fall	1E-14	10:1	*NWMO* (2011), Table A1
Kirkfield	8E-15	10:1	*NWMO* (2011), Table A1
Coboconk	4E-12	10-100:1	*NWMO* (2011), Table A1
Gull River	7E-13	10:1	*NWMO* (2011), Table A1
Shadow Lake	1E-09	10:1	*NWMO* (2011), Table A1
Cambrian	3E-06	1:1	*NWMO* (2011), Table A1
Upper Precambrian	1E-10	1:1	*NWMO* (2011), Table A1
Precambrian	1E-12	1:1	*NWMO* (2011), Table 4.17

The hydraulic conductivity values can be converted to permeability by assuming a fluid density of 1,250 kg/m^3 for brine and a dynamic viscosity of 0.002 Pa·s, which is suggested by *INTERA* (2011). Figure 3.11 illustrate the profile of horizontal hydraulic conductivity versus depth from the Guelph Formation to Precambrian, where the dashed lines indicate the interfaces of all geologic units.

As seen in Figure 3.11, the system hydraulic conductivity expresses distinctive heterogeneity and discontinuity. The K_H values for the Guelph Formation (3.0×10^{-8} m/s), the Shadow Lake Formation (1.0×10^{-9} m/s), and the Cambrian Formation (3.0×10^{-6}

m/s) are relatively high in the system, while other units reveal low K_h values about 3 to 8 orders of magnitude lower, between 10^{-15} m/s and 10^{-11} m/s.

However, the extremely low rock permeability of the Black River Group is not theoretically low enough to sustain the abnormal pressure for a long period. Lee and Deming (*Lee and Deming*, 2002) bring up a simplified formulation according to Bredehoeft and Hanshaw's case study of excess head throughout a sedimentary sequence (*Bredehoeft*, 1968). In their study of the over-pressures in the Anadarko Basin, they use this simple equation to calculate the approximate time for a hydraulic disturbance to diffuse through a layer of thickness:

$$t = z^2 \alpha \mu / 4k \tag{3.1}$$

where t is the time required for a hydraulic disturbance to diffuse [T]; z is the thickness of the layer [L]; k is the permeability of the media [L^2]; α is the pore compressibility of the media [LT^2/M]; and, μ is fluid viscosity [MT/L].

Thus, we can calculate the approximate permeability required for a 400 m thick low permeability media to preserve the high pressures for 3 Ma with a viscosity of 0.002 Pa·s and a compressibility of 10^{-9} Pa^{-1}. As a result, the permeability is 8×10^{-22} m^2 for 3 Ma, and for sealing for 200 Ma, an extreme low permeability of 1×10^{-23} m^2 is required. The low permeability Ordovician formation at Bruce site acts as a capable pressure seal for the underlying over-pressure in Cambrian sandstone.

3.2.4.2 Porosity and Rock Density

The Porosity and Rock Density for the descriptive hydrogeology units are listed in Table 3.3 and Table 3.4. These values are the arithmetic average for each layer, which is based on core laboratory testing results (*INTERA*, 2011; *Whitney and Lee*, 2009). A portion of these values are adopted in this thesis for the 1-D numerical modelling.

Table 3.3: Estimates of rock grain density and liquid porosity of hydrogeological model layers

Model Layer	Grain Density (g/cm^3)	Liquid Porosity (%)	Reference
Clay till overburden	-	20	*NWMO* (2011), Tables 4.18 & A2
Lucas	2.84	7.7	*NWMO* (2011), Tables 4.18 & A2
Amherstburg (upper 20m)	2.84	7.7	*NWMO* (2011), Tables 4.18 & A2
Amherstburg (lower 20m)	2.84	7.7	*NWMO* (2011), Tables 4.18 & A2
Bois Blanc	2.84	7.7	*NWMO* (2011), Tables 4.18 & A2
Bass Islands (upper 20 m)	2.84	5.6	*NWMO* (2011), Tables 4.18 & A2
Bass Islands (lower 25 m)	2.84	5.6	*NWMO* (2011), Tables 4.18 & A2
Salina G Unit	2.78	17.2	*NWMO* (2011), Tables 4.18 & A2
Salina F Unit	2.80	10.0	*NWMO* (2011), Tables 4.18 & A2
Salina E Unit	2.82	10.0	*NWMO* (2011), Tables 4.18 & A2
Salina D Unit	2.93	8.9	*NWMO* (2011), Tables 4.18 & A2
Salina C Unit	2.74	20.5	*NWMO* (2011), Tables 4.18 & A2
Salina B Unit - Carbonate	2.81	14.5	*NWMO* (2011), Tables 4.18 & A2
Salina B Unit - Evaporite	2.93	8.9	*NWMO* (2011), Tables 4.18 & A2
Salina A2 Unit - Carbonate	2.86	12.0	*NWMO* (2011), Tables 4.18 & A2
Salina A2 Unit - Evaporite	2.93	8.9	*NWMO* (2011), Tables 4.18 & A2
A1 Unit - Upper Carb	2.73	7.0	*NWMO* (2011), Tables 4.18 & A2
A1 Unit - Lower Carb	2.73	1.9	*NWMO* (2011), Tables 4.18 & A2
Salina A1 Unit - Evaporite	2.93	0.7	*NWMO* (2011), Tables 4.18 & A2
Salina A0 Unit	2.79	3.2	*NWMO* (2011), Tables 4.18 & A2
Guelph	2.81	5.7	*NWMO* (2011), Tables 4.18 & A2
Goat Island	2.73	2.0	*NWMO* (2011), Tables 4.18 & A2
Gasport	2.73	2.0	*NWMO* (2011), Tables 4.18 & A2
Lions Head	2.73	3.1	*NWMO* (2011), Tables 4.18 & A2
Fossil Hill	2.73	3.1	*NWMO* (2011), Tables 4.18 & A2
Cabot Head	2.79	11.6	*NWMO* (2011), Tables 4.18 & A2
Manitoulin	2.72	2.8	*NWMO* (2011), Tables 4.18 & A2
Queenston	2.77	7.3	*NWMO* (2011), Tables 4.18 & A2
Georgian Bay	2.76	7.1	*NWMO* (2011), Tables 4.18 & A2
Blue Mountain	2.77	7.8	*NWMO* (2011), Tables 4.18 & A2
Cobourg - Collingwood Member	2.70	1.2	*NWMO* (2011), Tables 4.18 & A2
Cobourg - Lower	2.71	1.5	*NWMO* (2011), Tables 4.18 & A2
Sherman Fall	2.72	1.6	*NWMO* (2011), Tables 4.18 & A2
Kirkfield	2.71	2.1	*NWMO* (2011), Tables 4.18 & A2
Coboconk	2.69	0.9	*NWMO* (2011), Tables 4.18 & A2
Gull River	2.73	2.2	*NWMO* (2011), Tables 4.18 & A2
Shadow Lake	2.76	9.7	*NWMO* (2011), Tables 4.18 & A2
Cambrian	2.70	7.1	*NWMO* (2011), Tables 4.18 & A2
Upper Precambrian	2.59	3.8	*NWMO* (2011), Tables 4.18 & A2
Precambrian	-	0.005	*NWMO* (2011), Table 4.17

3.2.4.3 Pore Fluid TDS

The TDS concentrations are greater than 300 g/L for the intermediate and deep zones. The fluid density for the intermediate and deep zones are represented by an average value of 1,250 kg/m^3 for DGR hydrogeologic model, which is suggested by *INTERA* (2011).

Table 3.4: Hydrogeologic properties for two-phase flow modelling

Formation	ID	Density	Porosity	Permeability			Capillary Pressure Curves				Relative Permeability Curves				
				k_x	k_y	k_z	λ	S_{lr}	S_{ls}	S_{gr}	λ	S_{lr}	$1/a$	P_{max}	S_{ls}
		$[kg/m^3]$	[/]	$[m^2]$	$[m^2]$	$[m^2]$	[/]	[/]	[/]	[/]	[/]	[/]	$[MPa]$	$[MPa]$	[/]
Guelph	GUELR	2810	0.057	4.89E-15	4.89E-15	4.89E-15	0.718	0.14	1.00	0.08	0.718	0.14	1.0E5	2.0E8	1.00
Goast Island	GOATR	2730	0.020	3.26E-19	3.26E-19	3.26E-20	0.718	0.14	1.00	0.08	0.718	0.14	2.1E7	2.0E8	1.00
Gasport	GASPR	2730	0.020	3.26E-19	3.26E-19	3.26E-20	0.718	0.14	1.00	0.08	0.718	0.14	2.1E7	2.0E8	1.00
Cabot Head	CABOR	2790	0.116	1.47E-20	1.47E-20	1.47E-21	0.718	0.14	1.00	0.08	0.718	0.14	3.2E7	2.0E8	1.00
Manitoulin	MANIR	2720	0.028	1.47E-20	1.47E-20	1.47E-21	0.718	0.14	1.00	0.08	0.718	0.14	3.2E7	2.0E8	1.00
Queenston	QUEER	2770	0.073	3.26E-21	3.26E-21	3.26E-22	0.718	0.14	1.00	0.08	0.718	0.14	3.2E7	2.0E8	1.00
Georgian Bay	GEORR	2760	0.071	4.89E-21	4.89E-21	4.89E-22	0.706	0.26	1.00	0.12	0.706	0.26	2.4E7	2.0E8	1.00
Blue Mountain	BLU1R	2770	0.078	8.16E-21	8.16E-21	8.16E-22	0.656	0.05	1.00	0.00	0.656	0.05	4.3E7	7.0E8	1.00
Cobourg - Collingwood	COBCR	2700	0.012	3.26E-21	3.26E-21	3.26E-22	0.626	0.00	1.00	0.13	0.626	0.00	4.0E7	6.0E8	1.00
Cobourg - Lower	COBLR	2710	0.015	3.26E-21	3.26E-21	3.26E-22	0.549	0.00	1.00	0.00	0.549	0.00	3.3E7	1.5E9	1.00
Sherman Fall	SHERR	2720	0.016	1.63E-21	1.63E-21	1.63E-22	0.626	0.00	1.00	0.14	0.626	0.00	2.1E7	3.0E8	1.00
Kirkfield	KIRKR	2710	0.021	1.31E-21	1.31E-21	1.31E-22	0.626	0.00	1.00	0.14	0.626	0.00	2.1E7	3.0E8	1.00
Coboconk	COBOR	2690	0.009	6.53E-19	6.53E-19	6.53E-22	0.626	0.00	1.00	0.14	0.626	0.00	2.1E7	3.0E8	1.00
Gull River	GULLR	2730	0.022	1.14E-19	1.14E-19	1.14E-22	0.547	0.020	1.00	0.00	0.547	0.020	3.4E5	6.0E7	1.00
Shadow Lake	SHADR	2760	0.097	1.63E-16	1.63E-16	1.63E-19	0.350	0.00	1.00	0.00	0.350	0.00	1.3E5	7.0E8	1.00
Cambrian	CAMBR	2700	0.071	4.89E-13	4.89E-13	4.89E-13	0.718	0.14	1.00	0.08	0.718	0.14	1.0E5	2.0E8	1.00
Precambrian	PRCAM	2700	0.005	1.63E-19	1.63E-19	1.63E-19	0.718	0.14	1.00	0.08	0.718	0.14	1.0E5	2.0E8	1.00
Fracture	FRACT	2760	0.071	4.89E-21	4.89E-21	4.89E-22	0.706	0.26	1.00	0.12	0.706	0.26	2.0E6	2.0E7	1.00

3.2.4.4 Relative Permeability and Capillary Pressure Function

The relative permeability is described in detail in section 4.3.4. The capillary pressure relation in two-phase flow as a function of saturation is considered to be van Genuchten like (see equation 4.14) and estimated through laboratory testing.

$$P_{cap} = -P_0([S^*]^{1/\lambda} - 1)^{1-\lambda} \tag{3.2}$$

where $S^* = (S_l - S_{lr}/(S_{ls} - S_{lr})$ and $-P_{max} \leq P_{cap} \leq 0$.

In the van Genuchten model for the capillary pressure, P_{cap} is the capillary pressure [M/LT^2]; P_0 is the air-entry pressure for the media [M/LT^2]; P_{max} is the maximum pressure allowed [M/LT^2]; S_l is the saturation of the liquid [/]; S_{lr} is the residual saturation of liquid [/]; S_{ls} is the irreducible water saturation [/]; and, λ is a parameter fitted for van Genuchten model [/].

According to Intera Laboratory Petrophysical Testing Report for DGR-2 Core (*Whitney and Lee*, 2009), twenty vertical preserved core samples were collected for petrophysical testing from the Queenston, Georgian Bay, Blue Mountain and Collingwood shales, from the Cobourg, Sherman Fall, Gull River argillaceous limestones, and from the Cambrian sandstone. The laboratory petrophysical test has determined the bulk density of DGR-2 cores, permeability and porosity on both "as received" and "clean and dry" cores. The "as received" samples were collected from the DGR-2 borehole and sent to the laboratory. The water, oil and remaining salt were then extracted from the "as received" sample and dried to produce the "clean and dry" samples. High pressure mercury injection analysis was performed on the "clean and dry" cores, and by fitting the van Genuchten curves to laboratory data for each core with proper optimization procedure, the parameters for capillary pressure- saturation relation were estimated for air-mercury condition. Derived from the approximate threshold mercury entry pressure, equivalent gas-brine threshold pressure and other pore fluid pairs are calculated for site modelling purpose. The resulting parameters for capillary pressure function are recorded in Intera Technical report TP-08-05 (*Calder*, 2009) and listed in Table 3.4.

The actual in-situ formation are saturated by multiple-phases (brine, oil and gas), thus "as received" results underestimate the intrinsic permeability of samples. The "clean

and dry" permeability is more representative of the intrinsic permeability and were used to characterize the rock properties. After capillary pressure curve parameters are estimated, the relative gas permeability curve was determined by fitting the van Genuchten curves to the "as received" measurement, and divided by the "clean and dry" gas permeability (*Calder*, 2009). This produces parameters for relative permeability function of Table 3.4.

The estimated van Genuchten curves for capillary pressure and relative permeability with respect to each unit are shown in Figure 3.12 and Figure 3.13. Some units share the same parameters, therefore they are represented by one common curve. The discontinuity discovered in the Georgian Bay Formation shares the identical curve with the adjacent formation, which is a high curve with a high entry pressure. The van Genuchten curves introduces air-entry pressure to account for the pressure needed to replace water. Because the capillary pressure gradient at and above the threshold saturation is extremely high, it is possible to see discontinuities in capillary pressure at the interfaces of two different media with different air-entry pressures.

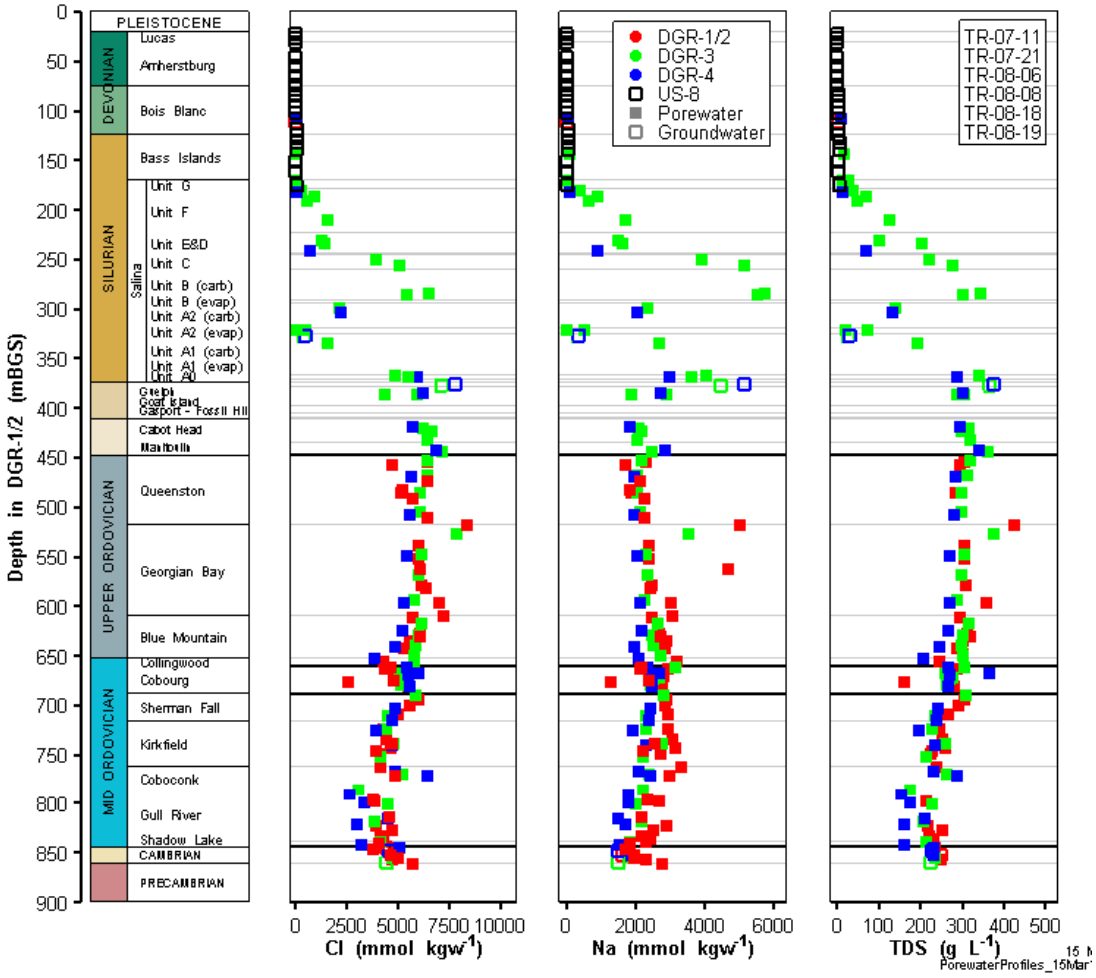

Figure 3.4: Profiles of Cl, Na and TDS concentrations from US-8 and DGR boreholes. Adopted from *INTERA* (2011).

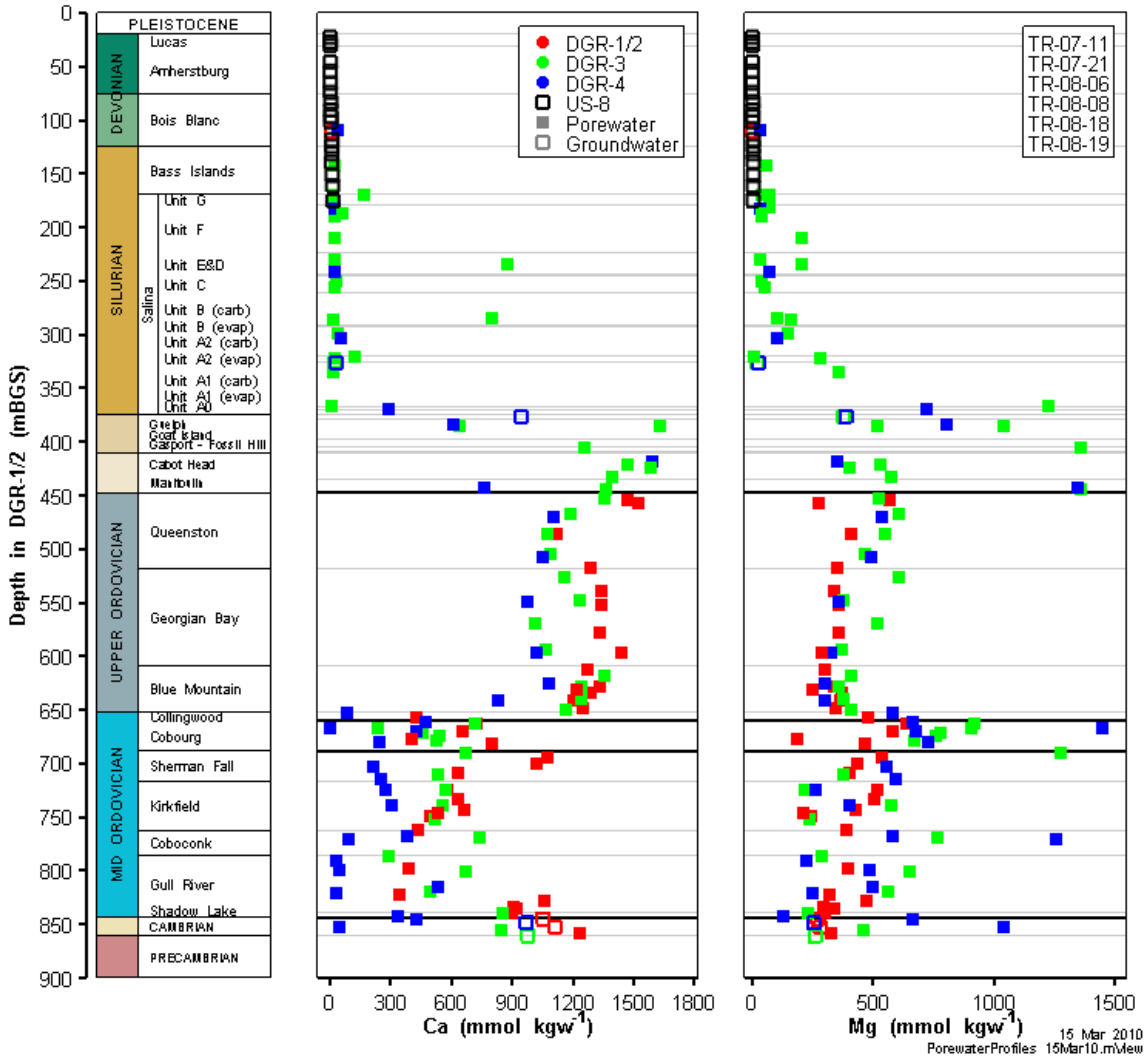

Figure 3.5: Profiles of Ca and Mg concentrations from US-8 and DGR boreholes. Adopted from *INTERA* (2011).

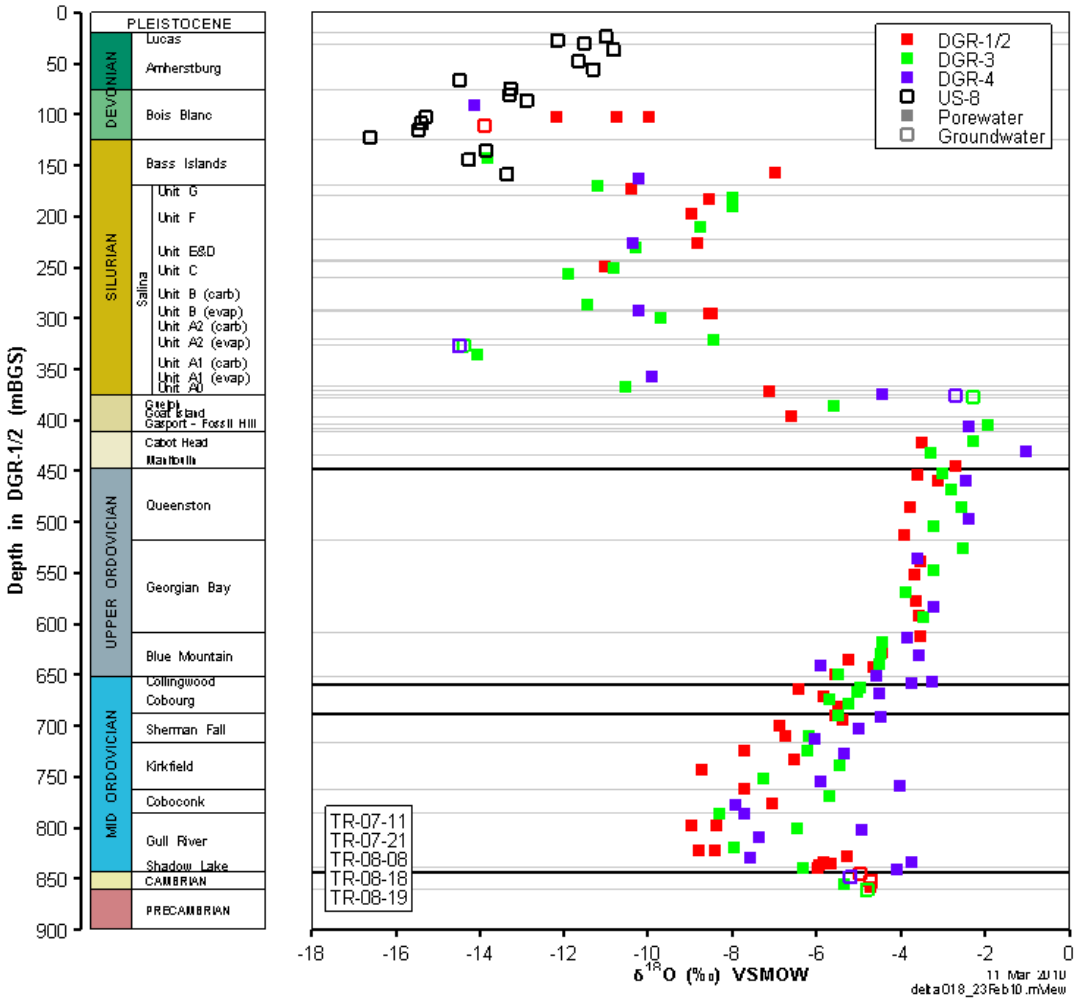

Figure 3.6: $\delta^{18}O$ profile for the DGR boreholes. Adopted from *INTERA* (2011).

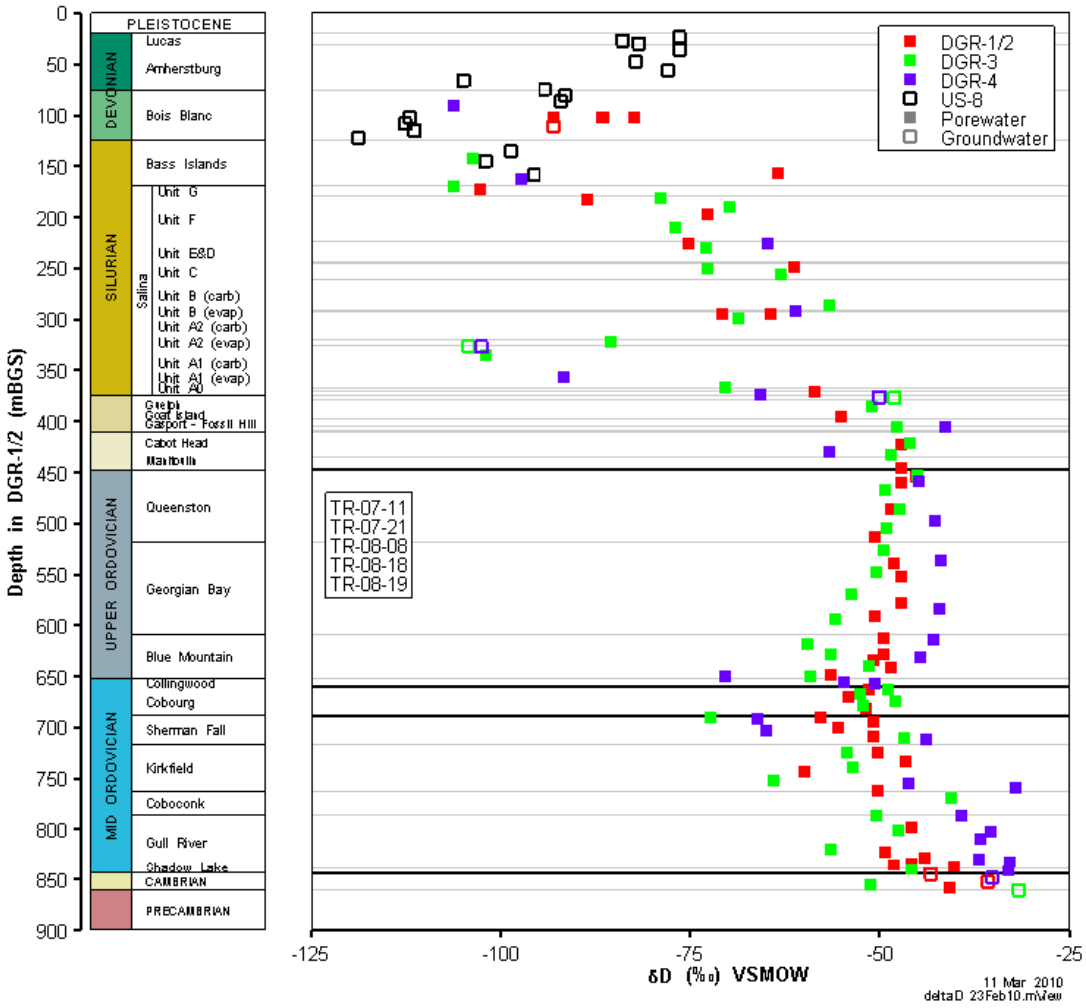

Figure 3.7: δD profile for the DGR boreholes. Adopted from *INTERA* (2011).

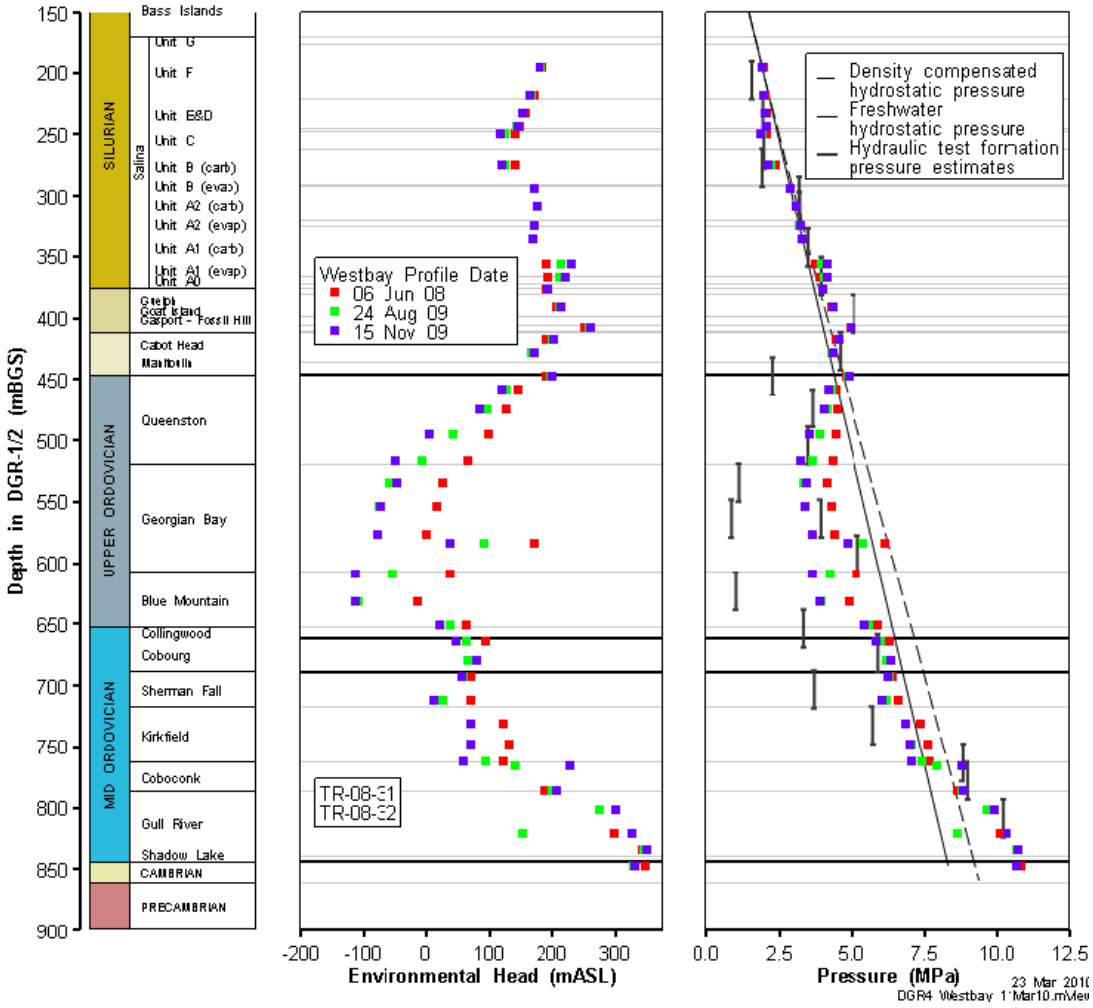

Figure 3.8: Measured Westbay Pressure and estimated head profile for the DGR-4 borehole. Adopted from *Sykes et al.* (2011).

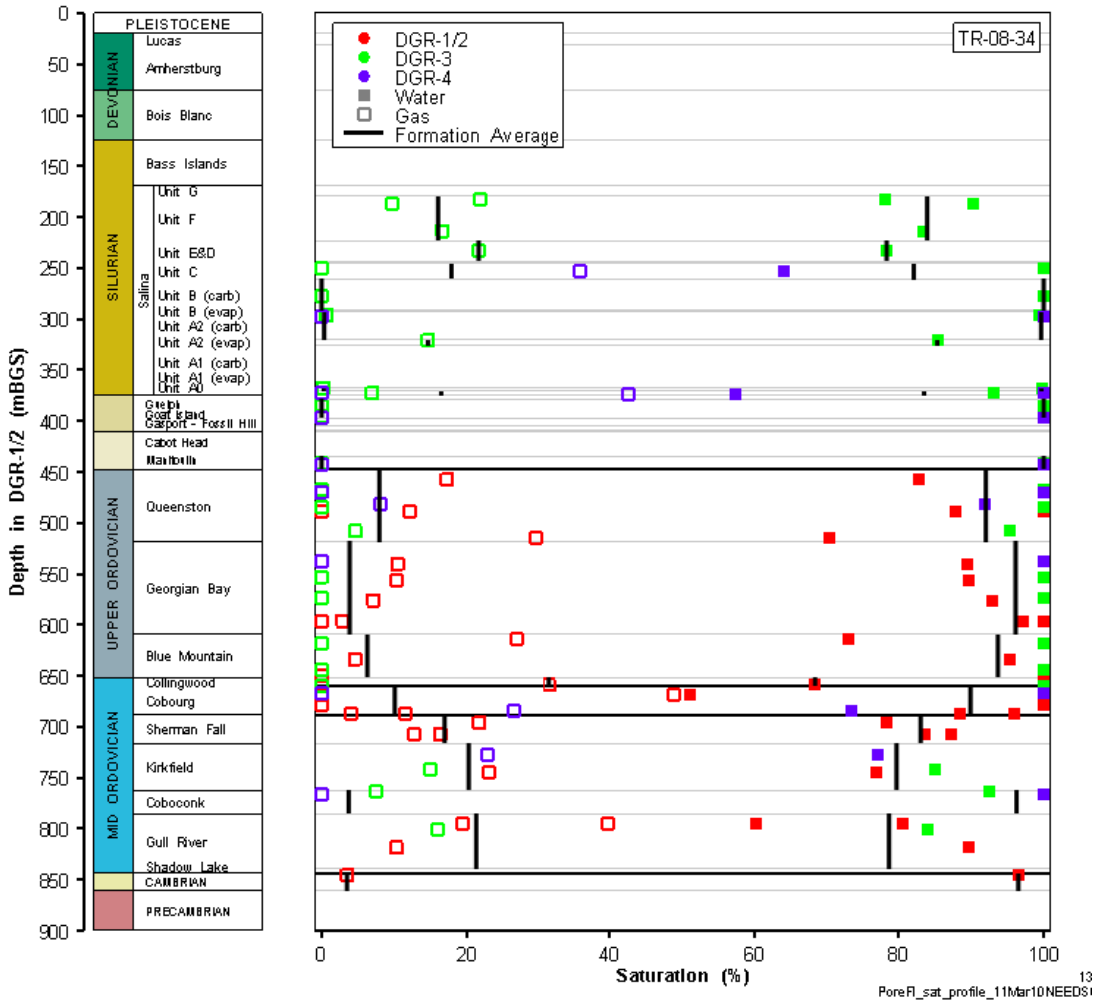

Figure 3.9: Pore fluid saturation profiles in confined DGR cores. Adopted from *INTERA* (2011).

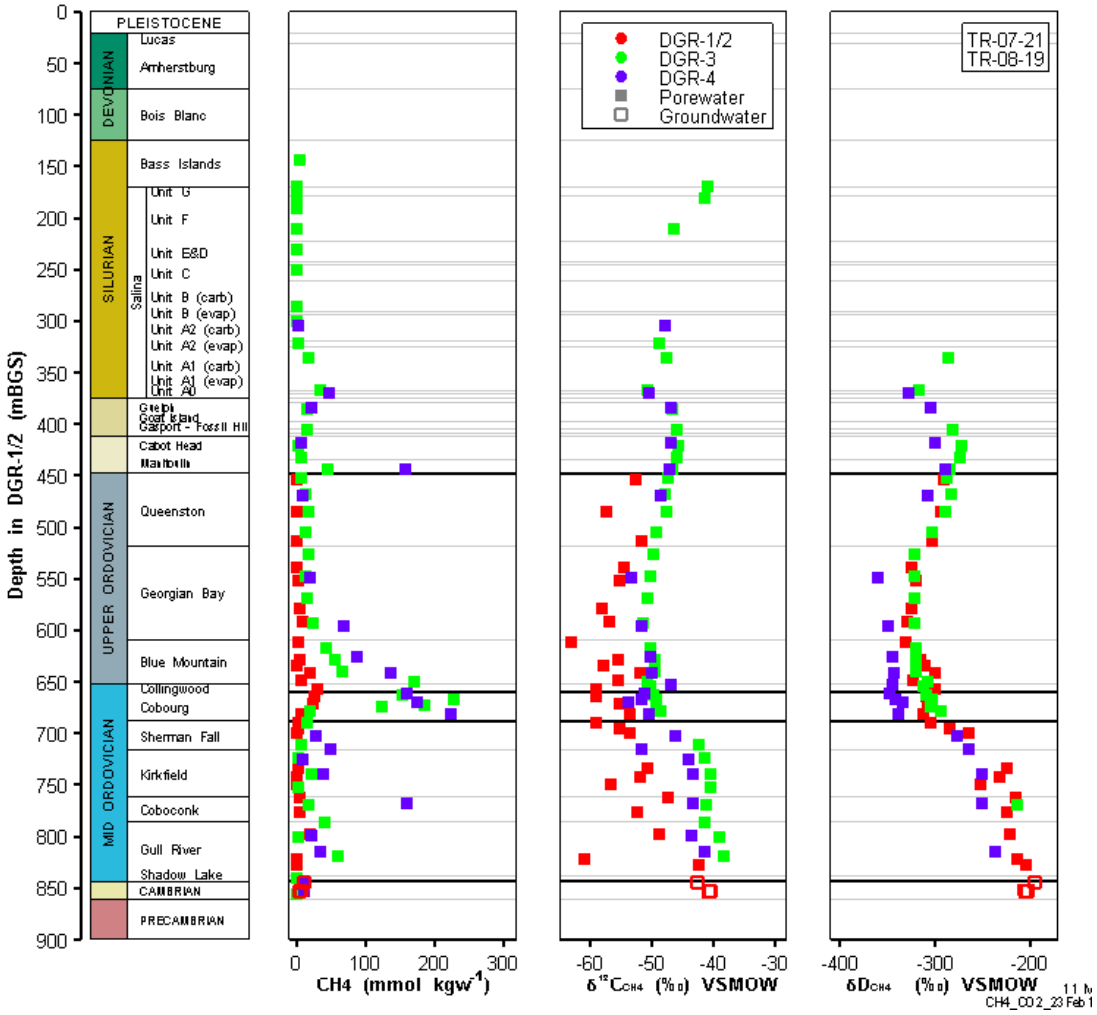

Figure 3.10: Profiles of CH_4 apparent porewater and groundwater concentrations and $\delta^{13}C$ and δD in CH_4 in DGR boreholes. Adopted from *INTERA* (2011).

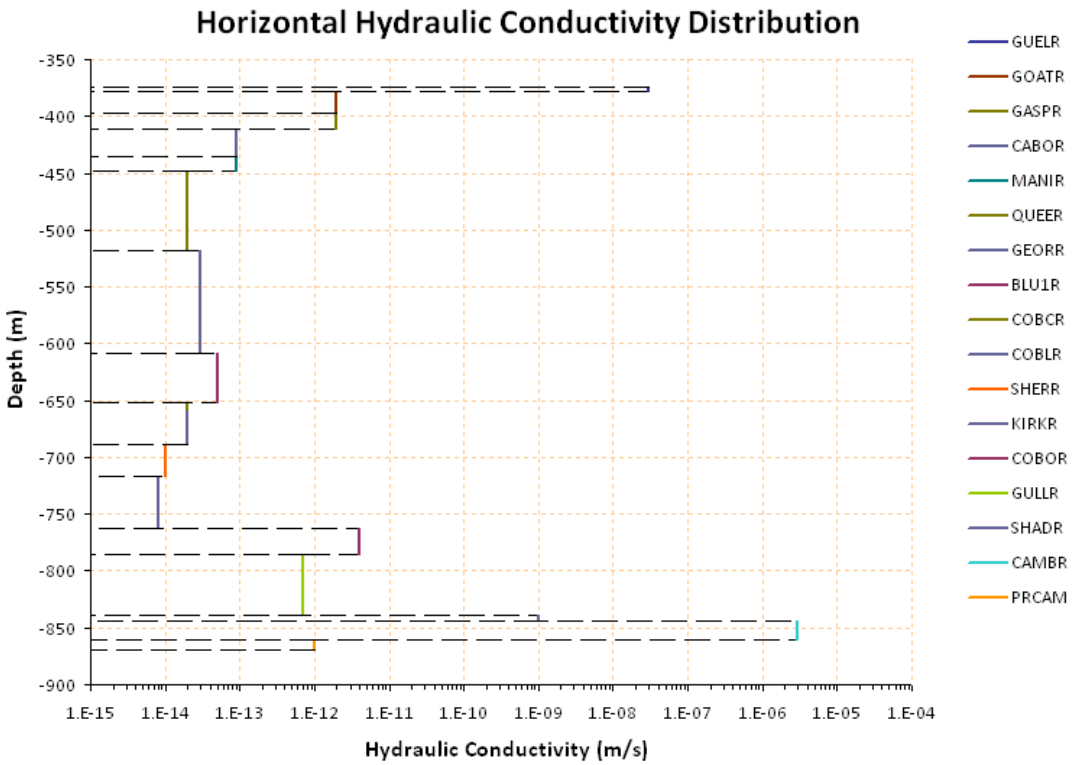

Figure 3.11: Profile of laboratory hydraulic conductivity for all units defined in the computational model.

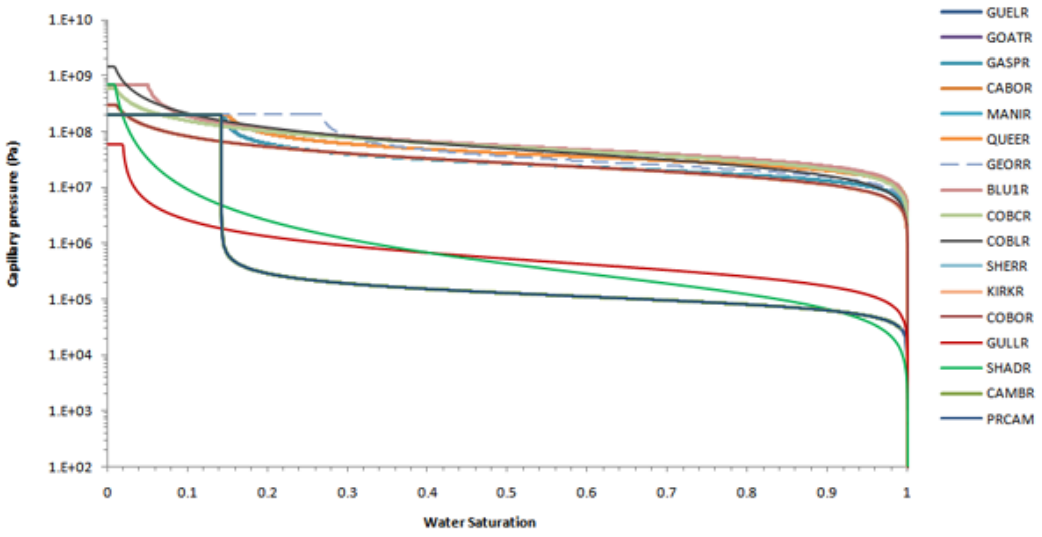

Figure 3.12: Capillary pressure curves using van Genuchten function versus water saturation for two-phase flow modelling.

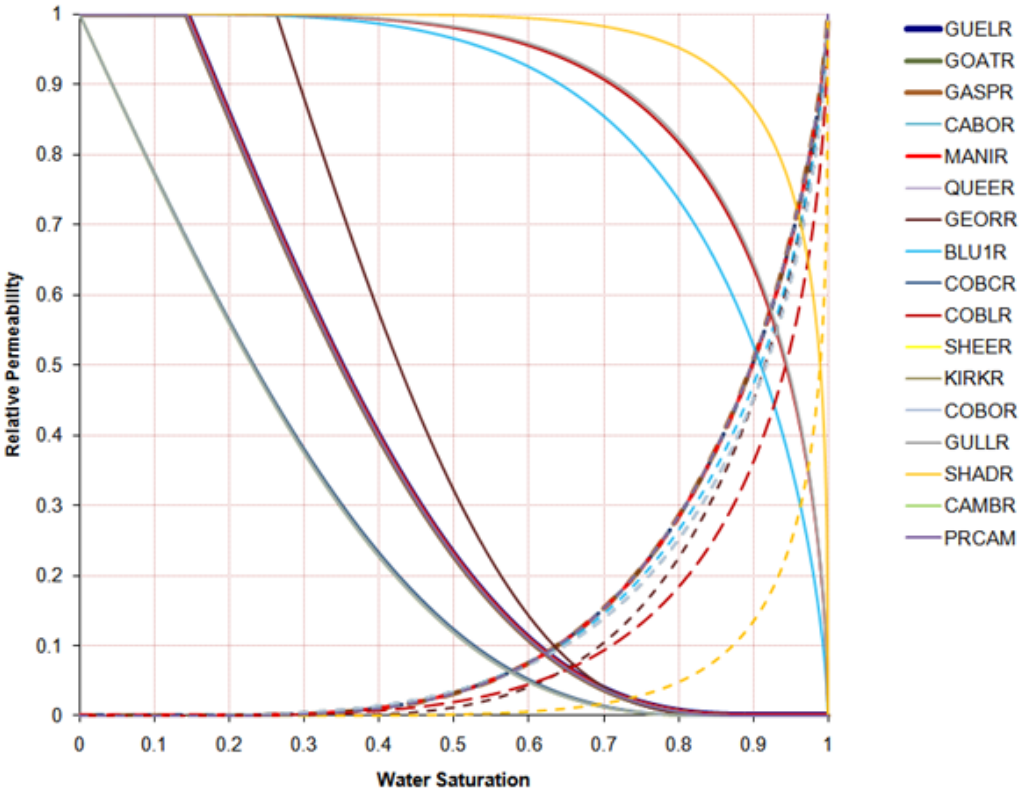

Figure 3.13: Relative permeability curves using van Genuchten function versus water saturation for two-phase flow modelling. The solid lines indicate the gas relative permeability, and the dashed lines indicate the liquid relative permeability.

Chapter 4

Two-Phase Flow Modelling

4.1 Study of Two-Phase Flow in Low Permeability Porous Media

Two-phase flow through low permeability media has been studied by several researchers, e.g., *Deming et al.* (2002); *Shosa and Cathles* (2001); *Duijn et al.* (1995); *Marschall et al.* (2005); *Hoteit and Firoozabadi* (2008). The flow pattern has been investigated at both the microscopic and macroscopic scale. Special attention was paid to the layered low permeability sedimentary basins, which are commonly pressure sealed.

Deming et al. (2002), based on former studies of static and dynamic concepts of groundwater movement in deep formations, developed a theory of self-sealing through gas generation in sedimentary basins. The purpose was to explain the over-pressuring in old sedimentary basins by the self-sealing theory, when the over-pressure situation cannot be explained by ongoing sedimentation and compaction disequilibrium.

They choose the Anadarko Basin in Oklahoma, U.S. as the study area, where extensive over-pressure was discovered at a depth of about 2 km or more. The over-pressuring was simulated by catagenic gas generation and maintained by a combination of vertical and horizontal gas capillary seals (*Deming et al.*, 2002). The over-pressure areas are most confined to distinct compartments considered as impervious media. They made two specific predictions in the conceptual model. The first is that anomalous pressures are

associated with the presence of gas; the second is that ambient fluid (or gas) pressures should undergo rapid changes across capillary barriers (*Deming et al.*, 2002). They consider the influence of gas capillary seals that act at the interface of a high permeability medium and low permeability medium, on fluid movement and saturation. Through their observation, a curious result was found that gas has preferentially invaded the sandy layers, while shales were water-saturated.

Two conceptual models illustrating two types of capillary barriers are suggested. One is that gas enters the media with saturated pore water, thus the sealing capacity is the capillary pressure of one gas-water interface. Another concept is the additive capillary seals. Consider that gas bubbles exist initially at the pore throat, therefore water flow through the system needs to exceed the sum of all individual capillary pressure at each interface. In their study, *Deming et al.* (2002) adopted the second concept for the Anadarko Basin.

These concepts provide important information in modelling two-phase flow in heterogeneous sediments. It suggests taking into account the related mechanism of capillary sealing, by adjusting model parameters to obtain a realistic simulation.

Duijn et al. (1995) examined the capillary effects through a heterogeneous porous medium. The heterogeneous condition is achieved by varying the absolute permeability and porosity spatially. They were interested in investigating the pressure discontinuity or continuity that occurred across the interfaces of discontinuous permeability and porosity. They noticed that the capillary pressure could be discontinuous if positive threshold pressures exist. This happens when the wetting phase saturation on the more permeable side (a medium with a coarse structure) is above the threshold saturation s^* (Figure 4.1), and that the capillary pressure on the other side (a medium with a fine structure) of the interface would be undefined, as the non-wetting phase is immobile.

They designed two specific problems with a single heterogeneity and provided analytical solutions to illustrate the behaviour of saturations and discontinuity of capillary pressure. In their cases, the capillary pressure was proved to be discontinuous in all conditions except for one circumstance. In the stationary convection diffusion problem, an interesting discovery was found that the non-wetting fluid was entrapped in the comparatively permeable medium, when positive threshold pressures were adopted.

Furthermore, a numerical algorithm was developed by *Duijn et al.* (1995) to understand the interaction of a free boundary with a heterogeneity. Similar cases were considered to

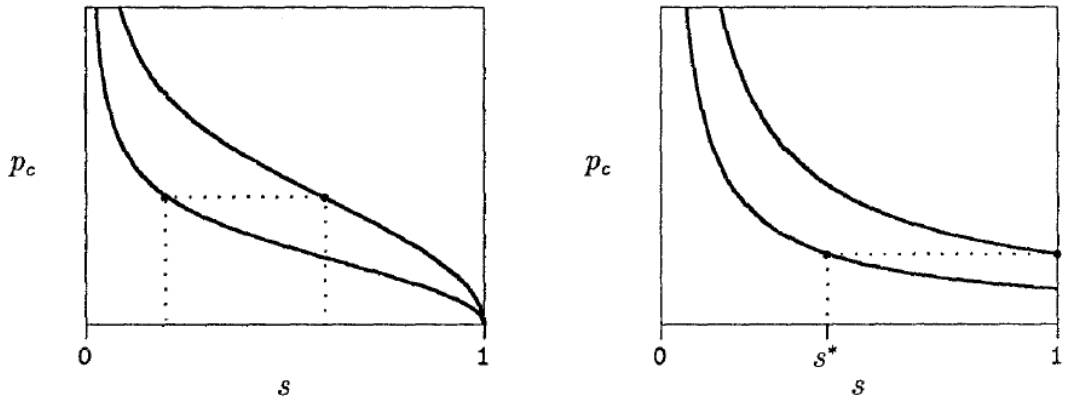

Figure 4.1: Capillary pressure p_c as a function of the reduced water saturation s. The upper curves correspond to a porous medium with a fine structure, the lower ones to a medium with a coarse structure. The threshold pressure at $s = 1$ is either zero (left) or positive (right).

provide comparative and extensive results based on the analytical studies. They examine the impact of threshold pressure of a defined saturated porous media on the movement of an oil-water front, that pore water was not replaced immediately but after a short time when enough oil saturations had been built up to move on. In the other example, an oil blob initially was present in a medium with periodic permeability. During a long-time of water flooding through the medium, considerable amounts of oil was trapped in the high permeability regions and become stationary in state. This conclusion corresponds to the analytical convection-diffusion case. The relation of parameters to the trapped oil saturation suggests practical options to decrease the amount of trapped oil, in the view of remediation.

Duijn et al. (1995) provide important evidence of the pressure and saturation distribution in heterogeneous media of a simple two-phase flow system.

Marschall et al. (2005), from both a microscopic view of pore structure and a macroscopic view of flow and transport mechanisms, studied the gas transport properties of the Opalinus Clay, which is considered as a potential host reservoir in Switzerland for radioactive waste, to understand the gas-liquid flow pattern through low permeability formations. Their study emphasized a careful understanding of the microstructure of the rock, as transport of non-wetting fluids in a low permeability formation is largely controlled by the rock structure and texture (*Marschall et al.*, 2005). According to the

phenomenological description of the Opalinus Clay by Nagra, *Marschall et al.* (2005) discussed the following subdivisions of the basic transport mechanisms:

- advective-diffusive transport of gas dissolved in the porewater;
- viscosity-capillary two-phase flow;
- dilatancy-controlled gas flow;
- gas transport along macroscopic tensile fractures.

They expect micro-fractures to form due to gas pressure increasing within argillaceous media with low tensile strength, when pressure is not exceeding the minimum principle effective stress. This is accompanied by an increase in permeability, thus the transport properties (rock permeability, relative permeability and capillary pressure relation) cannot be viewed as invariant (*Marschall et al.*, 2005). When gas pressure is rapidly built-up, macroscopic fractures develop, and gas flow in it can be seen as single-phase flow.

Three gas threshold pressure tests and two long-term gas injection tests were conducted to determine the gas transport properties in the Opalinus Clay. Evidence shows that when gas entry pressure is less than the minimum principle effective stress acting within the rock, classical flow concepts of immiscible displacement in porous media can be applied to such problems (*Marschall et al.*, 2005). In addition, dilatancy-controlled gas transport also impacts the two-phase flow in Opalinus Clay, due to the enhancement of permeability by micro-structuring, as long as the gas generation is slow and balanced by the porewater displacement. Meanwhile, tests show that high gas injection pressure could cause tensile fractures, but they are unrealistic in situ and excluded as a possible threat of waste disposal.

4.2 Popular Two-Phase Flow Models

Generally, to describe a two-phase flow system, the following processes should be considered:

1. Two-phase flow in porous media subject to relative permeability for all phases, capillary effects, and phase transfer effects.

2. Heat transport coupled with multiphase fluid transport.

3. Change of the thermodynamic and transport properties with system temperature and pressure.

All these behaviour have been studied and are reported in literature, and analytical models have been developed for single and coupled processes. A practical multiphase flow model requires the inclusion of all these physical and chemical processes with respect to space and time, which results in coupled governing equations and constraints. Many groundwater modelling efforts use finite-difference methods to discretize and solve the governing partial differential equations, and many of these models require a relatively fine-grid discretization to accurately represent the selected process in areas of interest where gradients vary rapidly in space (*Mehl and Hill*, 2002). For science and engineering study and application, matrices representing the equations for each grid need to be solved efficiently and simultaneously within limited memory and CPU resources.

Popular numerical groundwater models include SWIFT (GeoTrans), MODFLOW (USGS), FEFlow (Wasy Ltd.). These groundwater models are designed for saturated single-phase flow; only a few are developed for multicomponent multiphase flow in porous media. The creation of computer codes for modelling multiphase flows in industrial facilities is very complicated, time-consuming and expensive (*Kolev*, 2007). In the following section, codes that provide analysis of gas transport in porous media are introduced, including TOUGH, STOMP, NUFT.

TOUGH (Transport of Unsaturated Groundwater and Heat)

TOUGH Model has been developed for over 20 years, originated from the first released code by *Pruess et al.* (1999). TOUGH is a multidimensional numerical model designed for simulating multiphase flow in porous and fractured media. Coupled flow and transport governing equations are solved using the Integral Finite Difference Method (IFDM). A more comprehensive version TOUGH2-MP is adopted in this research and discussed in detail in the following section.

STOMP (Subsurface Transport Over Multiple Phases)

STOMP was developed by Mark White of Pacific Northwest Laboratory (*Nichols et al.*, 1997). The simulator's fundamental purpose is to produce numerical pre-

dictions of thermal and hydrogeologic flow and transport phenomena in variably saturated subsurface environments, which are contaminated with volatile or non-volatile organic compounds (*Nichols et al.*, 1997). The partial differential governing equations are solved by the Integrated Finite-Volume Method (IFVM).

NUFT (Nonisothermal Unsaturated-Saturated Flow and Transport model)

NUFT was designed by John Nitao of Lawrence Livermore National Laboratory (*Nitao*, 1996). For the purpose of monitoring subsurface contaminant transport, a suite of multiphase, multicomponent mass and energy transport models for numerical solution of non-isothermal flow and transport in porous media are combined into a single code. (*Nitao*, 1996). These modules are independent to each other and have their own specifications to fit various situations respectively. The NUFT model is based on the Finite-Volume Method (FVM).

In summary, these simulators are all capable of solving a combination of complex equations involving coupled fluid, heat, mass transport, and mass transfer. They also have similar physical, chemical, and thermal governing equations for defining the governing domain. Although they are built on similar bases, the methodology or assumptions used by each simulator differ. The resultant simulations generally have the same trends but with tiny deviations. The comparisons show a strong reliability of these computer models.

4.3 TOUGH2-MP Model

Several enhanced versions of the TOUGH model have been released to public to include more functional properties. The newest diversion of Tough series is iTOUGH2 (inverse TOUGH2), which is designed for model calibration in multi-phase flow system.

The TOUGH2-MP Model is a massive parallel version of the TOUGH2 code. It is professionally designed for multi-phase mass/heat flow in porous media and fractures. TOUGH2-MP is a more efficient version of TOUGH2, which can perform on multi-CPUs or platforms to improve its computational efficiency. Since its development, the parallel code has been successfully applied to large-scale simulations with up to several million grid blocks (*Zhang et al.*, 2008)

The functions of TOUGH2-MP model are accomplished by different modules called EOS (equation of state) modules. Each EOS module deals with a unique type of problem. Each problem should be simplified into a set of state variables and coupled boundary or initial conditions. For instance, the EOS3 module is designed for two-phase fluid/heat flow, in which case the flow system is represented by pure water and an ideal gas.

4.3.1 Model Overview

4.3.1.1 TOUGH2-MP Code Architecture

For solving complicated time-consuming problems, TOUGH2-MP adopted the domain decomposition method (DDM). The idea behind this approach is to divide the computational domain into a series of sub-domains (*Zhang et al.*, 2008). By solving the solutions simultaneously for sub-domains, an optimized global solution is sought. This allows the application of a parallel computation approach.

The numerical computational scheme is based on a fully implicit formulation with Newton iteration. For a typical simulation time step, three steps are conducted for each Newton iteration:

1. updating thermophysical parameters
2. assembling the Jacobian matrix
3. solving the linearized system of equations

The most important part of TOUGH2 code is its ability to distribute computational time for these three parts for parallel simulation, and incorporating parallel scheme in domain decomposition, grid element reordering, data input and output optimizing, and efficient message exchange between processors (*Zhang et al.*, 2008).

The TOUGH2-MP code adopted the same numerical scheme as the TOUGH2 code, which is based on the Integral Finite-Difference (IFD) method. The conservation equations in TOUGH2, involving mass of air, water and chemical components as well as heat, are discretized in space using the IFD method (*Zhang et al.*, 2008). Time is discretized using a first-order backward finite difference scheme. A Newton/Raphson iterative scheme is

used simultaneously to solve these discrete equations. The TOUGH2-MP model includes 12 modules, they are described in the TOUGH2 user manual (*Pruess et al.*, 1999). The descriptions are not reproduced in this thesis. Each module is designed for a specific circumstance reflecting a real problem, which is defined by input state variables. In this study, EOS3-module is adopted to solve the two-phase flow problem in a 1-D water-air system during a dynamic evolution over long period of time.

4.3.2 Multiphase Flow

Multiphase flow widely exists in all kinds of natural environment such as rain, snow, tornado, water and air circulation, and even in the human body. Moreover, it is a critical part in a variety of conventional and nuclear power plants, the chemical and biological industry, as well as oil and gas production. There are many complications that emerge when multiple components exist in multiple phases. These complications include unexpected non-linear effects that arise from the tortuosity on saturations, coupled advection, dispersion and diffusion over all phases, and pressure-dependent multiphase transfer (*Sorey et al.*, 1980). Additionally, for components that easily partition between gaseous and aqueous phases, diffusion of these components are turning out to be complex and Fick's law is becoming insufficient to describe the complications (*Pruess et al.*, 1999).

The simulation of the target formations in this study is modelled as two-phase air-water flow. The actual brines that occupying the pores have a density of approximately 1,250 kg/m^3, which is evenly dispersed between the Guelph Formation and the Precambrian basement. Thus, for simplification and as a first approximation, the brines are modelled as water with a constant density, and the gas is modelled as air. Consequently, we are only concerned about the two-phase flow of a wetting (water) and a non-wetting (air) flow in the deep geologic sediments.

4.3.3 Phase Transfer

Conventionally, the phases of a multiphase multicomponent system are gas phase, aqueous phase and non-aqueous phase (NAPLs). Within each phase, multicomponents can co-exist. In the conceptual model of this study, only two components (water and air) and two-phases (gas and liquid) are considered.

The gases typically included in most conceptual models are non-condensible gases such as air, CO_2, CH_4, H_2 and N_2. In a gas-aqueous mixed system, the solubility of the gas phase in the liquid is determined by the temperature and pressure of the environment, and varies with the property of the fluids themselves. Generally, when temperature increases, the dissolved gas would be released from the liquid; while with pressure increases, gas tends to dissipate more into the liquid. Solubility of a gas in a liquid is interpreted by Henry's law, equation 4.1 indicates that the solubility of a gas in a liquid is directly proportional to the partial pressure of the gas:

$$P_g = K_h x \tag{4.1}$$

where P_g is the partial pressure of the gas solute above the solution [M/LT^2]; K_h is Henry's law constant, which is depend on solute, solvent, and temperature [M/LT^2]; and, x is the fraction of the dissolved gas in the aqueous phase [/].

Henry's law has two parts in common practice, the first part states that the solubility of a gas in a liquid increases as pressure increases; the second part states that the solubility of a gas in a liquid decreases as temperature increases. Therefore, during the deposition period, generated non-condensible gases would partially dissolve into liquids, and go to equilibrium by dynamic flow; during the erosion and deglaciation, pressure was released and reduced, resulting in an increment in the gas content, which brings the equilibrium to a different state.

4.3.3.1 Water and Air

In a system composed of pure water and air, the constituent masses with respect to their phases are: liquid water, gaseous water (vapor), dissolved air, and gaseous air. The following processes are considered in modelling:

- Partition of components among the possible phases
- Flow of air and water in the geologic system
- Transport of soluble air accounting for advection, dispersion and diffusion.

All these processes have their corresponding mathematical descriptions and formulations that have been well documented in literature.

In addition, air is approximated as an ideal gas, and additivity is assumed for the air (P_a) and vapor (P_v) partial pressures in the gas phase, $P_g = P_a + P_v$ (*Zhang et al.*, 2008). Air solubility is affected by temperature, but the variations are not significant. Henry's constant for air dissolution in water differs slightly with respect to temperature, from 6.7×10^3 MPa at 20°C to 1.0 $\times10^4$ MPa at 60°C and reaches 1.1×10^4 MPa at 100°C (*Loomis*, 1928). Since the gas pressures explored in a deep geologic system are unlikely to reach an extremely high pressure (50 MPa), and air solubility is small, the variation of K_h values will not cause significant effects in a simulation. Therefore, a constant $K_h = 10^4$ MPa is adopted.

The assumed conceptual model is the most basic and simple case for two-phase flow. No chemical reactions occur and no intermediates are produced. As a preliminary inspection into the groundwater movement in this complicated geological system, we would like to simplified the process by representing the components as air and water.

4.3.4 Relative Permeability Functions

In a multi-phase flow system, mobility of a given phase is a function of the saturation of the phases as pores are occupied by multiple fluids with different saturations. The effective permeability or mobility of a phase is estimated using the relative permeability (k_r), which is considered dimensionless and generally expressed as a function of the degree of saturation. There are various functions available to describe the relation between fluid saturations and their relative permeabilities, with these being determined empirically from experimental data. Typical functions include: linear functions, Corey's curves (1954), Grant's curves, Fatt and Klikoff's function (1959), van Genuchten-Mualem model, function of Verma et al. (1985), and ECM function (1994). All these common functions of k_r are included in TOUGH2-MP model, for multiphase flow calculation.

The van Genuchten-Mualem model (*van Genuchten*, 1980) is chosen for this study. The basic form is:

$$k_{rl} = \begin{cases} \sqrt{S^*}\left\{1-(1-[S^*]^{\frac{1}{m}})^m\right\}^2 & \text{if } S_l < S_{ls}, \\ 1 & \text{if } S_l \geq S_{ls}. \end{cases} \tag{4.2}$$

where,

$S^* = (S_l - S_{lr})/(S_{ls} - S_{lr})$, and $m = 1 - 1/n$.

In this equation, S_l is the saturation of a liquid [/]; S_{ls} and S_{lr} indicate saturated and residual saturation of the given liquid, respectively [/]; S^* thus is the effective saturation of that liquid; and, m is notated as a parameter of van Genuchten's equation where n is often written as β [/].

Corey demonstrated a relation between oil and gas relative permeability according to numerous experimental observations of oil and gas flow through consolidated porous cores (*Corey*, 1954). Corey's function has been commonly used in geothermal studies, and in the study by *Sorey et al.* (1980), it is described in terms of water and steam. Incorporated in the TOUGH2-MP model, Corey's function is presented below (*Zhang et al.*, 2008):

$$k_{rg} = \begin{cases} 1 - k_{rl} & \text{if } S_{gr} = 0, \\ (1-\hat{S})^2(1-\hat{S}^2) & \text{if } S_{gr} > 0. \end{cases} \tag{4.3}$$

where,

$\hat{S} = (S_l - S_{lr})/(1 - S_{lr} - S_{gr})$ and subject to the restriction $0 \leq K_{rl}, k_{rg} \leq 1$.

In Corey's function, k_rl [/] is the relative permeability of liquid which is defined in the van Genuchten-Mualem model (see equation 4.2); and, S_{gr} is the residual gas saturation [/]. The other parameters presented in the Corey's function are identical to the parameters defined in the van Genuchten-Mualem mode (equation 4.2).

4.3.5 Mass Conservation

The basic form of mass balance equation adopted in the TOUGH2 model is defined by *Pruess* (1991a):

$$\frac{d}{dt}\int_{V_n} M^{(\kappa)} dV = \int_{\Gamma_n} \mathbf{F}^{(\kappa)} \cdot \mathbf{n} d\Gamma + \int_{V_n} q^{(\kappa)} dV \tag{4.4}$$

where κ denotes the mass components (water and air) [/]; V_n is an arbitrary sub-domain of the flow system [L^3]; $M^{(\kappa)}$ denotes the mass stored in the pores per unit volume for each component κ [M/L^3]; $\mathbf{F}^{(\kappa)}$ denotes the mass flux including advective flow and dispersive/diffusive flow through the bounding surface Γ_n [L/T]; $q^{(\kappa)}$ denotes the sources/sinks per unit volume generated within the sub-domain, with respect to each component [M/T]; and, $\mathbf{n}$ is a normal vector to the surface element $d\Gamma_n$ [/].

Thus, the mass accumulated in the sub-domain per unit time is the result of net mass flows into the arbitrary sub-domain per unit time, plus the unit mass/energy generated internally.

The left hand side of equation 4.4 is the mass accumulation term, in which $M^{(\kappa)}$ can be represented quantitatively by the physical properties of fluids (*Pruess*, 1991a):

$$M^{(\kappa)} = \phi \sum_{\beta=1}^{N} S_\beta \rho_\beta {X_\beta}^{(\kappa)} \tag{4.5}$$

where ϕ is the porosity of the porous media [/]; S_β is the saturation of phase β [/]; ρ is the mass density in phase β [M/L^3]; and, ${X_\beta}^{(\kappa)}$ is the mass fraction of component κ in phase β [/].

The mass flux term on the right hand side is a combination of advection, dispersion and diffusion over all phases in a multi-phase system.

4.3.5.1 Advective Mass Flux

Darcy's law is used to describe the advective mass flow through porous media. The formulation of Darcy's law for multi-phase version is extended from single phase flow simply by using it for each phase and replacing permeability by phase relative permeability. For an individual phase β, the Darcy flux is presented as:

$$\mathbf{F}_\beta = \rho_\beta \mathbf{u}_\beta = -k\frac{k_{r\beta}\rho_\beta}{\mu_\beta}(\nabla P_\beta - \rho_\beta \mathbf{g}) \tag{4.6}$$

where the flux is a vector, and $\mathbf{u}_\beta$ is the Darcy velocity (volume flux) in phase β [L/T]. Gravity is accounted for in a three-dimensional environment, as flow is not affected by vertical pressure gradient caused by gravity when assuming a hydrostatic condition. The gravitational pressure drop is excluded by subtracting it from the total pressure drop, which is the product of a gravitational acceleration vector in the vertical direction $\mathbf{g}$ [L/T^2], and the density of the fluid ρ_β [M/L^3]. k is the absolute permeability [L^2]. $k_{r\beta}$ is the relative permeability to phase β [/], which is formulated by van Genuchten's curve in this study (see section 4.3.4). μ_β is the viscosity of phase β [MT/L].

The advective mass flux should be accumulated over all phases for a component κ:

$$\mathbf{F}_{adv}^{(\kappa)} = \sum_\beta X_\beta^{(\kappa)} \mathbf{F}_\beta \tag{4.7}$$

Similarly, heat conservation can also be expressed using the heat accumulation term and heat flux term over all phases. However, we only consider isothermal multiphase mass flow in this study.

4.3.5.2 Dispersive and Diffusive Mass Flux

Darcy flow is accompanied by hydrodynamic dispersion, which also contributes to the mass transport in multiphase flow system.

In TOUGH2-MP, the dispersive mass flux for a component κ over all phases is expressed as follows (*Pruess et al.*, 1999):

$$\mathbf{F}_{dis}^{(\kappa)} = -\sum_\beta \rho_\beta \bar{\mathbf{D}}_\beta^{(\kappa)} \cdot \nabla X_\beta^{(\kappa)} \tag{4.8}$$

The hydrodynamic dispersion tensor ($\bar{\mathbf{D}}_\beta^{(\kappa)}$) is given by

$$\bar{\mathbf{D}}_{\beta}^{(\kappa)} = D_{\beta,T}^{(\kappa)}\bar{\mathbf{I}} + \frac{D_{\beta,L}^{(\kappa)} - D_{\beta,T}^{(\kappa)}}{u_{\beta}^{2}}\mathbf{u}_{\beta}\mathbf{u}_{\beta} \tag{4.9}$$

where,

$$\begin{aligned} D_{\beta,L}^{(\kappa)} &= \phi\tau_0\tau_{\beta}d_{\beta}^{(\kappa)} + \alpha_{\beta,L}u_{\beta}, \\ D_{\beta,T}^{(\kappa)} &= \phi\tau_0\tau_{\beta}d_{\beta}^{(\kappa)} + \alpha_{\beta,T}u_{\beta} \end{aligned} \tag{4.10}$$

are longitudinal and transverse dispersion coefficients [L^2/T]; $\mathbf{u}_{\beta}$ is the Darcy velocity (volume flux) in phase β [L/T]; $d_{\beta}^{(\kappa)}$ is the molecular diffusion coefficient for component κ in phase β [L^2/T]; $\tau_0\tau_{\beta}$ is the tortuosity term, where τ_0 is a porous medium dependent factor; and, τ_{β} is a coefficient depending on phase saturation ($\tau_{\beta} = \tau_{\beta}(S_{\beta})$) [/]. TOUGH2 adopts the *Millington and Quirk* (1961) model to describe the tortuosity-saturation relation:

$$\tau_0\tau_{\beta} = \phi^{1/3}S_{\beta}^{10/3} \tag{4.11}$$

In the equation 4.10, α_L and α_T are the longitudinal and transverse dispersivities [L]. Only special versions of TOUGH2 include the full hydrodynamic dispersion described in equation 4.9 and equation 4.10. The molecular diffusion is included in all versions, which is obtained by setting α_L and α_T to 0 in equation 4.9 and equation 4.10. This gives the diffusive flux term:

$$\mathbf{f}_{\beta}^{(\kappa)} = -\phi\tau_0\tau_{\beta}\rho_{\beta}d_{\beta}^{(\kappa)}\nabla X_{\beta}^{(\kappa)} \tag{4.12}$$

By applying Gauss divergence theorem to equation 4.4, the following PDE is obtained and used as the common form for finite difference approach:

$$\frac{\partial M^{(\kappa)}}{\partial t} = -div\mathbf{F}^{(\kappa)} + q^{(\kappa)} \tag{4.13}$$

4.3.6 Equation-of-State Modules

In TOUGH2, the properties and behaviour of fluid mixtures are described and provided by "equation-of-state" (EOS) modules. The EOS modules are used to assemble the mass/energy balance equations over components in all phases. Commonly encountered fluid component and phase mixtures are generalized into 12 EOS modules and implemented in TOUGH2 codes.

In this study, the EOS3 (water-air) module is adopted to set up the flow equations for numerical modelling, as gas and fluid are conceptualized to be air and water, respectively. According to the TOUGH2-MP manual (*Zhang et al.*, 2008), all water properties are represented by the steam table equations, and air is approximated as an ideal gas.

The primary variables for EOS3 is $(P_g, S_g + 10, T)$ for two-phase conditions, where P_g is the partial pressure of air, S_g is the saturation of air subject to a transformation of 10 to distinct the two-phase condition from the single-phase condition in the TOUGH2 code, and T is the temperature. The coupled partial pressure of water (P_w), is given by the relation between wetting and non-wetting fluids:

$$P_{non-wetting} = P_{wetting} + P_c \tag{4.14}$$

where P_c is the capillary pressure across the interface between air and water, which is determined by specified capillary function (van Genuchten in this study) for different saturation conditions during numerical iterations [M/LT^2].

The saturation of water S_w is obtained by subtracting S_g from 1.

Chapter 5

Analysis of Two-Phase Air and Water Flow in Low Permeability Rock

The two-phase air-water flow is simulated in a 1-D domain and performed using TOUGH2-MP with the EOS3 module. The object is to investigate the hypothesis that the existence of a gas phase in the Ordovician sediments at the Bruce site could result in the observed abnormal pressures. *Sykes et al.* (2011) have provided site-scale and regional-scale density-dependent flow analyses to support the hypothesis that the impact on transport of advection is negligible and transport is diffusion dominated in the Ordovician shale. They had included a 1-D simulation to evaluate the impact of a gas phase on the presence of abnormal pressures. In this thesis a 1-D model is developed based on the latest laboratory testing results and provides a sensitivity analysis of the impact of hydrogeologic parameters on the predicted pressure distribution in the Ordovician units.

All TOUGH2-MP runs were run on SHARCNET (Shared Hierarchical Academic Research Computing Network), which is a network that links colleges, universities and research institutes in southern Ontario on a "cluster of clusters" of high performance computers. Taking the advantage of running across multiple clusters on SHARCNET, runtimes are reduced from months to hours.

The following sections describe the conceptual model and results of this study.

5.1 Conceptual Model of Two-Phase Water-Air Flow

The 1-D model domain contains 17 formations and 1 discontinuity in the intermediate and deep zones, from the top of Niagarian Group (Guelph Formation, at a depth of 374.5 m) to the Precambrian basement (870 m). The depth and thickness information for the modelled units are identical to the units observed at the DGR boreholes (Table 3.1) as described by *INTERA* (2011). The units are subdivided and represented by a series of vertically layered gridblocks. Grid sizes were adopted from the study of *Sykes et al.* (2011). A thickness of approximately 0.5 m in height is defined for these blocks, resulting in 983 blocks for the whole domain. As suggested by *Sykes et al.* (2011), the discontinuity discovered at a depth of approximate 585 m in the Georgian Bay Formation is represented by a block with 0.5 m thickness (Figure 5.1).

The cross-section area of every two adjacent blocks is set to be 1 m^2. The grid blocks are in a Cartesian coordinate system. The input hydrogeologic parameters for the stratigraphic units are listed in Table 3.4. The rock grain density, porosity and hydraulic conductivity are from Table 3.2 and Table 3.3. The grain density for the Precambrian crystalline rock is assigned the same value as the Cambrian formation. The hydrogeologic parameters for two-phase air-water flow at the DGR site are summarized in section 3.2.4 and listed in Table 3.4. According to the study of *Sykes et al.* (2011), the discontinuity in the Georgian Bay Formation at a depth of 585 m in DGR-2 borehole was modelled using a capillary pressure curve that has the same parameters as the Georgian Bay Formation curve, but with a reduced air-entry pressure which gives a low capillary pressure curve that represents the loose permeable fracture feature. The suggested curve for the discontinuity is presented in Figure 5.2. The capillary pressure is expected to be continuous at the interfaces thus resultant water saturation could be discontinuous as the capillary pressure curves are in different levels.

Boundary condition and initial condition for the system are required for the TOUGH2 model to solve the partial differential equations. Therefore, reasonable boundary conditions and initial conditions are assumed for each TOUGH2 run as described in the following paragraphs.

A Dirichlet boundary condition of pressure is applied on the top and bottom of formation layers. This is implemented by assigning a large volume to the top and bottom grid blocks. The averaging volume of inner blocks is around 0.5 m^3, while the top and bottom blocks

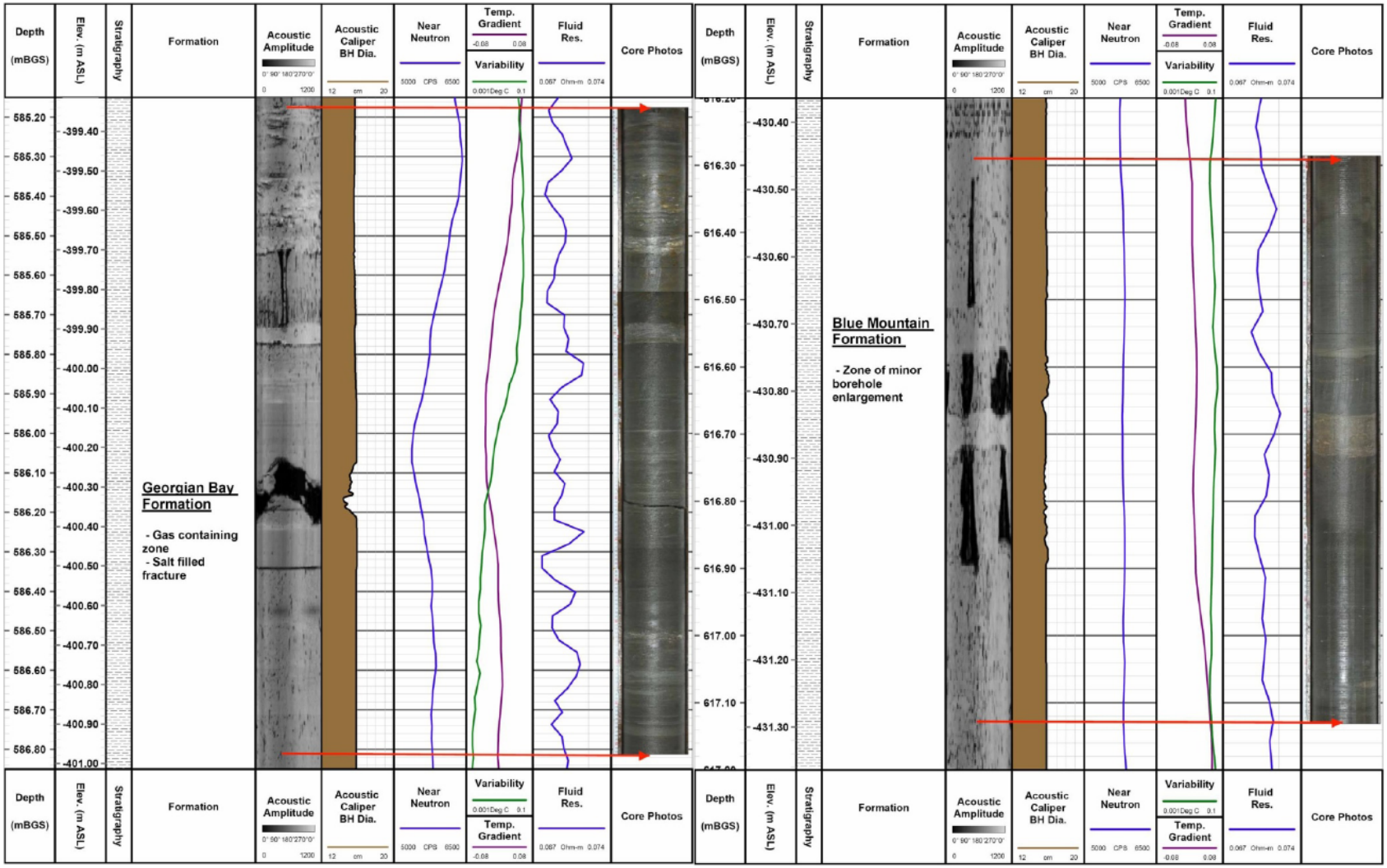

Note: From *INTERA* (2011).

Figure 5.1: ATV Logs, Selected Geophysical Logs and Core Photographs of Possible Gas-Containing Discontinuity (Left) in Georgian Bay Formation in DGR-2 and Zone of Minor Borehole Enlargement (Right) in Blue Mountain Formation in DGR-2

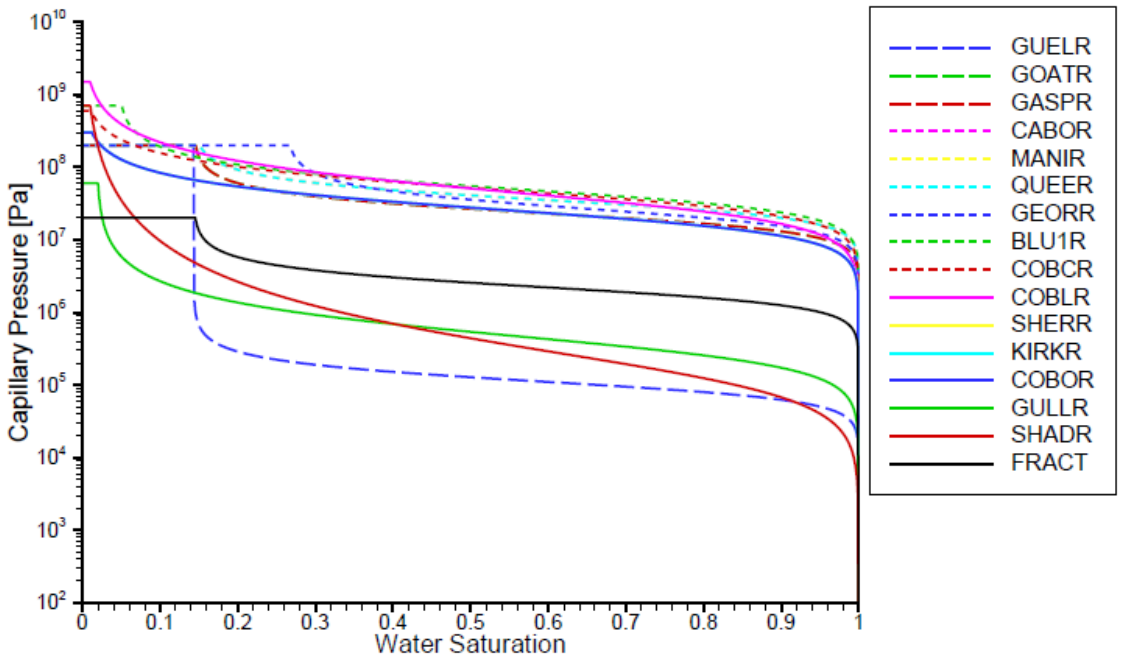

Figure 5.2: Capillary pressure curves for the two-phase flow analysis

are assigned a volume of 10^{20} m^3, so that the changes in conditions from fluid or heat exchange with the adjacent finite-size blocks within the flow domain can be ignored. The pressure for the Guelph Formation was set as 3.675 MPa while a pressure of 9.705 MPa was assigned to the Precambrian. These pressures were varied in the sensitivity analyses.

The initial condition for primary variables in TOUGH2-MP is specified for each grid block. For two-phase flow initialization, the primary variables (P, S, T) in EOS3 should be specified with reasonable values to identify a hypothetical beginning state of the flow system. Temperature T = 20°C is fixed for the isothermal assumption.

5.2 Two-Phase Flow with Air Generated in Ordovician

The initial gas saturations for all formations are zero; however, a gas generation term is added as a source term in the TOUGH2-MP GENER file. The air generator was implanted into the grid blocks between the Ordovician Queenston and Kirkfield formations,

so that air was generated with a low but uniform rate for a long time period, and then stopped at a specified time to see the further transport and distribution of gas phase in these heterogeneous sediments. The gas generation rate was initially assumed to be uniformly generated for 200 ka from the Coboconk to the Queenston inclusive (*Sykes et al.*, 2011). The total gas generation is assumed to be 98% of the air that would be contained in a volume of rock with gas saturation of 5%. An increased generation rate is evaluated in the following sections to see its sensitivity with respect to the under-pressure. Three types of boundary conditions are investigated showing very little impact for long-time simulations. The initial gas saturations are specified to be zero for all cases, thus the initial capillary pressure for all units is zero. As a result, the input initial gas pressure equals to the initial water pressure for all three cases as described in the following sections.

All the simulations were submitted and running on SHARCNET clusters, which allows users to utilize multiple clusters to solve their problems more efficiently. The CPU time is approximate 3 hours for a single run with 32 CPUs assigned to the simulation. If the simulation is running on 4 CPUs, it will take at least 24 hours to yield the final results. The actual time used in a single run is longer than CPU time, because the submitted job is listed in the queue according to the user's priority.

5.2.1 Hydrostatic Boundary Condition

The initial water pressure and water head are shown in Figure 5.3. Also shown in the plot of water head versus depth are the estimated freshwater heads based on the measured pressures in DGR-4 borehole. An assumed hydrostatic condition for all units from the Guelph Formation to the Precambrian formation was used for the base case analysis. Air is generated within the Ordovician formation and starts to replace the initially saturated water by exceeding the air-entry pressure. The water migrates due to the hydraulic gradient. Air is also partially dissolved into the aqueous phase and migrates within the domain by diffusion. The water pressure continuously decreases when air is generated and transported within the formations. Figure 5.4 shows the water pressure, water head, gas pressure, and capillary pressure simulated at 50 ka. The water pressures in the Ordovician formations are significantly under-pressured.

Figure 5.5 present the corresponding saturations at 50 ka. The gas saturation is highest at the discontinuity and capillary pressure is discontinuous at the discontinuity with relative

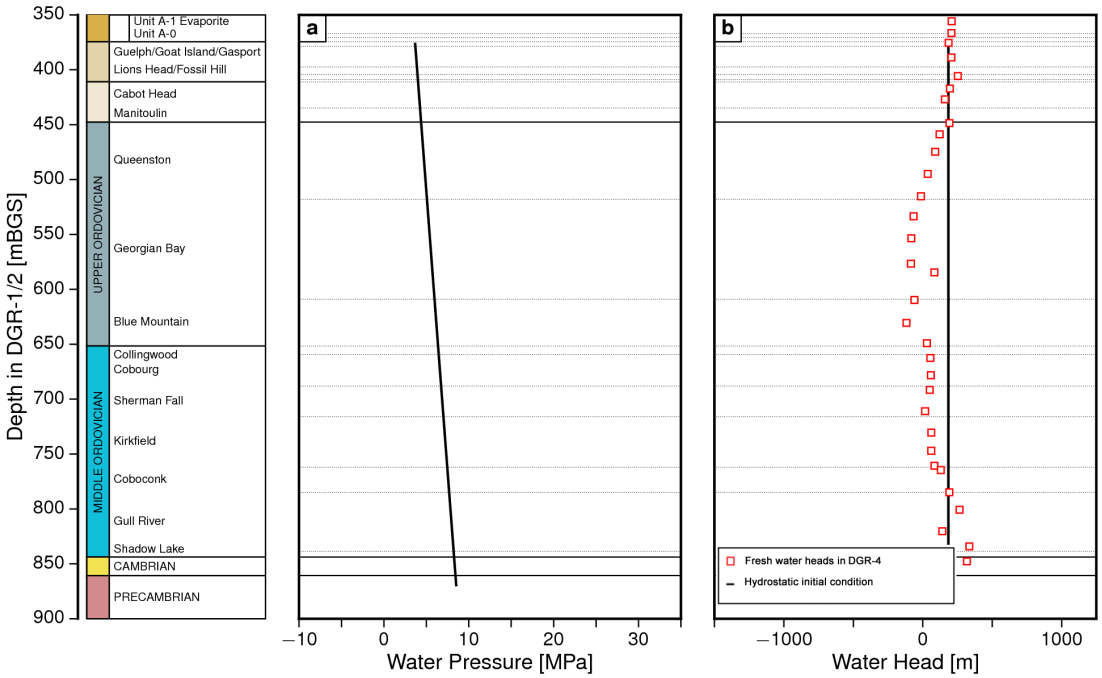

Figure 5.3: Hydrostatic initial conditions for the two-phase flow analysis. The estimated freshwater heads based on the measured pressures in DGR-4 borehole are shown the right figure.

higher value compared to the adjacent formations. The gas generation is continued after 50 ka and is not terminated until 200 ka, thus the amount of gas is still increasing after the presence of under-pressure and the level of under-pressure grows. After 200 ka, gas generation stops, the deficit water pressure tends to return to hydrostatic, with the gas partitioning into the water. Figure 5.6 shows the water pressure, water head, gas pressure, and capillary pressure simulated at approximately 1 Ma.

The gas and water saturation at 1 Ma are shown in Figure 5.7. The results of a longer period at 4 Ma are shown in Figure 5.8 and Figure 5.9. It is obvious in these figures that the water pressure is returning to the hydrostatic condition after the termination of air generation. The collection of air in the discontinuity at a depth of 585 m is evident with the highest gas saturation at that level.

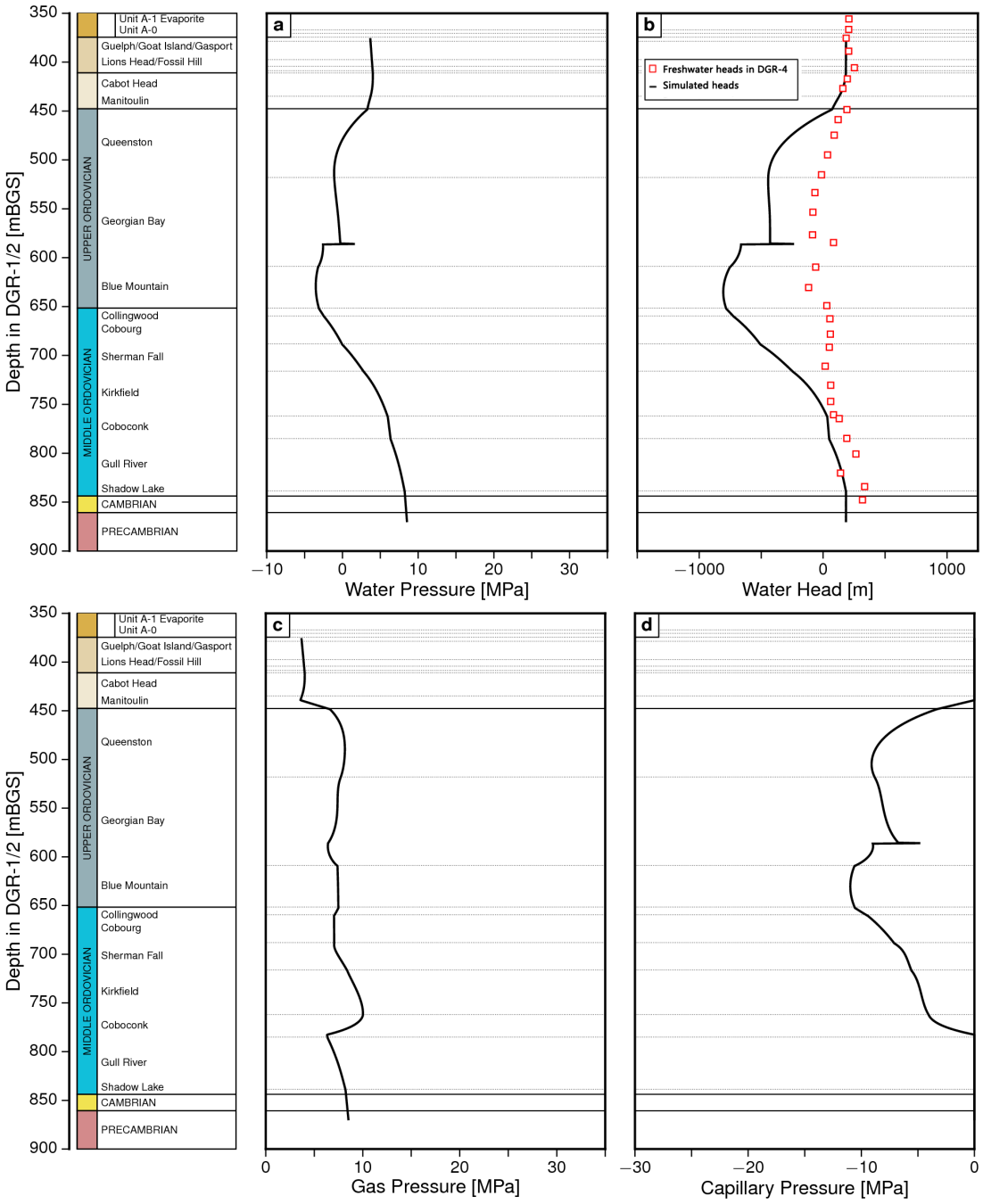

Figure 5.4: Two-phase gas-water flow analysis at 50 ka with air generation and hydrostatic initial condition.

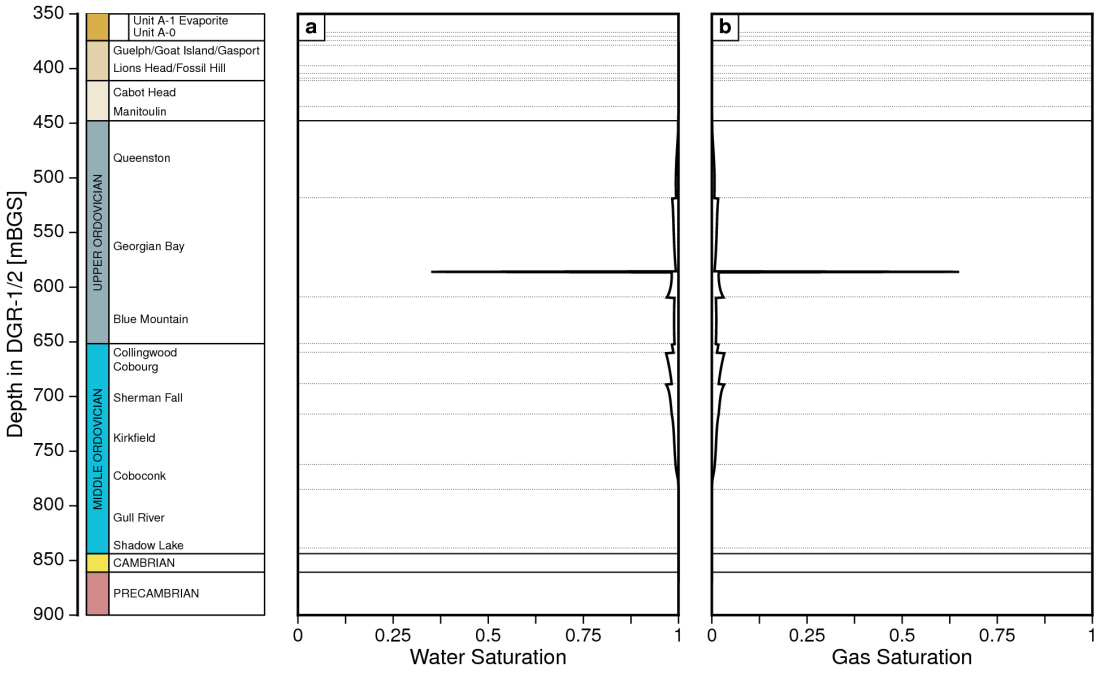

Figure 5.5: Saturations of two-phase water-gas flow at 50 ka with air generation and hydrostatic initial condition.

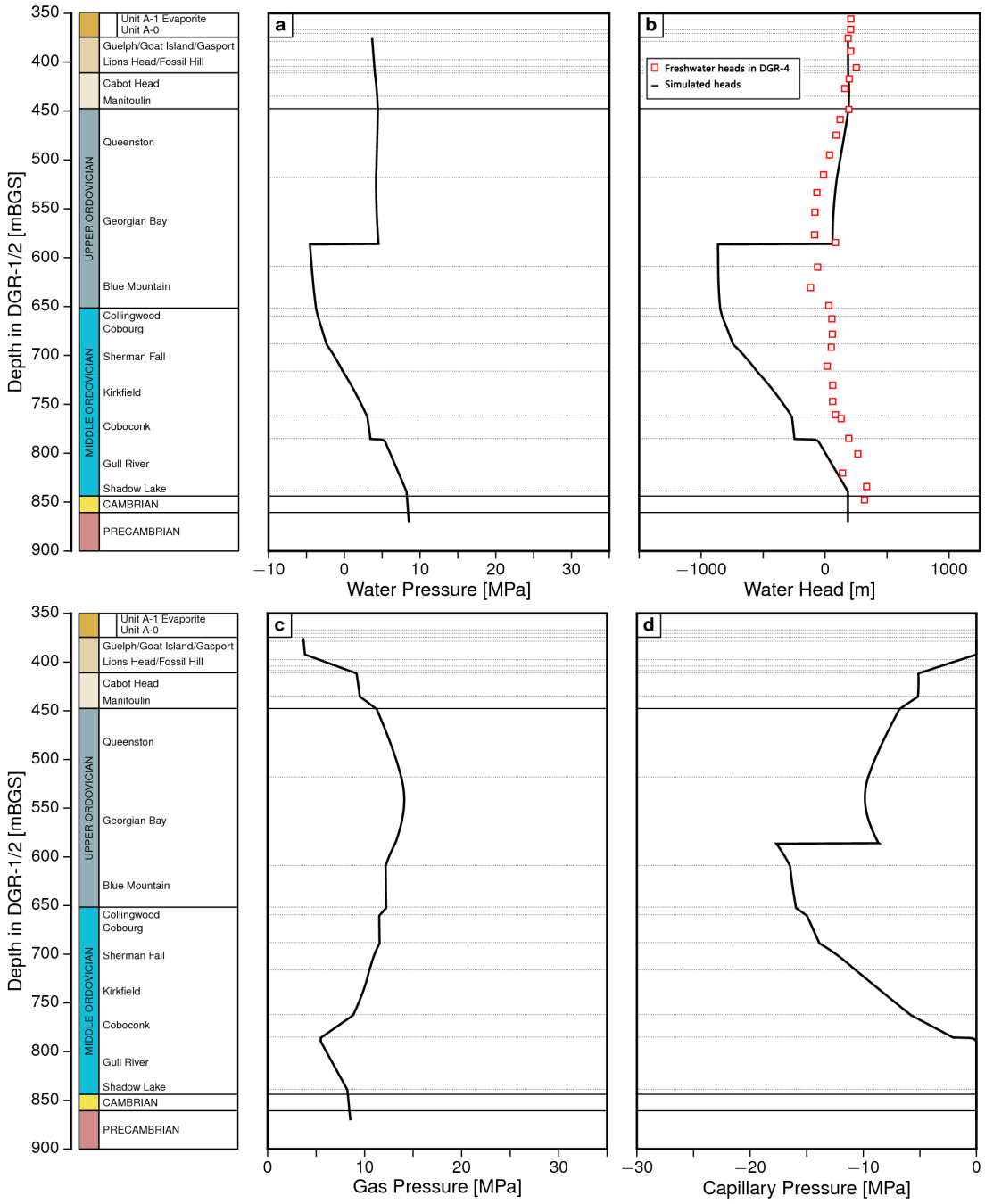

Figure 5.6: Two-phase gas-water flow analysis at 1 Ma with air generation and hydrostatic initial condition.

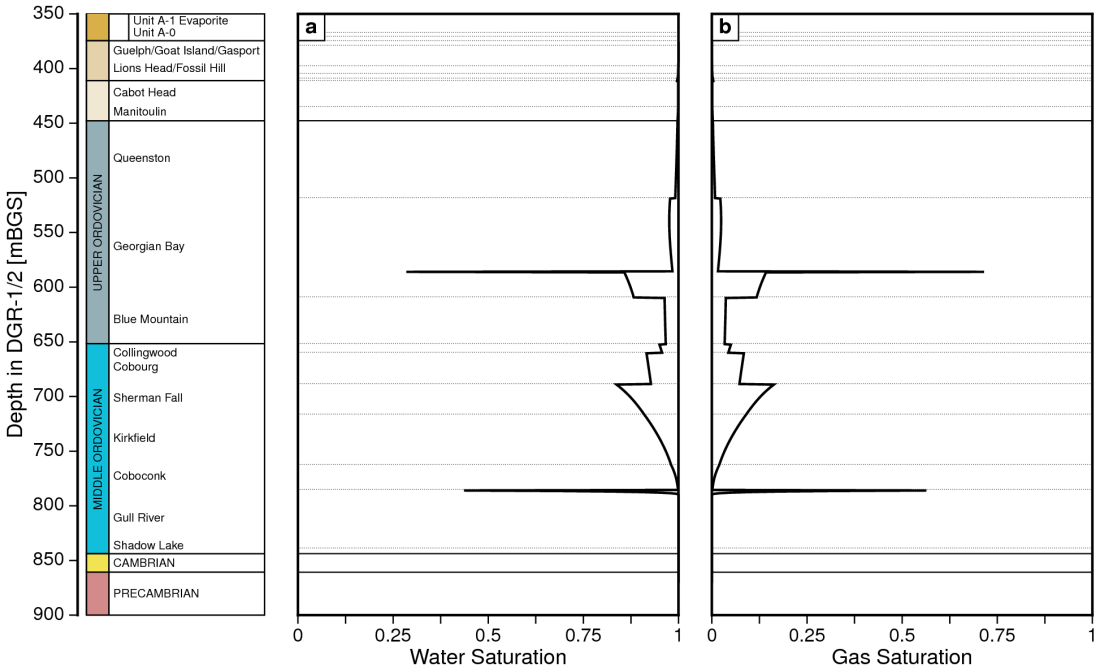

Figure 5.7: Saturations of two-phase water-gas flow at 1 Ma with air generation and hydrostatic initial condition.

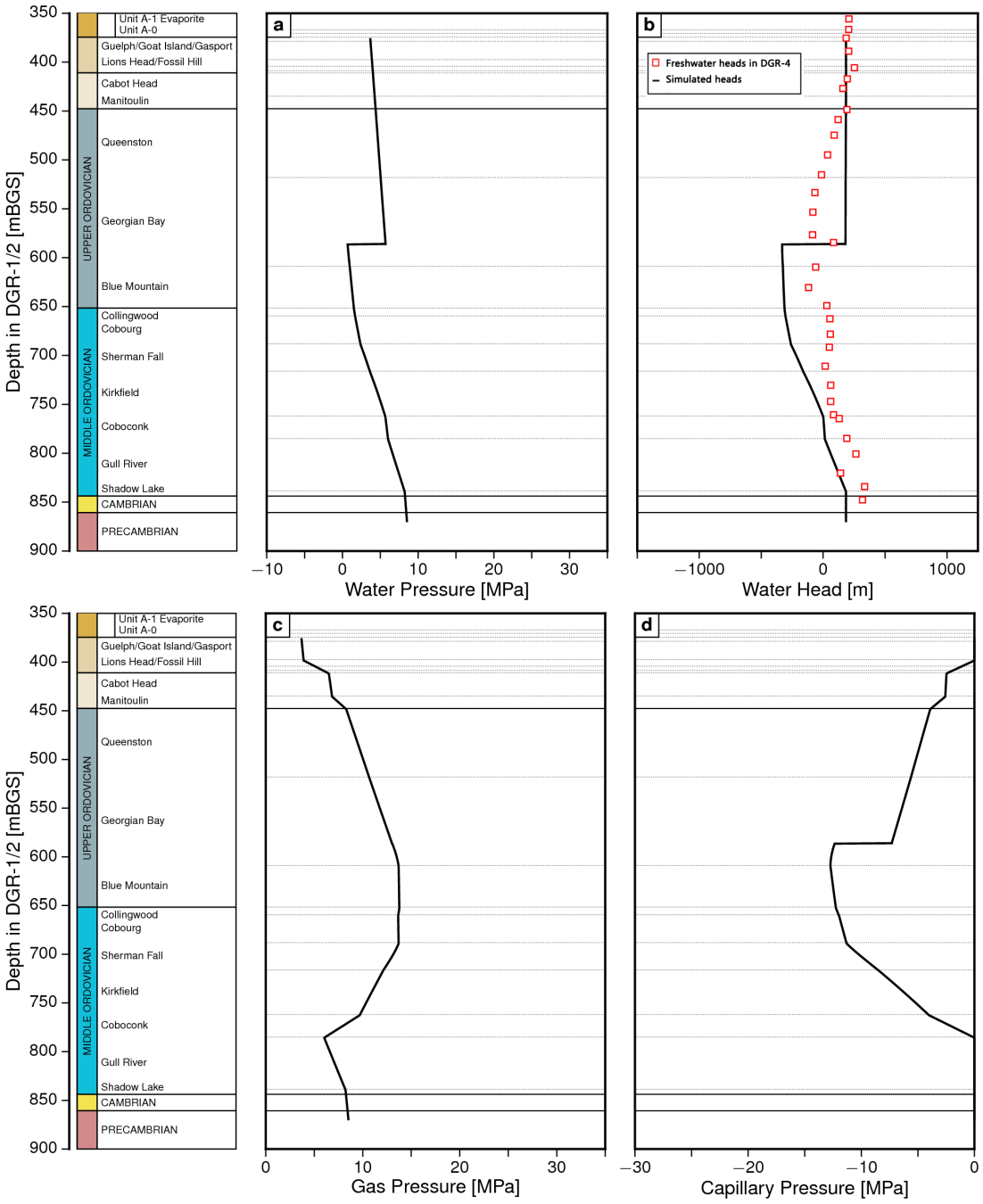

Figure 5.8: Two-phase gas-water flow analysis at 4 Ma with air generation and hydrostatic initial condition.

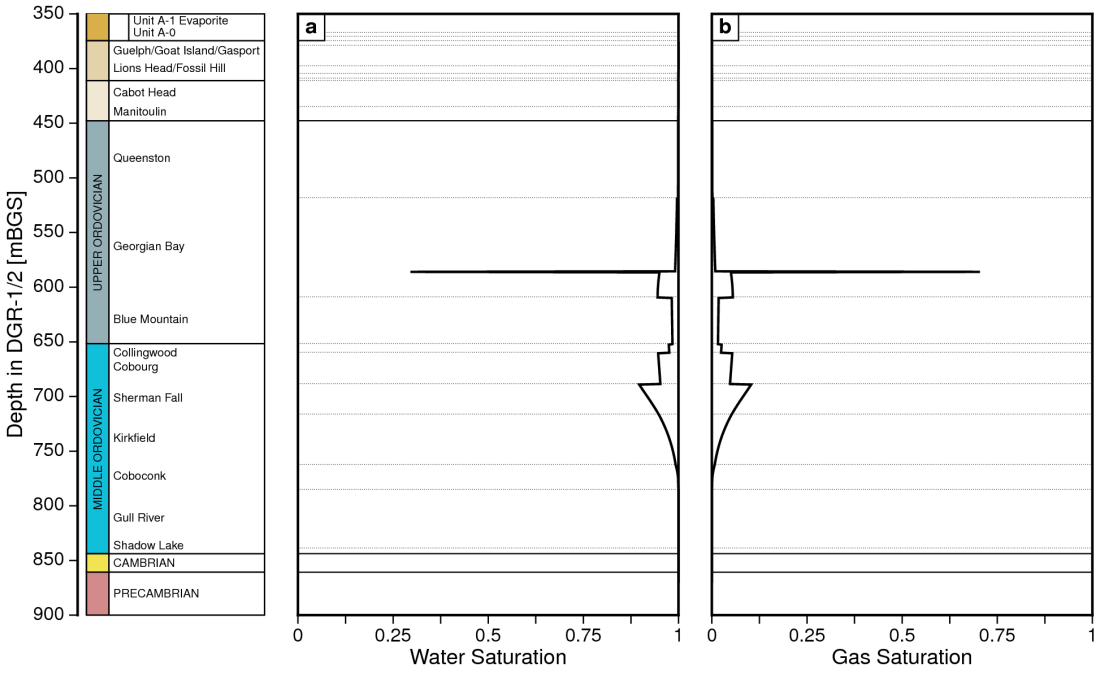

Figure 5.9: Saturations of two-phase water-gas flow at 4 Ma with air generation and hydrostatic initial condition.

5.3 Sensitivity Analyses

5.3.1 Over-pressure Boundary Condition in the Cambrian and Precambrian

This section uses identical hydrogeologic parameters as the base-case described in the previous section; however, the initial conditions are changed to account for the over-pressure in the Cambrian and Precambrian Formation. The initial water pressures (Figure 5.10) in the formations overlying the Cambrian remain hydrostatic, while an excessive water head of 120 m was assigned to the Gull River, Shadow Lake, Cambrian and Precambrian units (*Sykes et al.*, 2011). There were no changes in gas generation rate and initial gas saturation.

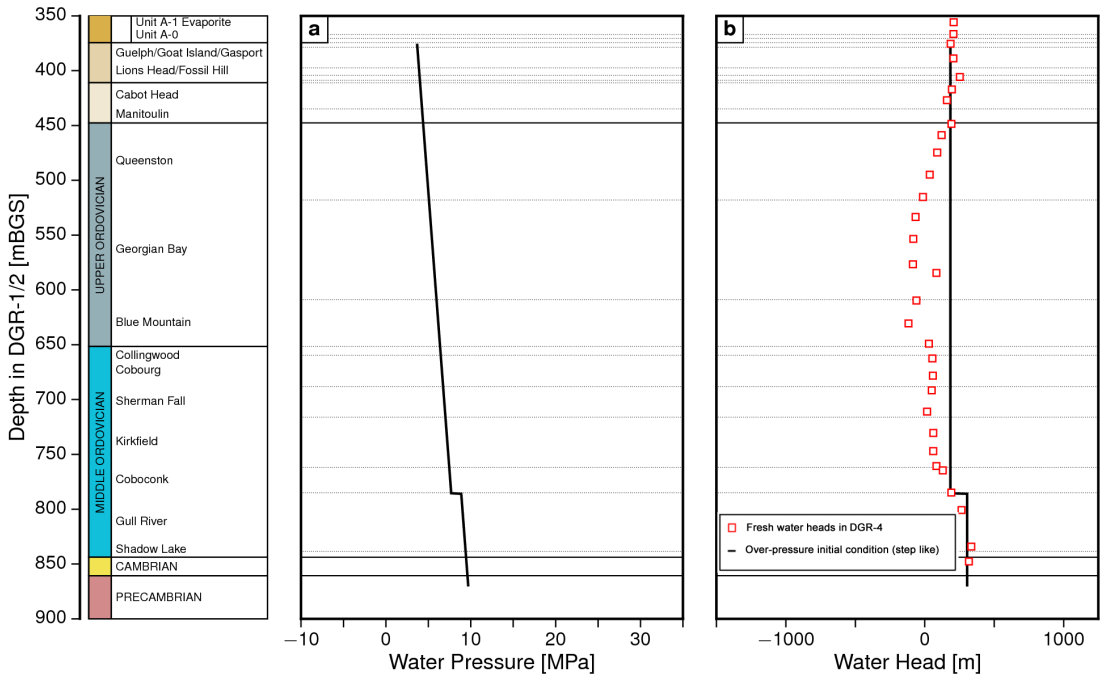

Figure 5.10: Initial condition with 120 m over-pressure of water head in the Gull River, Shadow Lake, Cambrian and Precambrian formations.

The resulting pressure profiles and saturations at 1 Ma and 4 Ma are shown in Figure 5.11, Figure 5.13, Figure 5.12 and Figure 5.14.

The distribution and discontinuity in saturations are similar with respect to hydrostatic case. The overall pressures are constrained to the boundary conditions specified for

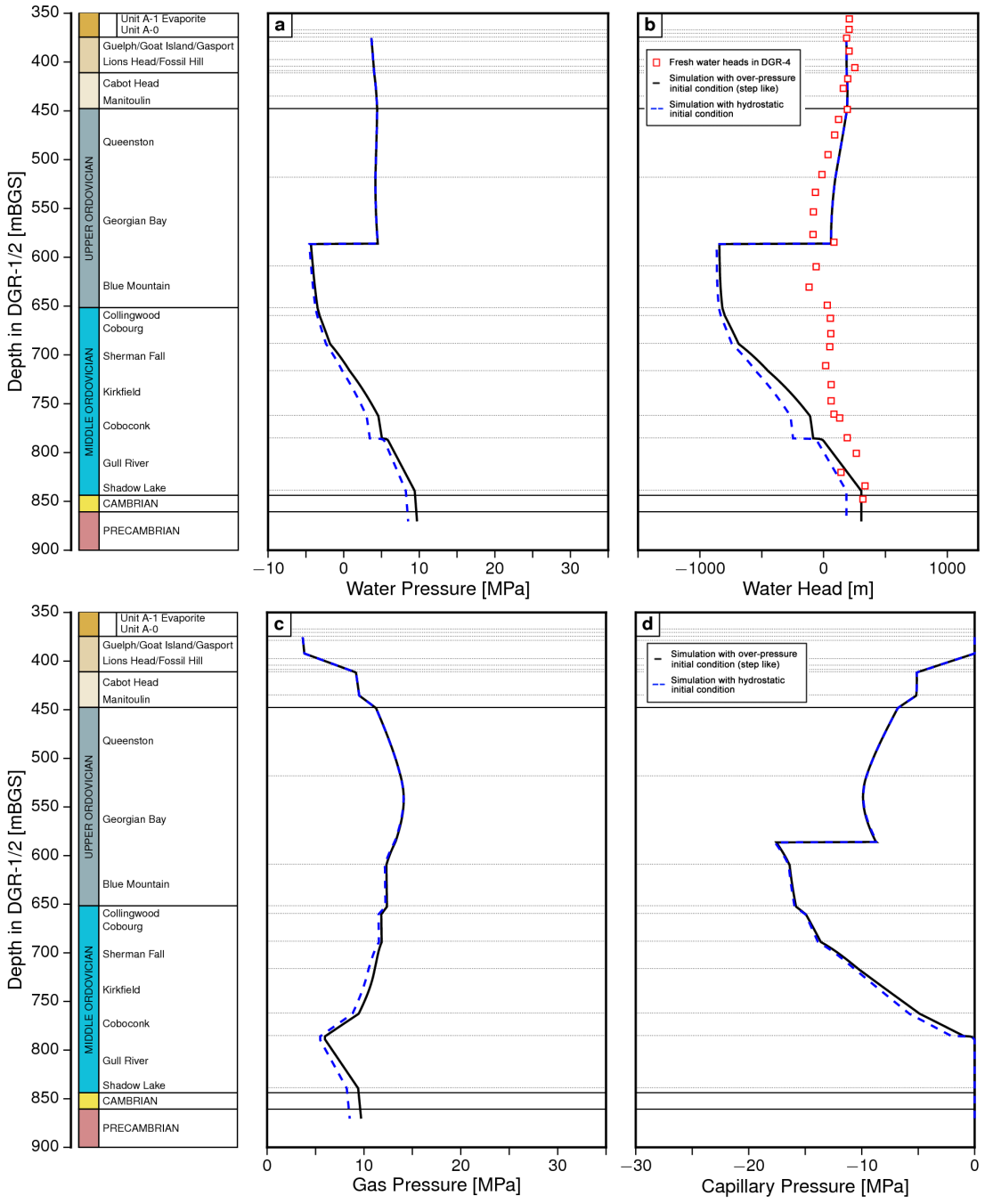

Figure 5.11: Two-phase gas-water flow analysis at 1 Ma with air generation and 120 m over-pressure of water head in the Gull River, Shadow Lake, Cambrian and Precambrian formations.

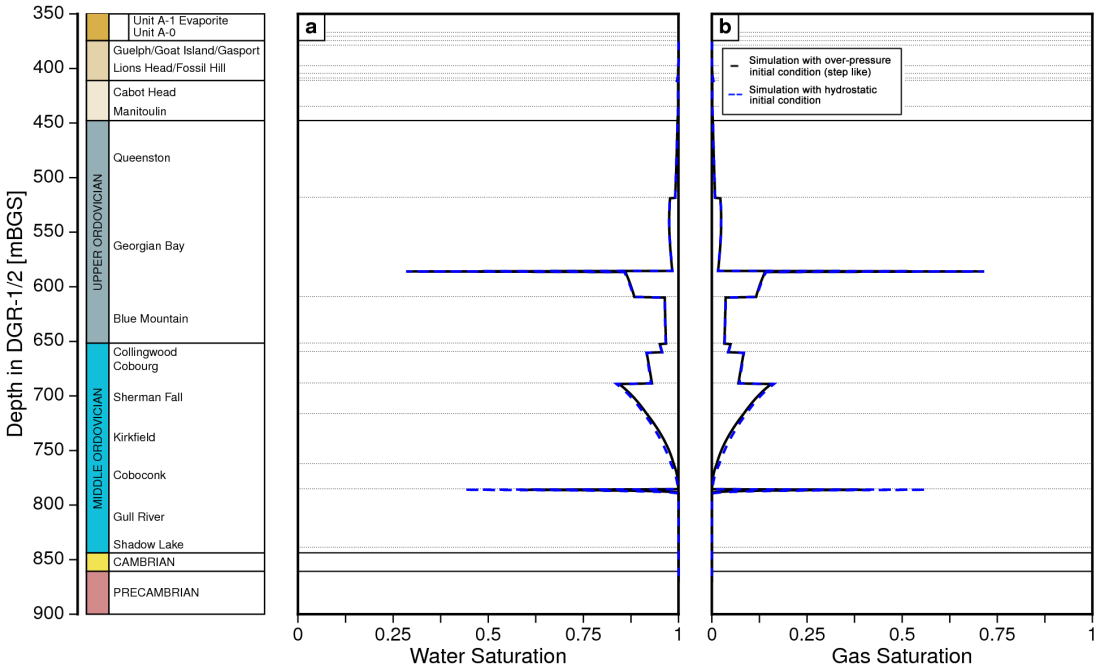

Figure 5.12: Saturations of two-phase water-gas flow at 1 Ma with air generation and over-pressure of water head in the Gull River, Shadow Lake, Cambrian and Precambrian formations.

the Guelph Formation and Precambrian. As the Precambrian is over-pressured, the pressures at 1 Ma and 4 Ma in the whole domain are slightly over-pressured compared to the hydrostatic case respectively, while the features and critical points of the profiles are similar. Compared to the hydrostatic case, it is obvious that the over-pressures in the Cambrian and Precambrian formations have no relation with the presence of the under-pressure in the Ordovician formations.

5.3.2 Gradually Increased Initial Water Pressure

The third initial condition is revised from the second one, while the formations between the bottom of Guelph Formation and top of the Shadow Lake Formation are not hydrostatic in the water head. Instead, the head is linearly increasing to the over-pressured Cambrian formation (Figure 5.15).

The water head in the Guelph Formation remains hydrostatic. The initial condition is smoothed with a uniform gradient between the Guelph formation and Shadow Lake

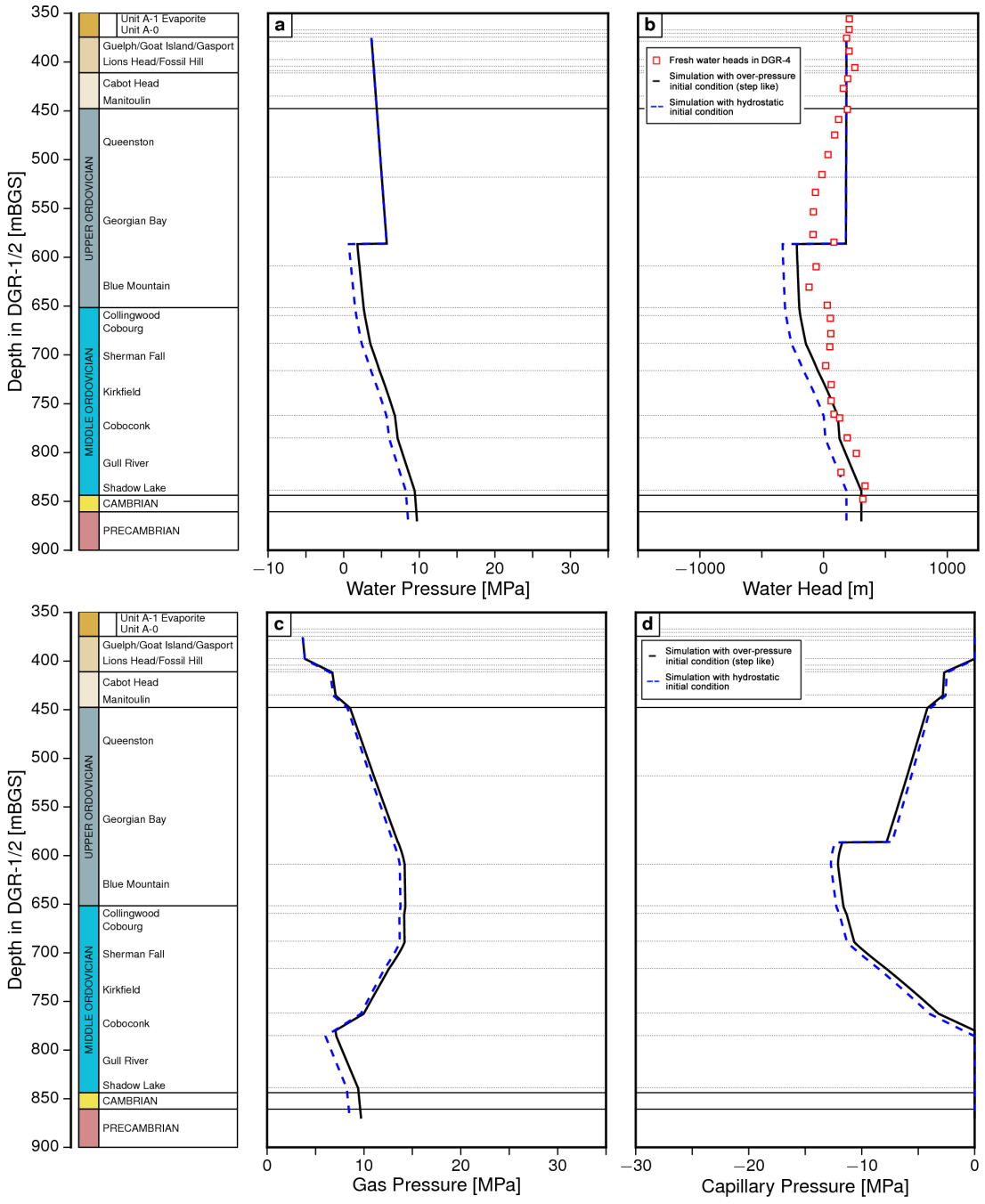

Figure 5.13: Two-phase gas-water flow analysis at 4 Ma with air generation and 120 m over-pressure of water head in the Gull River, Shadow Lake, Cambrian and Precambrian formations.

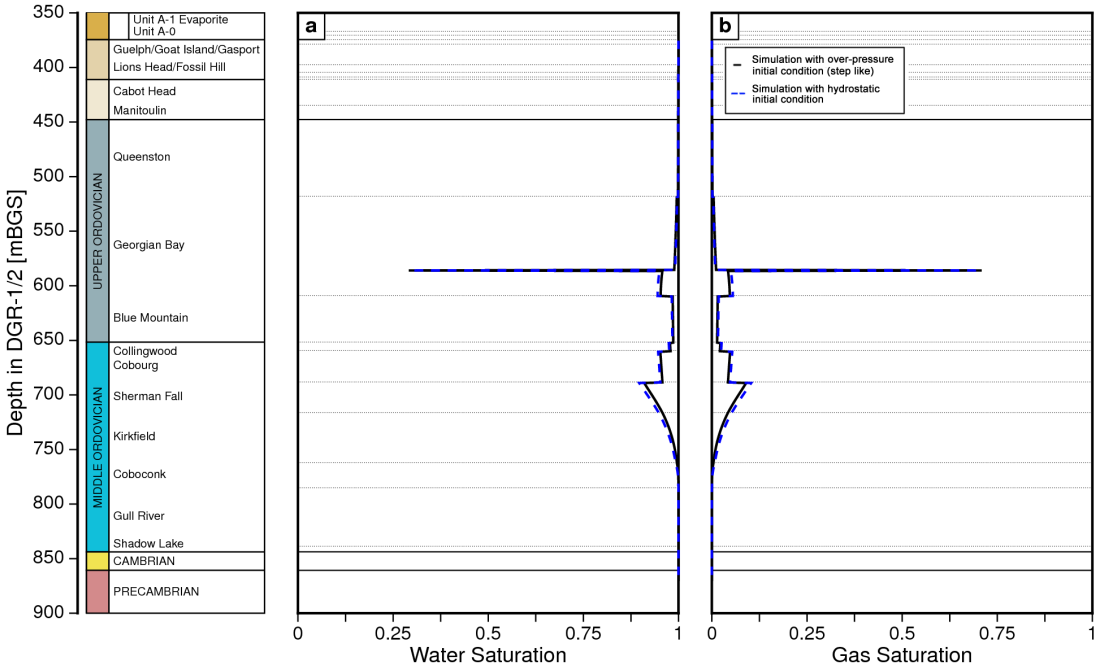

Figure 5.14: Saturations of two-phase water-gas flow at 4 Ma with air generation and over-pressure of water head in the Gull River, Shadow Lake, Cambrian and Precambrian formations.

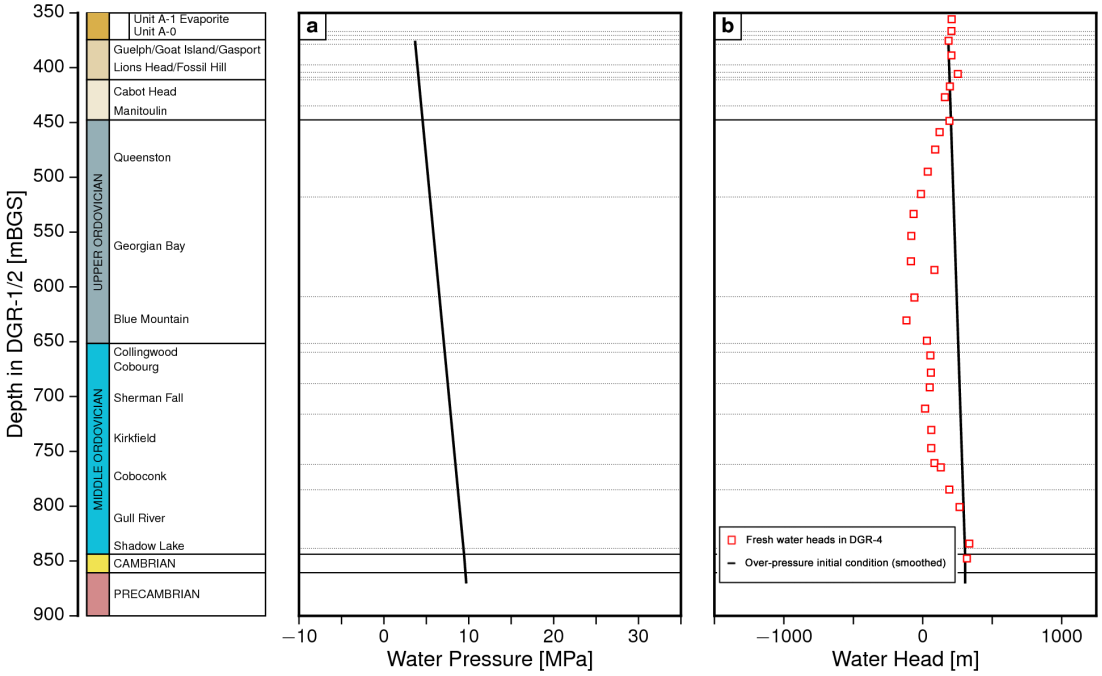

Figure 5.15: Initial condition with 120 m over-pressure of water head in the Cambrian and Precambrian and gradually increased heads in the Ordovician.

formation and reaches the over-pressure in the Cambrian aquifer and the Precambrian formation.

The results at 1 Ma and 4 Ma are shown in Figures 5.16, 5.18, 5.17 and 5.19. Compared to the previous case (with a step-like initial condition), this case is almost identical with a slight deviation, which is due to the difference in pressure gradient within the Ordovician formations. After a long time period (4 Ma), there is no significant impact of the initial condition on the pressures and saturations.

The case discussed here is used as the base case in the sensitivity analyses. It addresses a hydrostatic condition in the Guelph Formation and over-pressure heads between the Shadow Lake formation and the Precambrian formation with a smoothed trend, which is a reasonable assumption and more representative for the real environment.

Generally, a gas generation in the Ordovician would result in significant under-pressure in water pressure in the Ordovician formations. The water pressure returns to hydrostatic situation gradually but very slowly motion and driven predominantly by diffusion of soluble gas. The water pressure is constrained by the boundary conditions and the impact of initial water pressure is not significant in a long-time scale analysis (greater than 1 Ma). The following section will investigate the sensitivity of the pressure, head and saturation to the gas generation rate and the diffusivity and assess their impact.

5.3.3 A Fast Gas Generation Rate

A fast gas generation rate is achieved by increasing the base case gas generation rate by one order of magnitude, and reducing the gas production period by one order of magnitude so that the amount is equivalent to the base case. A faster generation rate has little impact on a long-time scale, however significant variations are observed on a short period. The water becomes under-pressured earlier than the base case, as more air is generated per unit time in the same volume. At approximately 4 ka (Figures 5.20 and 5.21), the water pressure deficit is significant compared to the base case where no visible changes in pressure had been revealed. After a simulation period of 1 Ma (Figures 5.22 and 5.23), the two cases are almost identical, showing that the impact of a fast gas generation rate has been dissipated soon after the termination of gas production.

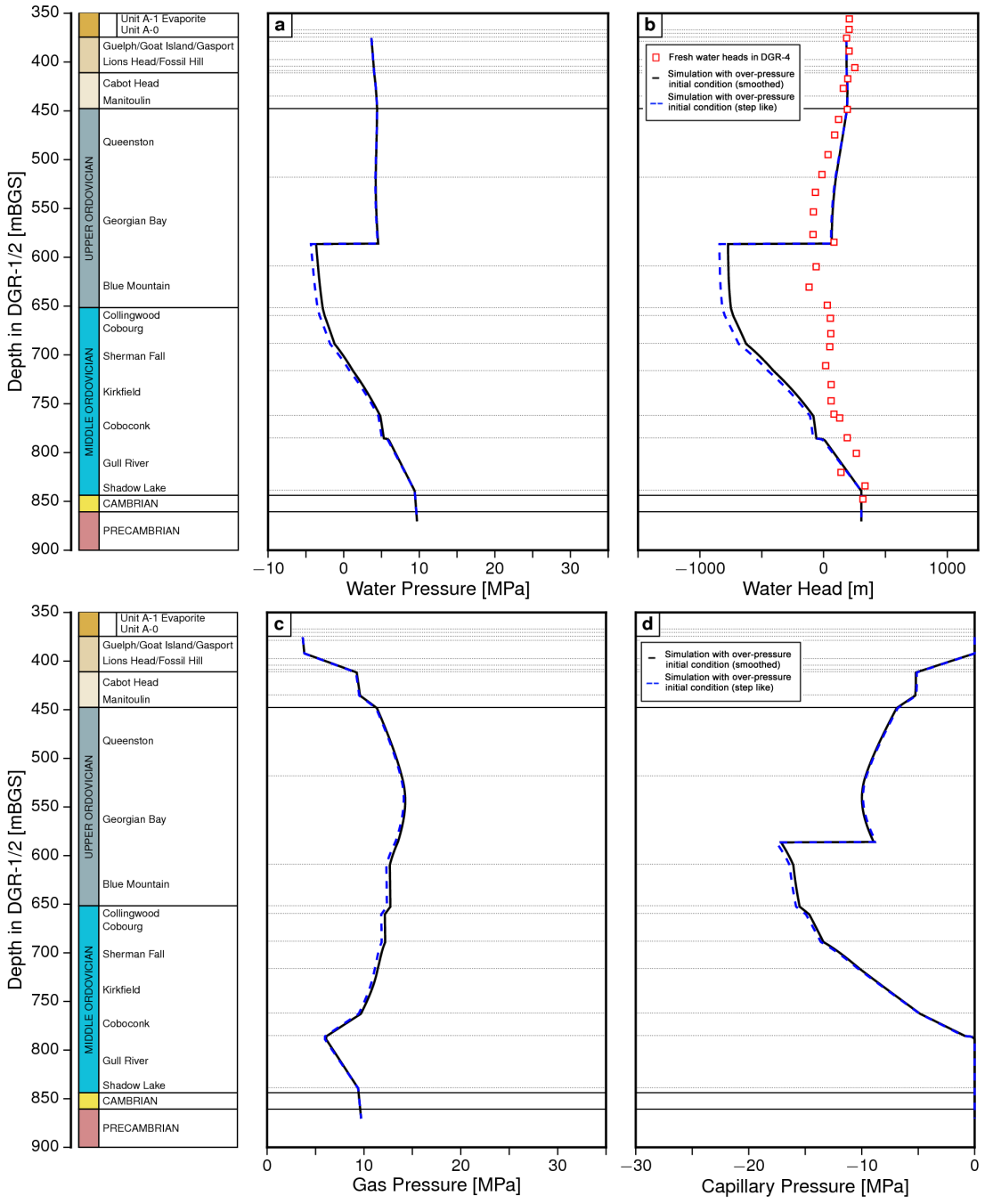

Figure 5.16: Two-phase gas-water flow analysis at 1 Ma with air generation, 120 m over-pressure at the Cambrian and Precambrian formations and a uniform Pressure increment in the Ordovician formations.

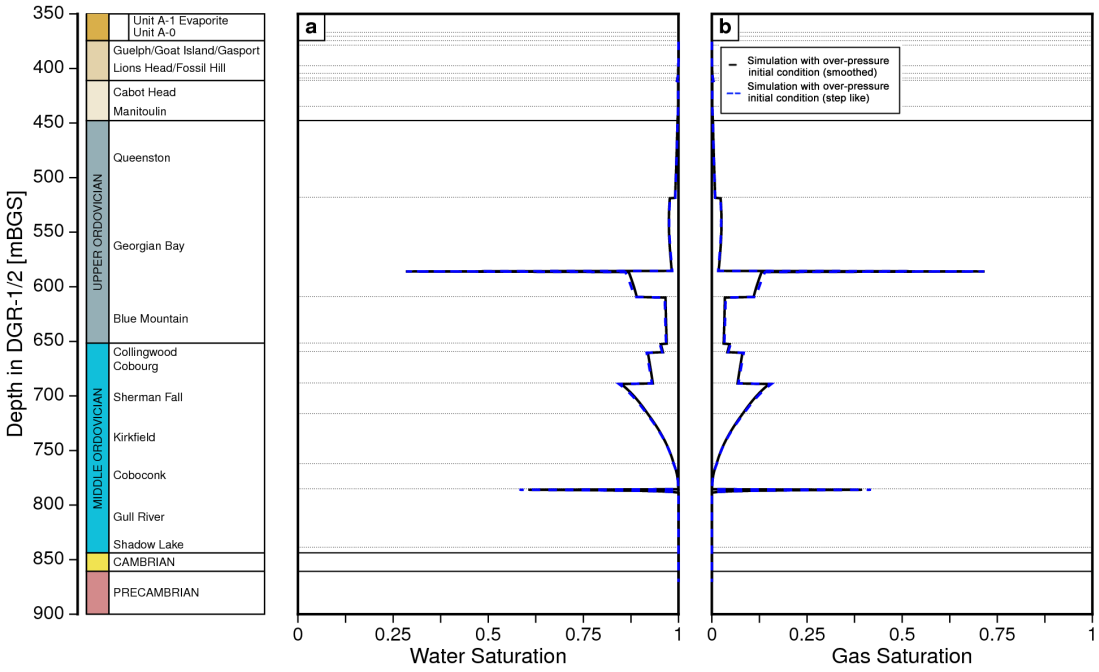

Figure 5.17: Saturations of two-phase water-gas flow at 1 Ma with air generation, 120 m over-pressure at the Cambrian and Precambrian formations and a uniform pressure increment in the Ordovician formations.

5.3.4 An Upgraded Diffusivity of Air in Water

The diffusivity of air in water is increased by one order of magnitude (from $0.25 \times 10^{-8} m^2/s$ to $0.25 \times 10^{-7} m^2/s$) compared to the base case. Investigations of pressure profiles and saturations at 50 ka are presented in Figures 5.24 and 5.25.

The gas saturation at 50 ka has almost identical features as the base case. The gas enriched discontinuity is consistent with the base case analysis. The water pressure has shown significant under-hydrostatic deficit after a short period of 50 ka that the generated air saturation is quite low in the Ordovician formations. However, the level of under-pressure in this case is moderately less than the level of under-pressure in the base case because more air is transported through diffusion in solute phase. This difference is more obvious in the 1 Ma simulation (Figures 5.26 and 5.27). In the 1 Ma simulation for a higher diffusivity, the water pressure is close to the hydrostatic condition there is no significant under-pressure observed in the Ordovician formations. The 4 Ma simulation results are displayed in Figures 5.28 and 5.29. The water pressure at 4 Ma has returned to hydrostatic condition and gas phase has fully partitioned into solute phase while not in the base case. This difference indicates that the rate of return and air dissipation

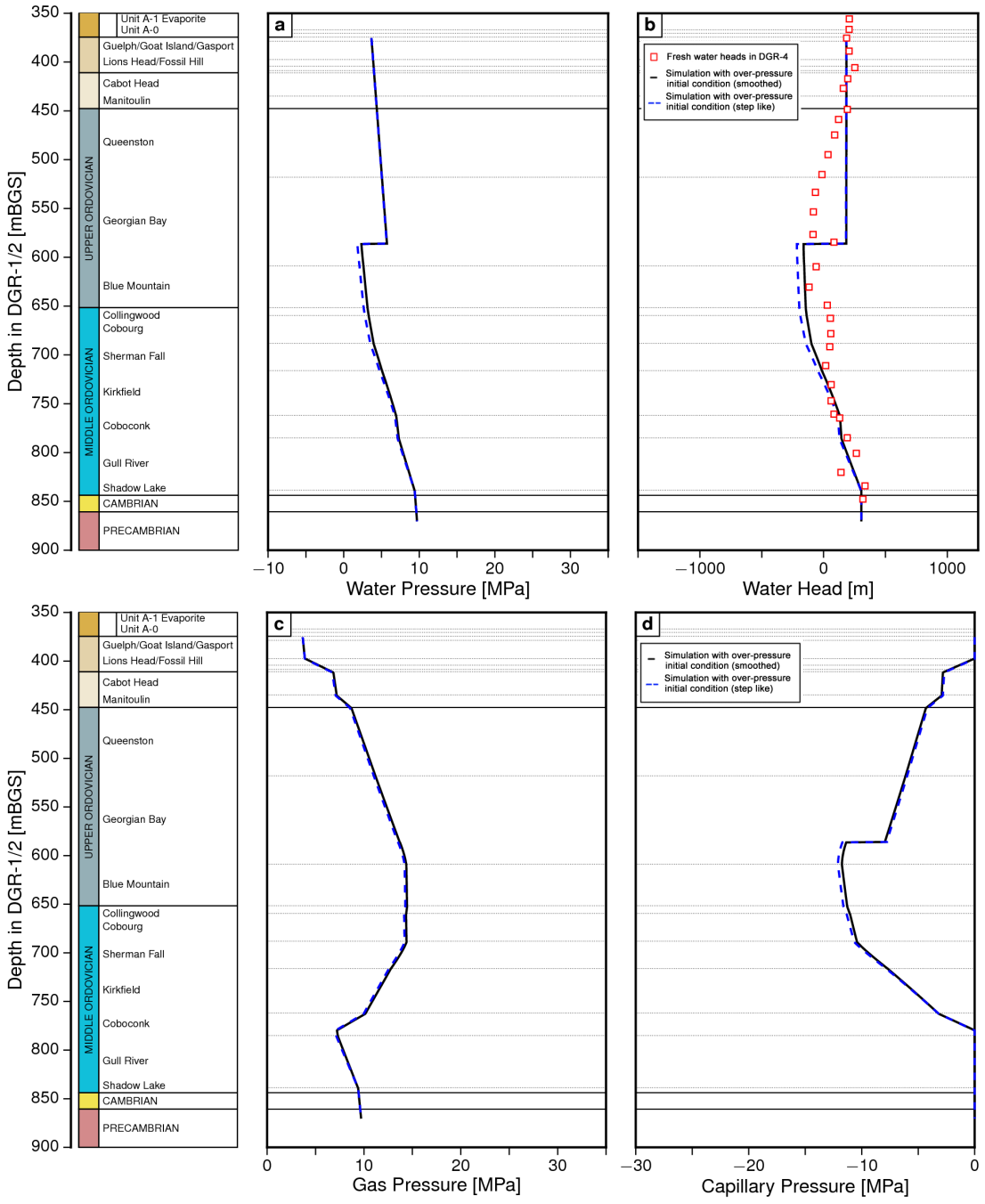

Figure 5.18: Two-phase gas-water flow analysis at 4 Ma with air generation, 120 m over-pressure at the Cambrian and Precambrian formations and a uniform pressure increment in the Ordovician formations.

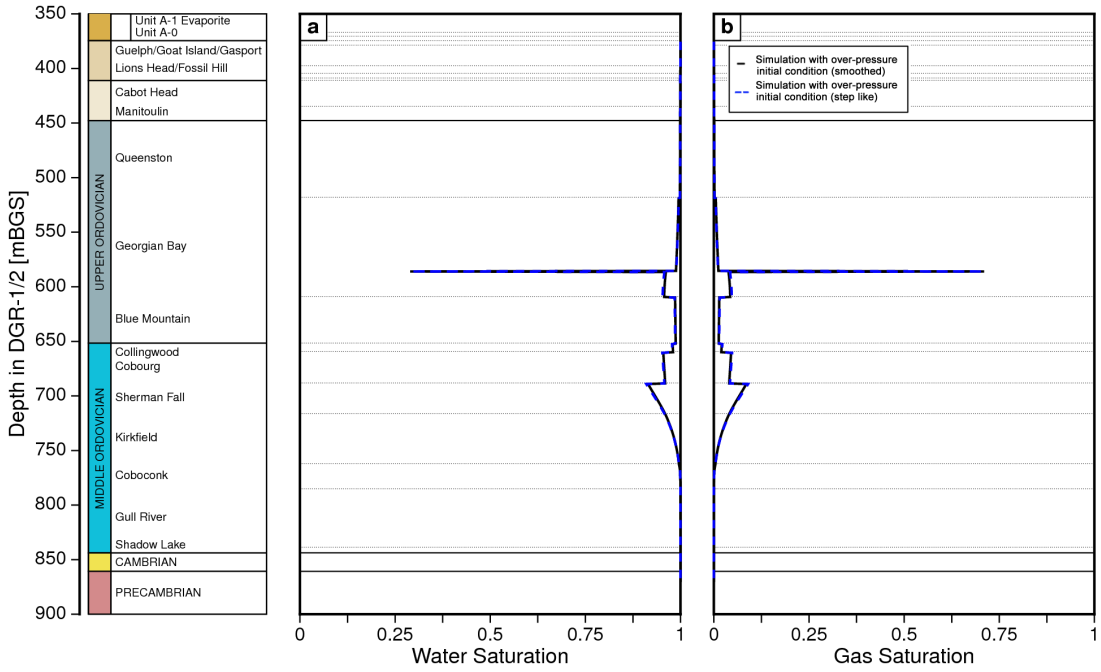

Figure 5.19: Saturations of two-phase water-gas flow at 4 Ma with air generation, 120 m over-pressure at the Cambrian and Precambrian formations and a uniform pressure increment in the Ordovician formations.

through diffusion is sensitive to the diffusion coefficient. In addition, this implies that for a long-term preservation of the under-pressure in low permeability rocks, the diffusivity of air must be low.

5.3.5 Sensitivity of the Pressure in the Discontinuity to the Two-Phase Flow Properties

In a parallel study to that of this thesis, *Sykes et al.* (2011) investigated the sensitivity of the water pressure and the saturations in the discontinuity in the Georgian Bay Formation to the capillary pressure saturation relationship used to describe the discontinuity. The three relationships investigated in the analyses of their study are shown in Figure 5.30. The capillary pressure versus saturation relationship for the medium case is typical of that used for a clay. For the sensitivity analyses an initial water pressure of zero (refer to Figure 5.31) was used with an initial gas saturation of 17%. The water pressure distribution at 100 ka for the high capillary pressure case is shown in Figure 5.32. For this case, the capillary pressure relationship for the discontinuity is the same as that

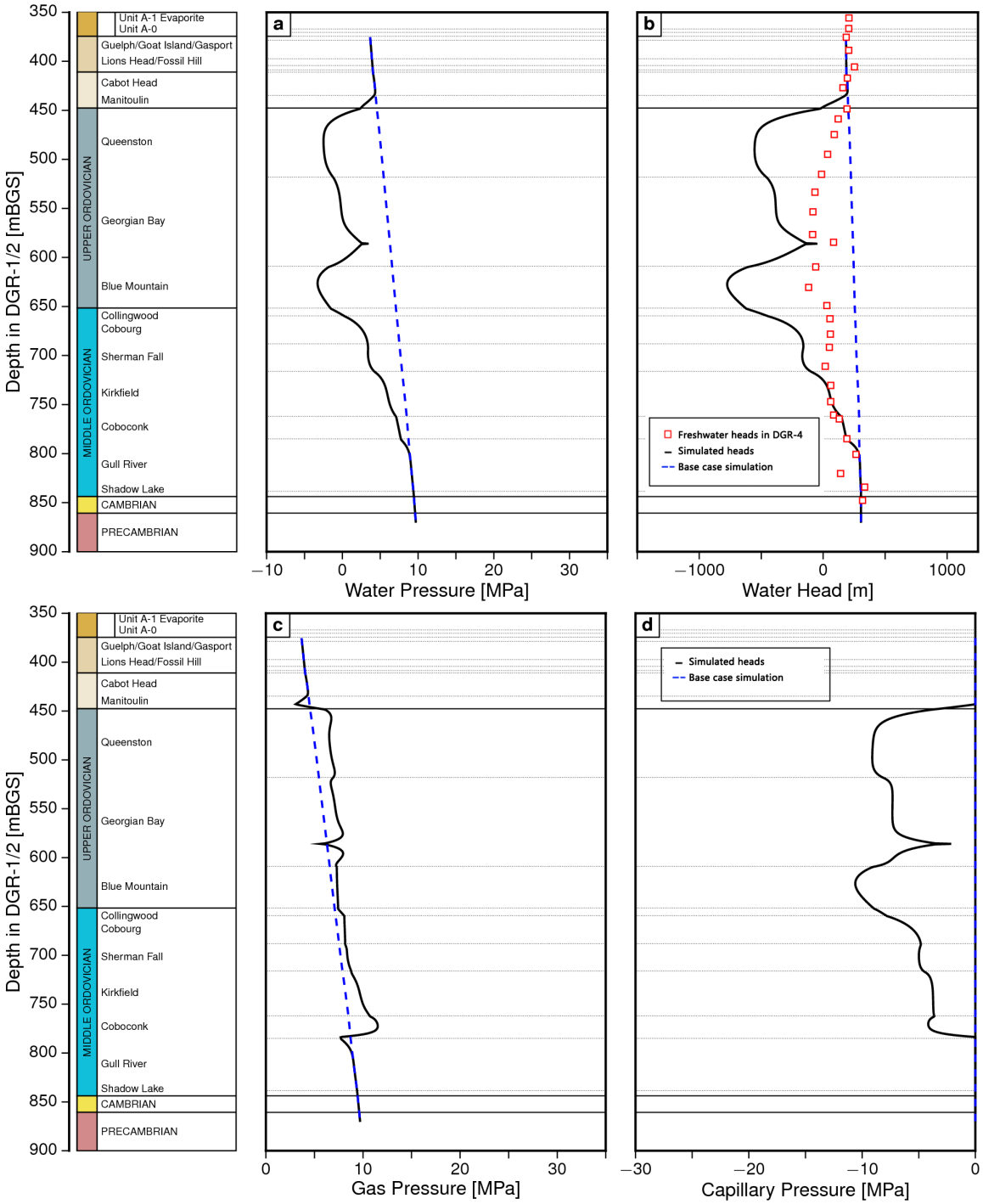

Figure 5.20: Two-phase gas-water flow analysis at 4 ka with a fast gas generation rate

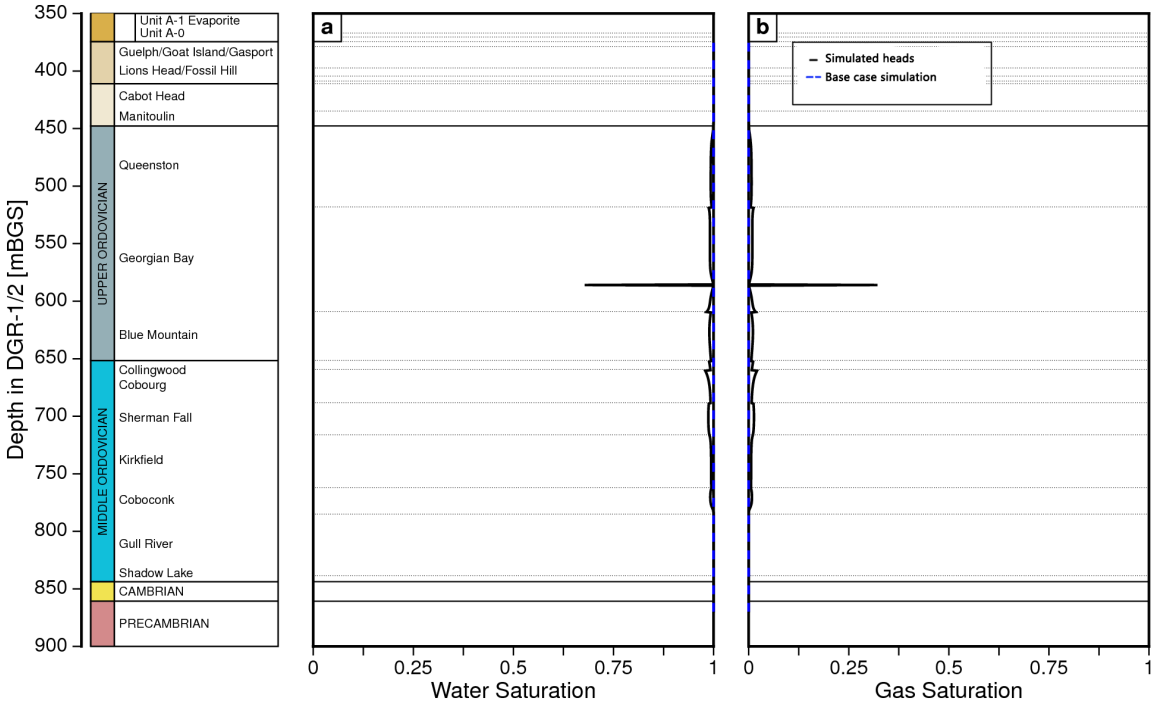

Figure 5.21: Saturations of two-phase water-gas flow at 4 ka with a fast gas generation rate

assigned to the Georgian Bay Formation so that the water pressure in the discontinuity is predicted to be the same as that of the shale matrix. The water pressure distribution at 100 ka for the low capillary pressure case is shown in Figure 5.33. The results for this analysis show a high pressure in the discontinuity with the gas saturation (not shown) also being high. The third case, a medium capillary pressure relationship, results in water pressures in the discontinuity (refer to Figure 5.34) that more closely match the pressure measured in the borehole interval containing the discontinuity. The analyses undertaken by *Sykes et al.* (2011) clearly show that the water pressure in the discontinuity is sensitive to the capillary pressure versus saturation relationship used to represent the discontinuity.

5.4 Summary of Two-Phase Flow Analysis

The generation of gas phase in the Ordovician shale and limestone has explained the under-pressure in the Ordovician. The discontinuity observed in the Georgian Bay Formation acts as a pressure barrier expressed in the capillary discontinuity at the discon-

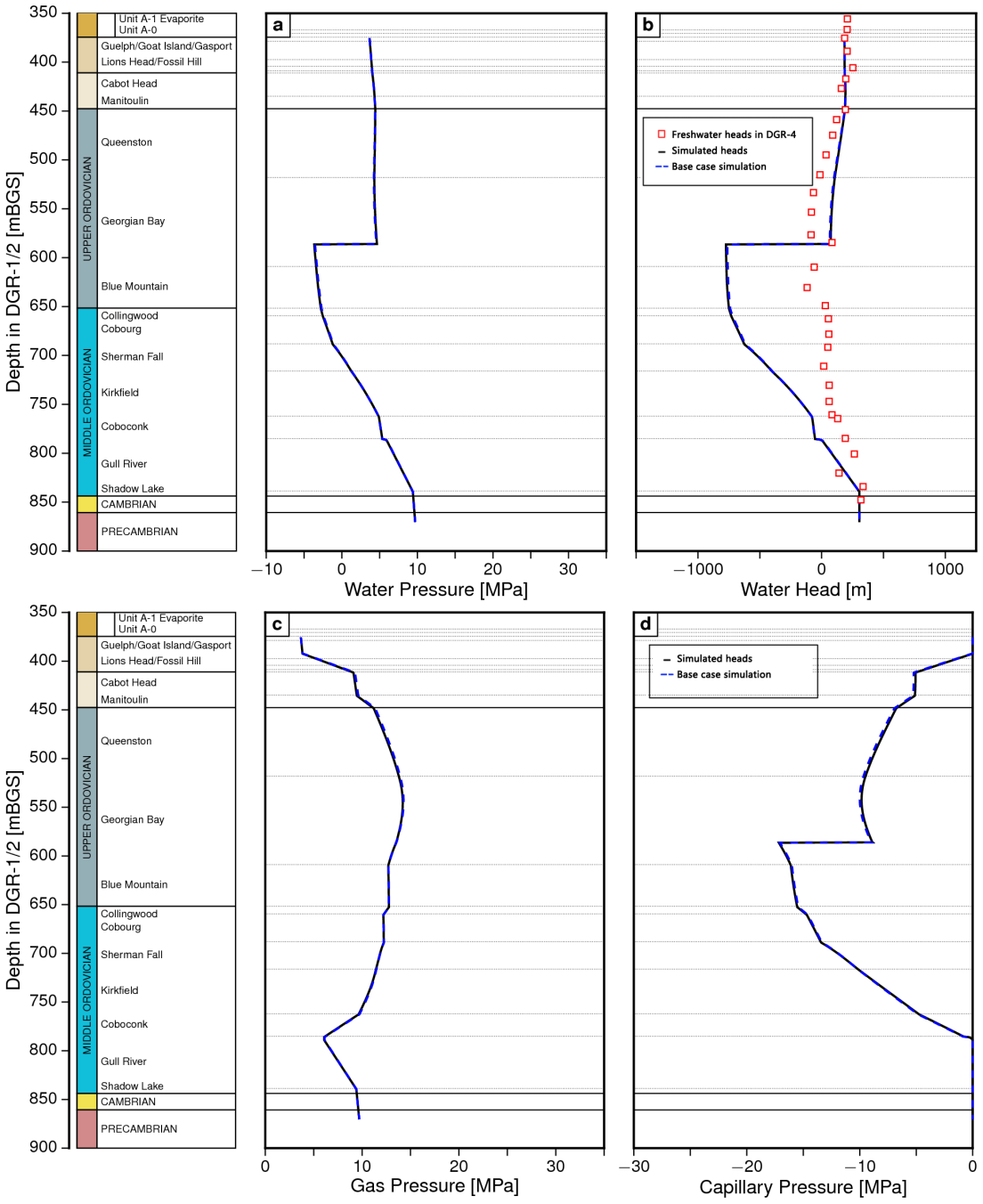

Figure 5.22: Two-phase gas-water flow analysis at 1 Ma with a fast gas generation rate.

tinuity. The capillary pressure at the bottom of the discontinuity is significantly higher than the one at the top.

Gas generation rate and variation of the initial condition could delay or speed up the migration of water and gas; however, they do not effectively change the distributions

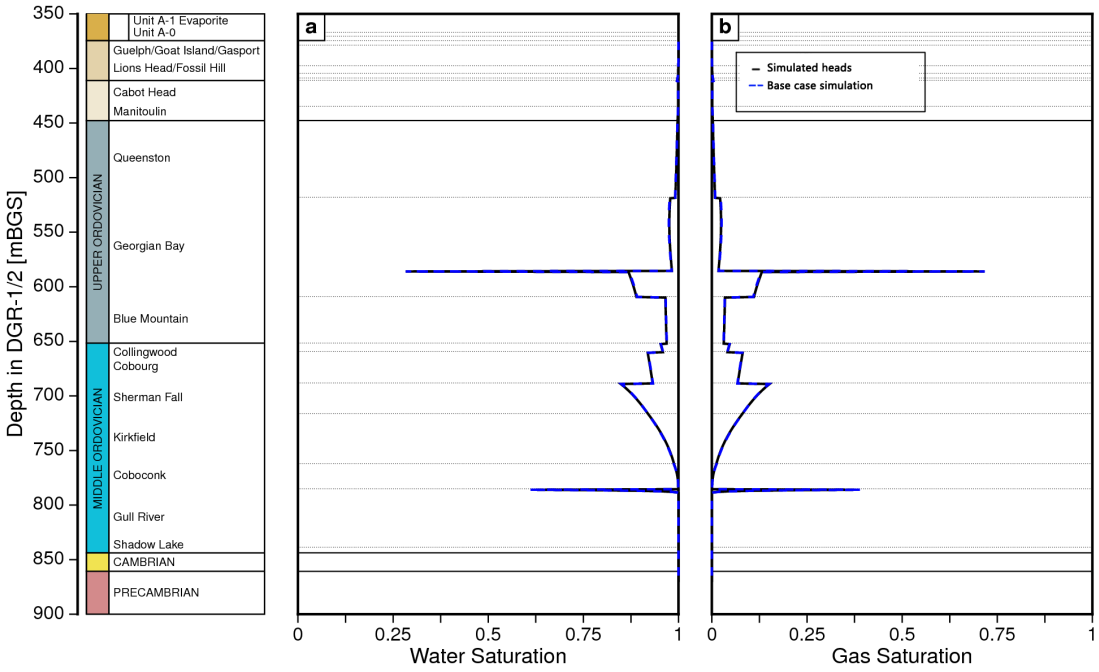

Figure 5.23: Saturations of two-phase water-gas flow at 1 Ma with a fast gas generation rate.

of gas and water in the heterogeneous sediments in a long-time simulation. The under-pressure in the Ordovician does not dissipate over a short period (50 ka) even after the termination of air generation (1 Ma). However, the return of the water pressure to hydrostatic condition gradually proceeds by the continuous diffusion of air into the solute phase.

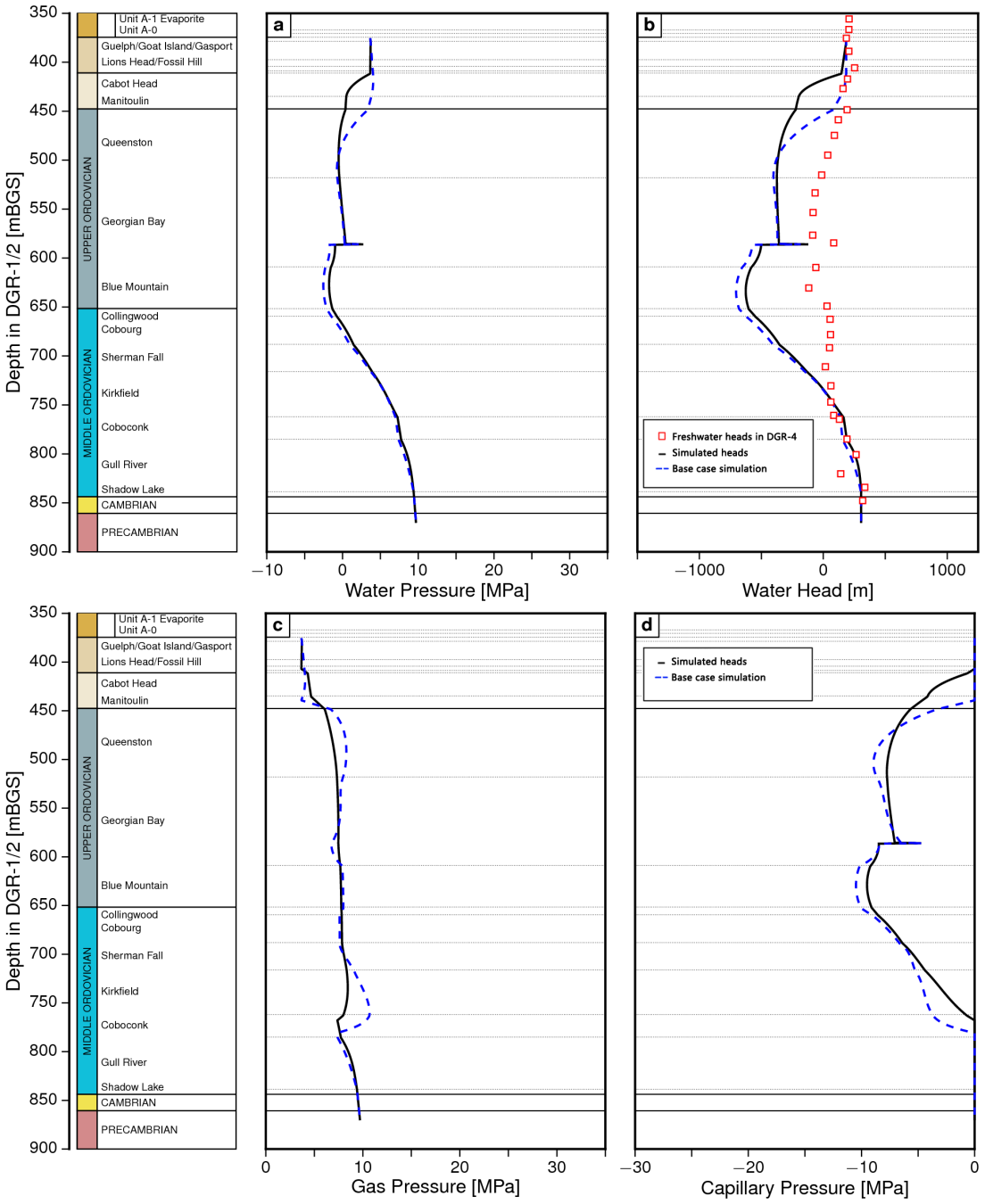

Figure 5.24: Two-phase gas-water flow analysis at 50 ka with an upgraded diffusivity.

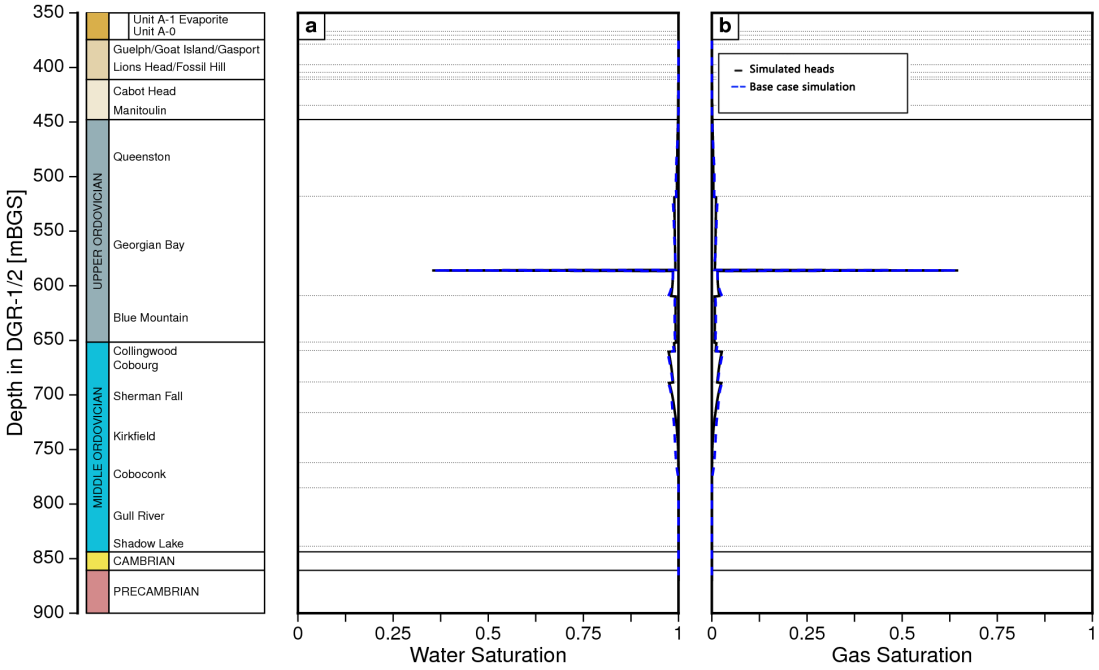

Figure 5.25: Saturations of two-phase water-gas flow at 50 ka with an upgraded diffusivity.

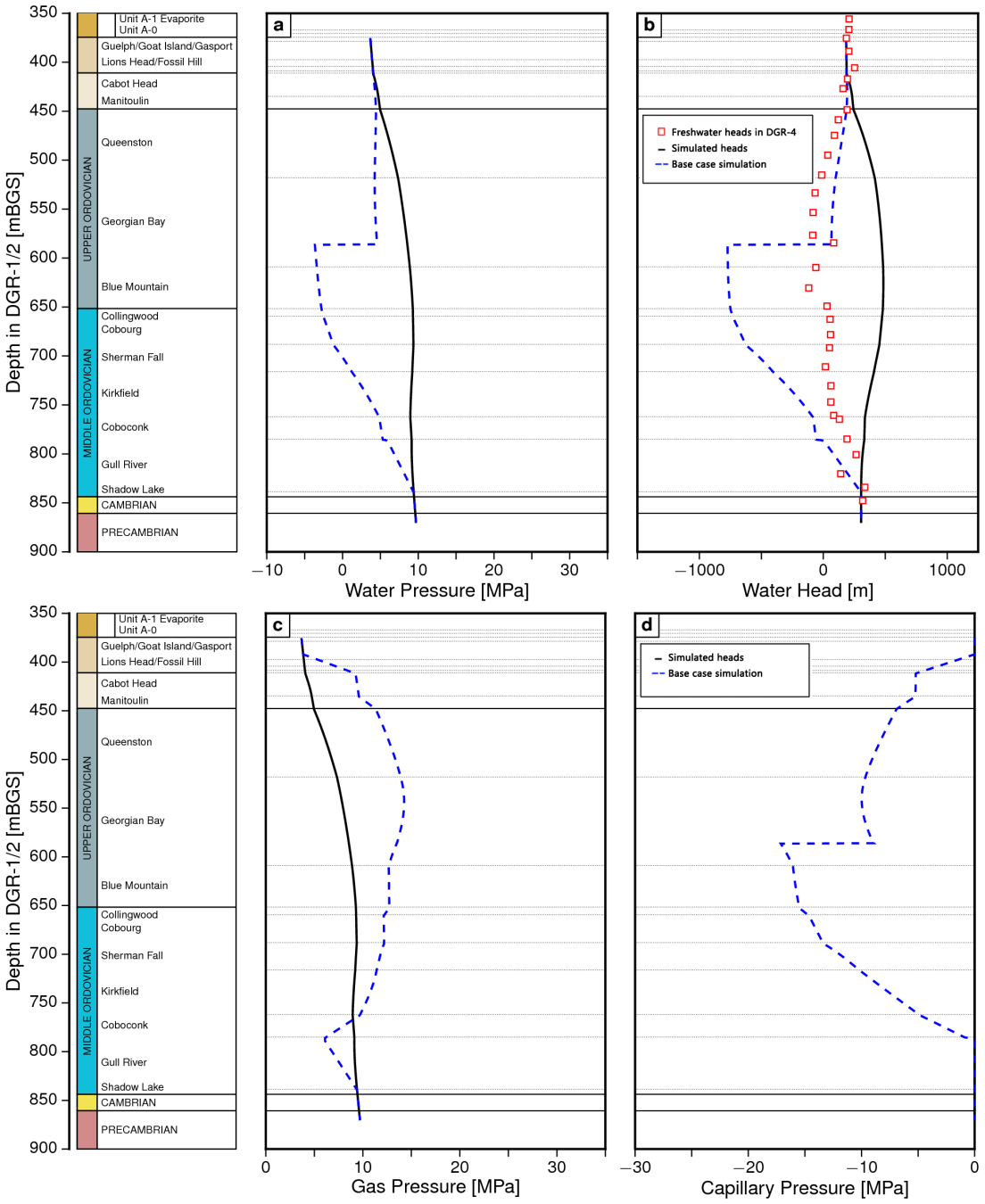

Figure 5.26: Two-phase gas-water flow analysis at 1 Ma with an upgraded diffusivity.

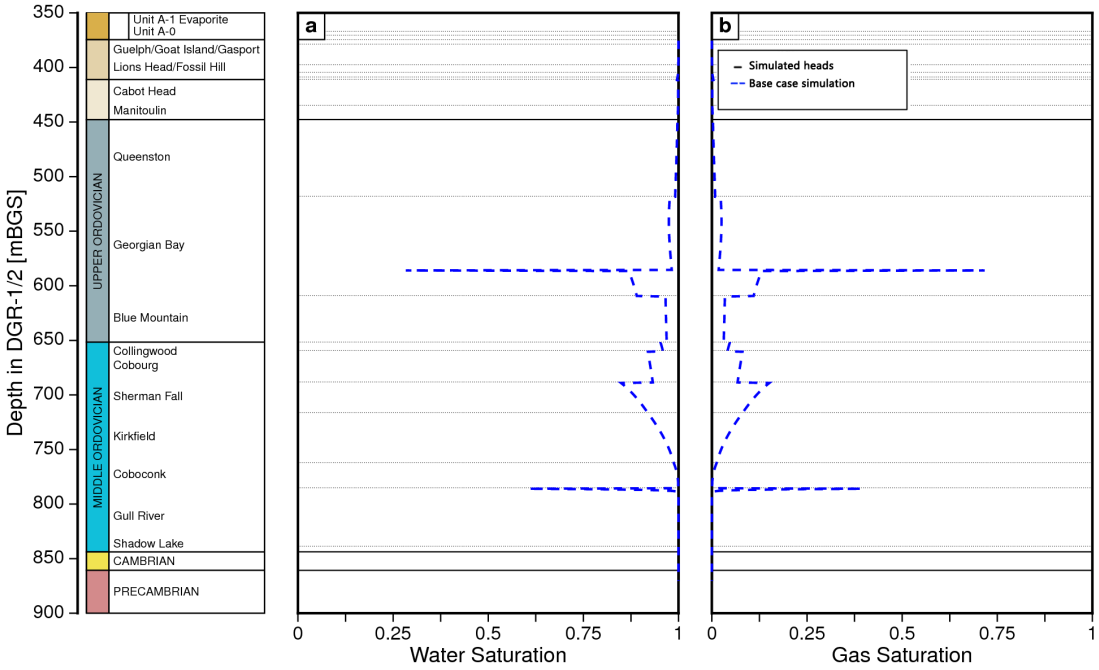

Figure 5.27: Saturations of two-phase water-gas flow at 1 Ma with an upgraded diffusivity.

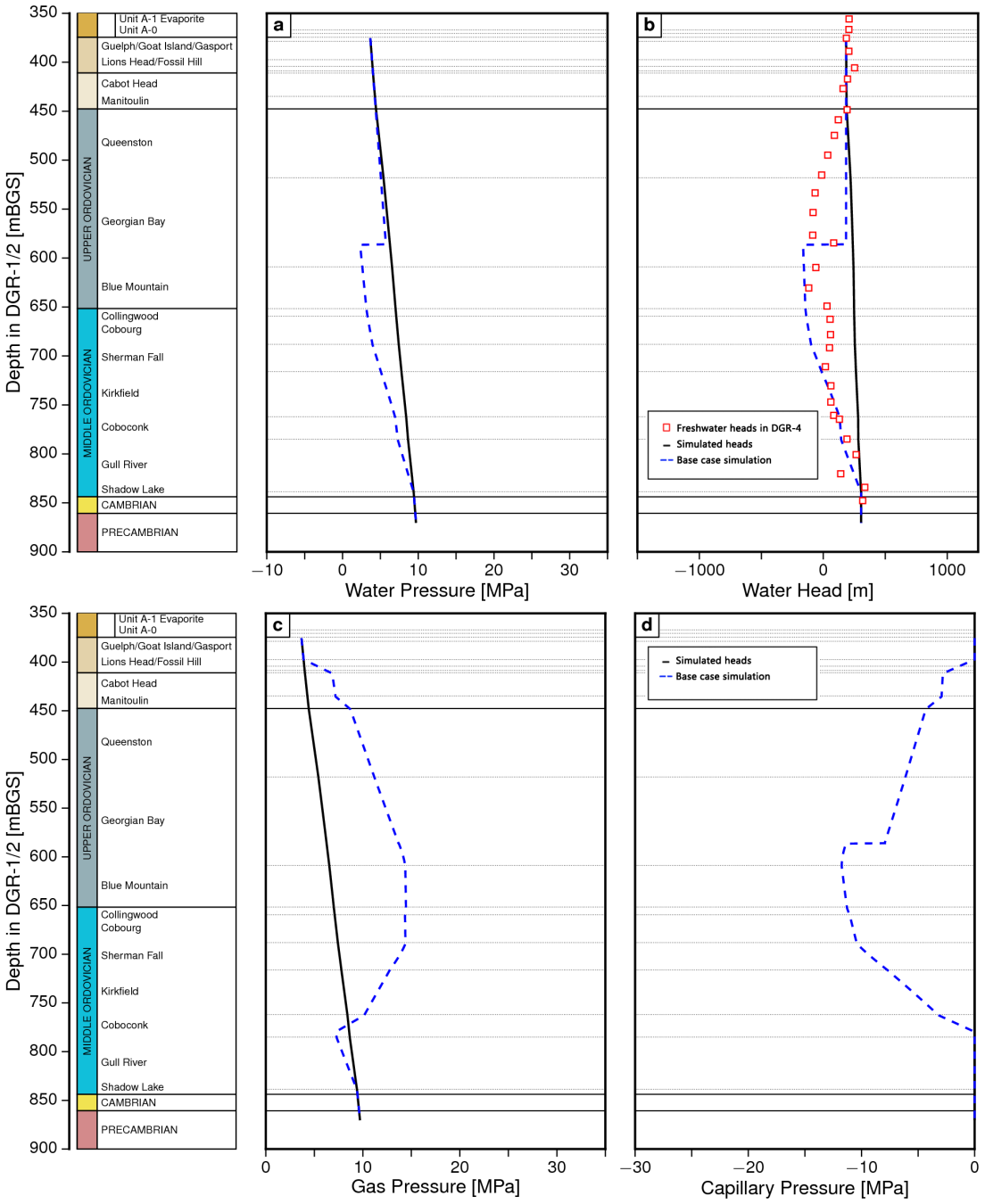

Figure 5.28: Two-phase gas-water flow analysis at 4 Ma with an upgraded diffusivity.

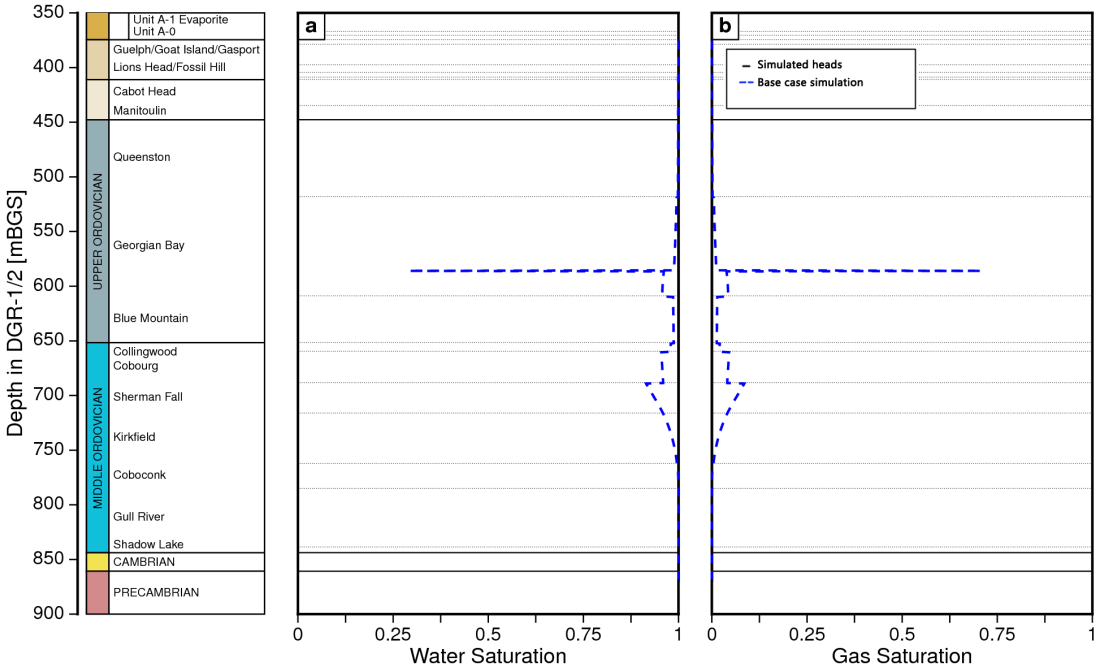

Figure 5.29: Saturations of two-phase water-gas flow at 4 Ma with an upgraded diffusivity.

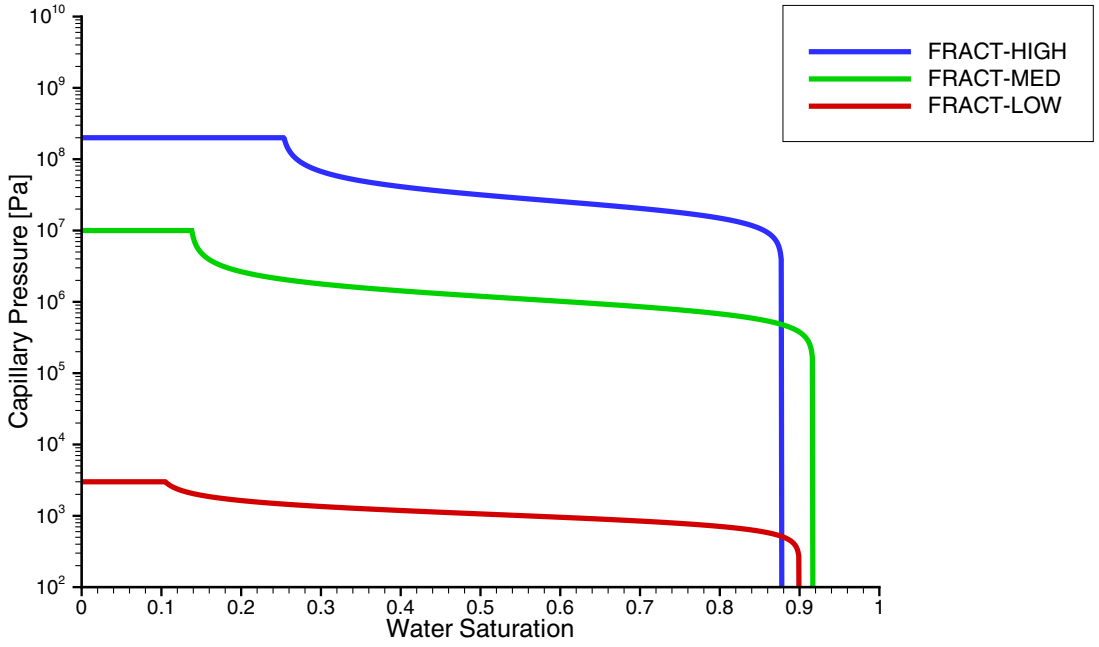

Figure 5.30: Capillary pressure versus saturation curves investigated in sensitivity analysis of discontinuity pressure. Adopted from *Sykes et al.* (2011).

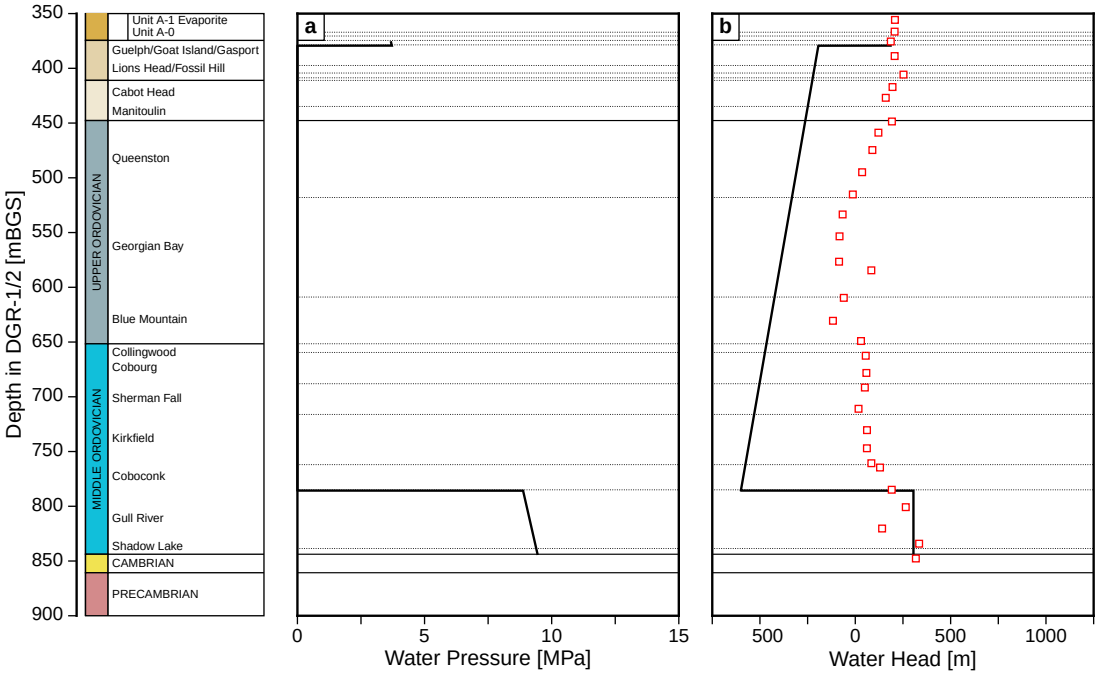

Figure 5.31: Initial water pressure for sensitivity analysis of discontinuity pressure. Adopted from *Sykes et al.* (2011).

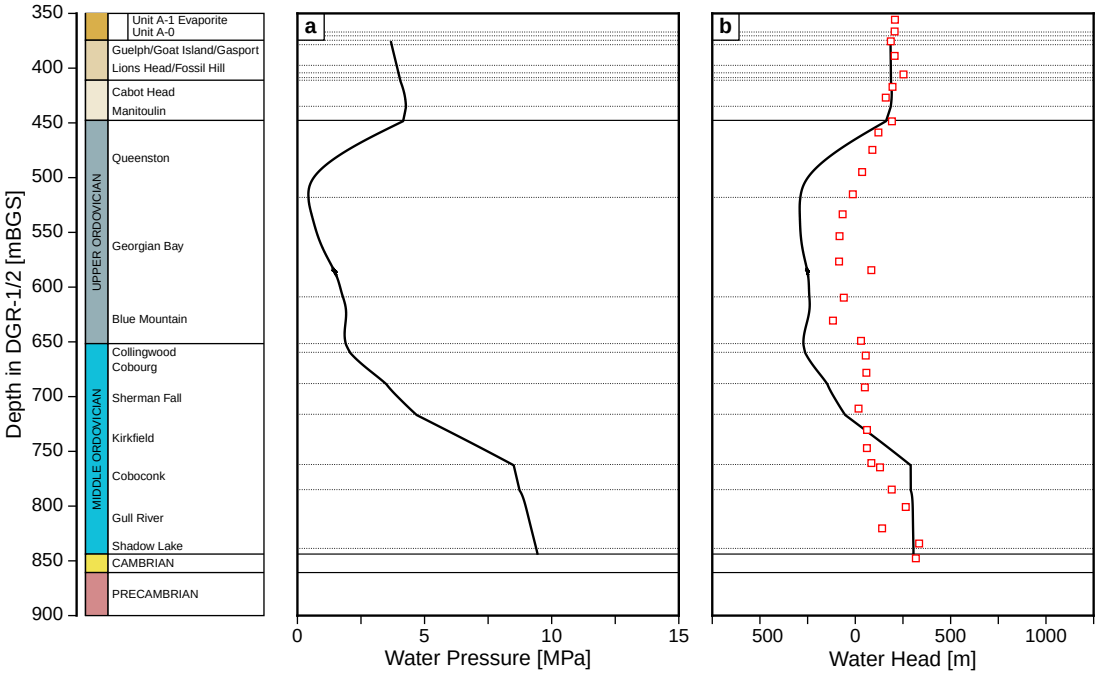

Figure 5.32: Water pressure at 100 ka for high capillary pressure versus water saturation relationship. Adopted from *Sykes et al.* (2011).

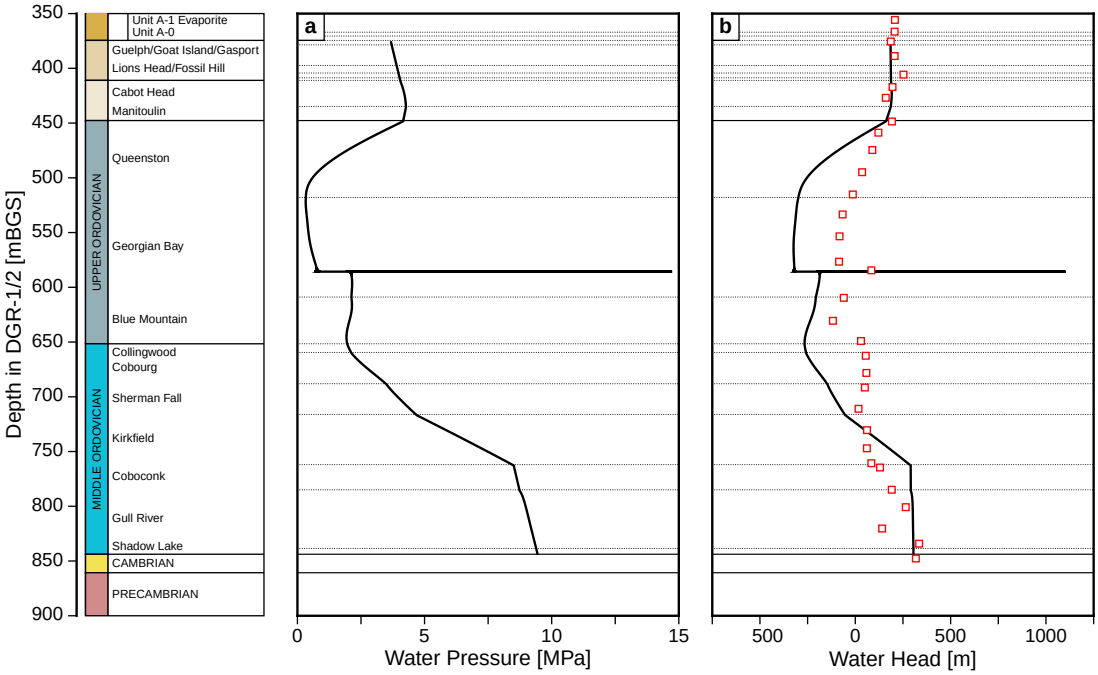

Figure 5.33: Water pressure at 100 ka for low capillary pressure versus water saturation relationship. Adopted from *Sykes et al.* (2011).

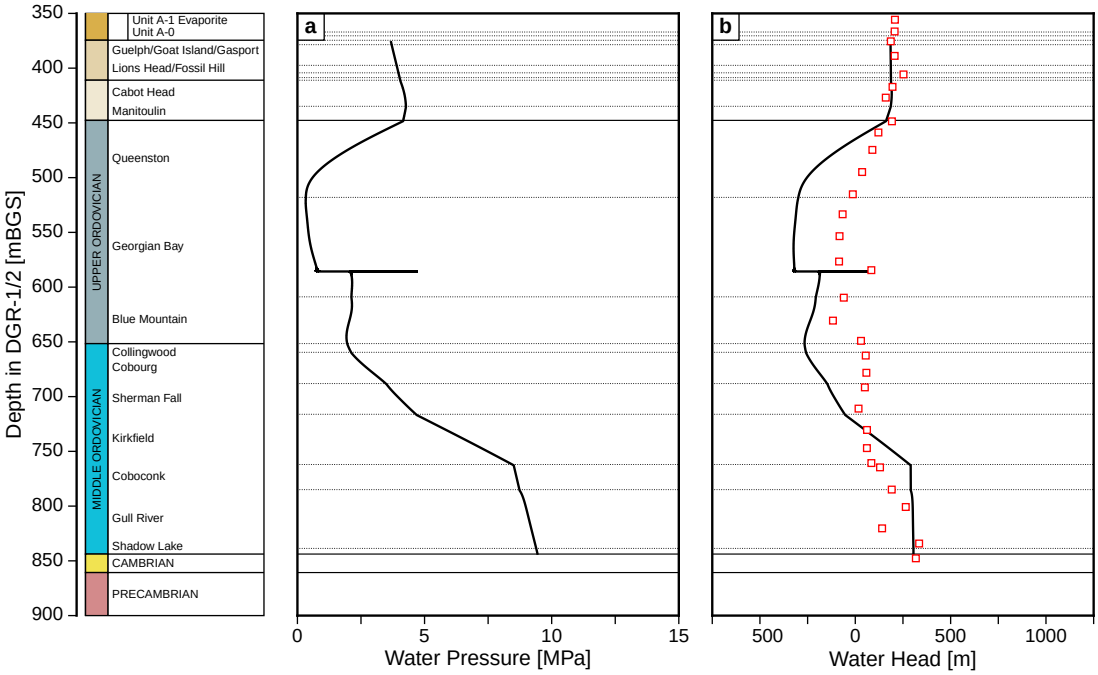

Figure 5.34: Water pressure at 100 ka for medium capillary pressure versus water saturation relationship. Adopted from *Sykes et al.* (2011).

Chapter 6

Conclusions

Two-phase flow and a sensitivity analyses have been presented in this study to explain the occurrence of abnormal under-pressures in the DGR boreholes at the Bruce site. Numerical simulations for the 1-D DGR site examined the conceptual model that the under-pressure in the Ordovician limestone and shales is a result of the presence of a gas phase. The in situ fluids (brine and methane) are represented by air and water and simulated using the TOUGH2-MP model. In the analyses, air represents methane.

The sensitivity simulation results are consistent with the under-pressure in the Ordovician formations. The presence of a gas phase and its migration in the Ordovician carbonates causes the under-pressure in water, with only a small amount of gas being required to reduce the water pressure. Different initial conditions, which are constrained to a hydrostatic head in the top Guelph Formation and a possible 120 m over-pressure head in the Cambrian and Precambrian formations, do not significantly alter the presence of the under-pressure water head in the Ordovician sediments. Different gas generation rates; however, were found to advance or postpone the dissipation of the under-pressure. The gas generation rate is not a factor that causes the under-pressure occurring in the Ordovician formations. The dominant factors that control the occurrence of under-pressures in the Ordovician formations are the diffusion coefficient and the low rock permeabilities. The long-term simulation indicates that it requires a low diffusivity to sustain the under-pressures in the Ordovician formations and delay its return to the hydrostatic condition. The return of under-pressured water head to a hydrostatic level consistent with the heads of the Guelph and Cambrian sandstone is controlled by the

partitioning of the gas from the air to the water phase and the diffusion coefficient in the water phase.

The presence of the discontinuity in the Georgian Bay Formation at a depth of 585 m in the DGR-2 borehole was modelled. The capillary pressure in the discontinuity is lower than that of the adjacent rock. This results in a high gas saturation and high water pressure for the discontinuity. The capillary pressure and water pressure above and below the discontinuity is discontinuous, with this indicating that, if parameterized as done here the discontinuity is a pressure barrier in the domain.

The phase saturations are distinctly discontinuous, which is determined by the heterogeneities of the formations as pressures are continuous at the interfaces of two adjacent geologic units. The low gas saturations indicate that the gas phase has dissolved into the water phase. The gas then migrates by diffusion constrained by the saturations at the domain boundary.

6.1 Model Limitations and Future Improvements

The conceptual model in this study is a 1-D analysis that does not consider the horizontal movement of a gas phase that could occur in a three-dimensional environment. The brine is represented by water that overestimates the mobility and viscosity. Hysteric behaviour is not included in the capillary pressure functions due to its complexity.

Future studies can include the simulation of methane and brine instead of air and water. Three-dimensional two-phase flow could be considered in site-scale analyses. Boundary conditions do not change in this study, they can be revised to include groundwater recharge/discharge at the top of the domain.

References

AECOM, and ITASCA CANADA (2011), Regional geology – southern Ontario, *NWMO DGR-TR-2011-15 R000*, AECOM Canada Ltd. and Itasca Consulting Canada, Inc. report for the Nuclear Waste Management Organization, Toronto, Canada.

Aminian, K., M. Tek, and J. Wilson (1982), Silurian-Niagaran reef belt around the Michigan Basin - a synergistic review, in *AIME Society of Petroleum Engineers annual technical conference and exhibition*, no. SPE11056 in Conference: 57, LA, USA.

Armstrong, D., and T. Carter (2006), An updated guide to the subsurface Paleozoic stratigraphy of southern Ontario, *Open File Report 6191*, Ontario Geological Survey.

Bailey Geological Services Ltd., and R. O. Cochrane (1984a), Evaluation of the conventional and potential oil and gas reserves of the Cambrian of Ontario, *Open File Report 5499*, Ontario Geological Survey.

Bethke, C. M. (1986), Inverse hydrologic analysis of the distribution and origin of Gulf Coast-type geopressured zones, *Journal of Geophysical Research*, *91*(B6), 6535–6545.

Bredehoeft, J. D. (1968), On the maintenance of anomalous fluid pressures: I. Thick sedimentary sequences, *Geological Society of America Bulletin*, *79*(9), 1097–1106.

Calder, N. (2009), Two-phase flow parameters determined from DGR-2 laboratory petrophysical data, *Tech. Rep. TR-08-05*, Intera Engineering.

Carpenter, A. B. (1978), Origin and chemical evolution of brines in sedimentary basins, *Oklahoma Geological Survey Circular*, *79*, 60–77.

Catacosinos, P. A., and P. A. Daniels (1991), Stratigraphy of Middle Proterozoic to Middle Ordovician formations of the Michigan basin, in *Early sedimentary evolution of the Michigan basin*, Geological Society of America Special Paper 256.

Catacosinos, P. A., P. A. Daniels, Jr., and W. B. Harrison (1991), Structure, stratigraphy, and petroleum geology of the Michigan Basin, in *Interior Cratonic Basins*, edited by M. W. Leighton, AAPG memoir, 51, chap. 30, pp. 561–601, American Association of Petroleum Geologists.

Clayton, R. N., I. Friedman, D. L. Graf, T. K. Mayeda, W. F. Meets, and N. F. Shimp (1966), The origin of saline formation waters. I. Isotopic composition, *Journal of Geophysical Research*, *71*, 3869–3882.

Coniglio, M., M. J. Melchin, and M. E. Brookfield (1990), Stratigraphy, sedimentology and biostratigraphy of Ordovician rocks of the Peterborough-Lake Simcoe area of southern Ontario, 1990 Eastern Section Meeting, hosted by Ontario Petroleum Institute, Field Trip Guidebook no.3, p. 82, American Association of Petroleum Geologists.

Coniglio, M., Q. Zheng, and T. R. Carter (2003), Dolomitization and recrystallization of middle Silurian reefs and platformal carbonates of the Guelph Formation, Michigan Basin, southerwestern Ontario, *Bulletin of Canadian Petroleum Geology*, *51*(2), 177–199.

Corey, A. T. (1954), The interrelation between gas and oil relative permeabilities, *Producers Monthly*, (NNA.19900720.0036), 38–41.

Craig, H. (1961), Isotopic variations in meteoric waters, *Science*, *133*, 1702–1703.

Davis, C. M. (1964), *Readings in the Geography of Michigan*, Ann Arbor.

Deming, D., C. Cranganu, and Y. Lee (2002), Self-sealing in sedimentary basins, *Journal of Geophysical Research*, *107*(B12), ETG2–1 – ETG2–9.

Dorr, J. A., and D. F. Eschman (1970), *Geology of Michigan*, 117-119 pp., University of Michigan Press: Ann Arbor.

Duan, Z., and S. Mao (2006), A thermodynamic model for calculating methane solubility, density and gas phase composition of methane-bearing aqueous fluids from 273 to 523 k and from 1 to 2000 bar., *Geochimica et Cosmochimica Acta*, *70*(13), 3369–3386.

Duijn, C. V., J. Molenaar, and M. J. Deneef (1995), The effect of capillary forces on immiscible two-phase flow in heterogeneous porous media, *Transport in Porous Media*, *21*, 71–93.

Golder Associates Limited (2003), LLW Geotechnical Feasibility Study, Western Waste Management Facility, Bruce Site, Tiverton, Ontario, *Tech. rep.*, Golder Associates Limited.

Hinze, W. J., R. L. Kellogg, and N. W. O'Hara (1975), Geophysical studies of basement geology of southern penisula of Michigan, *AAPG Bulletin*, *59*(9), 1562–1584.

Hobbs, M. Y., S. K. Frape, O. Shouakar-Stash, and L. R. Kennell (2011), Regional hydrogeochemistry – southern Ontario, *Tech. Rep. NWMO DGR-TR-2011-12 R000*, Nuclear Waste Management Organization, Toronto, Canada.

Hoffman, P. F. (1988), United plates of America, the birth of a craton: Early Proterozoic assembly and growth of Laurentia, *Annual Review of Earth and Planetary Sciences*, *16*, 543–603.

Holman, J. A. (1995), *Ancient Life of the Great Lakes Basin*, 287 pp., University of Michigan Press: Ann Arbor.

Hoteit, H., and A. Firoozabadi (2008), Numerical modeling of two-phase flow in heterogeneous permeable media with different capillarity pressure, *Advances in Water Resources*, *31*, 56–73.

INTERA (2011), Descriptive geosphere site model, *NWMO DGR-TR-2011-24 R000*, Intera Engineering Ltd. report for the Nuclear Waste Management Organization, Toronto, Canada.

Kharaka, Y. K., and J. S. Hanor (2005), Deep fluids in the continents: 1. sedimentary basins, in *Treatise on Geochemistry, Surface and Groundwater, Weathering, and Soils*, edited by J. I. Drever, chap. 5, pp. 499–540.

Kolev, N. I. (2007), *Multiphase Flow Dynamics Fundamentals*, 3rd ed., Berlin ; New York : Springer.

Lee, Y., and D. Deming (2002), Overpressures in the Anadarko basin, southwestern Okalahoma: Static or dynamic?, *AAPG Bulletin*, *86*(1), 145–160.

Loomis, A. G. (1928), Solubilities of gases in water, in *International Critical Tables of Numerical Data, Physics, Chemistry and Technology*, vol. III, edited by E. W. Washburn, C. J. West, N. E. Dorsey, F. R. Bichowsky, and A. Klemenc, pp. 255–261, McGraw-Hill, New York.

Marschall, P., S. Horseman, and T. Gimmi (2005), Characterisation of gas transport properties of the Opalinus clay, a potential host rock formation for radioactive waste disposal, *Oil & Gas Science and Technology - Rev. IFP*, *60*(1), 121–139.

Martini, A. M., J. M. Budai, L. M. Walter, and M. Schoell (1996), Microbial generation of economic accumulations of methane within a shallow organic-rich shale, *Nature*, *383*(6596), 155–158.

Mehl, S., and M. C. Hill (2002), Development and evaluation of a local grid refinement method for block-centered finite-difference groundwater models using shared nodes, *Advances in Water Resources*, *25*, 497–511.

Millington, R. J., and J. P. Quirk (1961), Permeability of porous solids, *Trans. Faraday Soc.*, *57*, 1200–1207.

Neuzil, C. E. (1995), Abnormal pressures as hydrodynamic phenomena, *American Journal of Science*, *295*, 742–786.

Nichols, W. E., N. J. Aimo, M.Oostrom, and M. D. White (1997), STOMP-subsurface transport over multiple phases application guide, *Tech. rep.*, Pacific Northwest National Laboratory.

Nitao, J. J. (1996), *Reference Manual for the NUFT Flow and Transport Code, Version 1.0*, Earth Sciences Department, Lawrence Livermore National Laboratory.

NWMO (2011), Geosynthesis, *Tech. Rep. NWMO DGR-TR-2011-11 R000*, Nuclear Waste Management Organization, Toronto, Canada.

Pruess, K. (1991a), TOUGH2 - A General Purpose Numerical Simulator for Multiphase Fluid and Heat Flow, *Tech. Rep. LBL-29400*, Lawrence Berkeley Laboratory Report, CA.

Pruess, K., C. Oldenburg, and G. Moridis (1999), Tough2 users guide, version 2.0., *Tech. Rep. LBNL-43134*, Earth Sciences Division, Lawrence Berkeley National Laboratory.

Sanford, B. V. (1993), St. lawrence platform, in *Sedimentary Cover of the Craton in Canada*, edited by D. F. Stott and J. D. Aitken, Number 5 in Geology of Canada, pp. 709–798, Geological Survey of Canada.

Saripalli, K. P., R. J. Seme, P. D. Meyer, and B. P. McGrail (2002), Prediction of diffusion coefficients in porous media using tortuosity factors based on interfacial areas, *Ground Water*, *40*(4), 346–352.

Shosa, J. D., and L. M. Cathles (2001), Experimental investigation of capillary blockage of two phase flow in layered porous media, in *GCSSEPM Foundation 21st Annual Research Conference, Petroleum Systems of Deep-Water Basins*, pp. 725–739.

Sorey, M. L., M. A. Grant, and E. Bradford (1980), Nonlinear effects in two-phase flow to wells in geohermal reservoirs, *Water Resources Research*, *16*(4), 767–777.

Sykes, J. F., S. D. Normani, and Y. Yin (2011), Hydrogeologic modelling, *Tech. Rep. NWMO DGR-TR-2011-16 R000*, Nuclear Waste Management Organization, Toronto, Canada.

van Genuchten, M. T. (1980), A closed-form equation for predicting the hydraulic conductivity of unsaturated soils, *Soil Sci. Soc.*, *44*, 892–898.

Whitney, C., and R. Lee (2009), Laboratory Petrophysical Testing of DGR-2 Core, *Tech. Rep. TR-07-18*, Core Laboratories.

Zhang, K., Y.-S. Wu, and K. Pruess (2008), User's Guide for TOUGH2-MP - A Massively Parallel Version of the TOUGH2 Code, *Tech. Rep. LBNL-315E*, Earth Science Division, Lawrence Berkeley National Laboratory.